



**MATHMODEL'20**

**IV INTERNATIONAL SCIENTIFIC CONFERENCE**  
**09 - 12 DECEMBER, 2020, BOROVETS, BULGARIA**

---

# **MATHEMATICAL MODELING**

---

# **PROCEEDINGS**

**YEAR IV ISSUE 1(4)/2020**

**ISSN (Print) 2535-0978**

**ISSN (Online) 2603-3003**

Published by  
**SCIENTIFIC-TECHNICAL UNION of MECHANICAL ENGINEERING - INDUSTRY 4.0**  
**Sofia, BULGARIA**



**IV INTERNATIONAL SCIENTIFIC CONFERENCE**

# **MATHEMATICAL MODELING**

**Year IV**

**Volume 1/4**

**DECEMBER 2020**

ISSN 2535-0978 (Print)  
ISSN 2603-3003 (Online)

# **PROCEEDINGS**

**09 – 12 DECEMBER, 2020,  
BOROVETS, BULGARIA**

**PUBLISHER:  
SCIENTIFIC TECHNICAL UNION OF MECHANICAL  
ENGINEERING “INDUSTRY-4.0”**

108, Rakovski Str., 1000 Sofia, Bulgaria

**tel.** (+359 2) 987 72 90,

**tel./fax** (+359 2) 986 22 40,

[office@mathmodel.eu](mailto:office@mathmodel.eu)

[www.mathmodel.eu](http://www.mathmodel.eu)

# INTERNATIONAL EDITORIAL BOARD

Chairman:		
<b>Prof. ANDREY FIRSOV</b> Peter the Great St.Petersburg Polytechnic University		RU
<b>Members:</b>		
Abilmazhin Adamov, Prof.	L.N.Gumilyov Eurasian National University	KZ
Alexander Guts, Prof.	Omsk State University	RU
Alexei Zhabko, Prof.	Saint Petersburg State University	RU
Andrey Markov, Prof.	Baltic State Technical University	RU
Andrii Matviichuk, Prof.	Kyiv National Economics University	UA
Andrzej Nowakowski, Prof.	University of Lodz	PL
Anton Makarov, Dr.	Saint Petersburg State University	RU
Armands Gricans, Assoc. Prof.	Daugavpils University	LV
Artūras Dubickas, Prof.	Vilnius University	LT
Avinir Makarov, Prof.	Saint Petersburg State University of Industrial Technologies and Design	RU
Christo Boyadjiev, Prof.	Institute of Chemical Engineering, BAS	BG
Daniela Marinova, Dssoc. Prof.	Technical University of Sofia	BG
Dimitrios Poulakis, Prof.	Aristotle University of Thessaloniki	GR
Evgeniy Smirnov, Assoc. Prof.	Volgograd State Technical University	RU
Galia Angelova, Prof. DSc	Institute of Information and Communication Technologies, BAS	BG
Giovanni Borgioli, Assoc. Prof.	University of Florence	IT
Haskiz Coskun, Prof.	Karadeniz Technical University of Trabzon	TR
Idilia Bachkova, Prof.	University of Chemical Technology and Metallurgy	BG
Irena Stojkovska, Prof.	Ss. Cyril and Methodius University in Skopje	NM
Ivana Štajner-Papuga, Prof.	University of Novi Sad	RS
Kanagat Aldazharov, Assoc. Prof.	Kazakh Economics University	KZ
Karl Kunisch, Prof.	University of Graz	AT
Mahomed Agamirza ogly Dunyamalyev, Prof.	Azerbaijan Technical University	AZ
Marius Giuclea, Prof.	The Bucharest University of Economics Studies	RO
Mihail Okrepilov, Prof.	D.I. Mendeleev Institute for Metrology (VNIIM)	RU
Milena Racheva, Assoc. Prof.	Technical University of Gabrovo	BG
Mohamed Kara, Dr.	Ferhat Abbas Sétif 1 University	DZ
Mohamed Taher El-mayah, Prof	MTI University	EG
Neli Dimitrova, Prof.	Institute of Mathematics and Informatics, BAS	BG
Nina Bijedic, Prof.	Dzemal Bijedic University of Mostar	BA
Oleg Obradović, Prof.	University of Montenegro	ME
Olga Pritomanova, Assoc. Prof.	Oles Honchar Dnipropetrovsk National University	UA
Özkan Öcalan, Prof.	Akdeniz University of Antalya	TR
Pașc Găvruta, Prof.	Politehnic University of Timisoara	RO
Pavel Satrapa, Assoc. Prof.	Technical University of Liberec	CZ
Pavel Tvrdík, Prof.	Czech Technical University in Prague	CZ
Pavlina Yordanova, Assoc. Prof.	Shumen University	BG
Petr Trusov, Prof.	Perm State Technical University	RU
Rannveig Björnsdóttir, Prof.	University of Akureyri	IS
Roumen Anguelov, Prof.	University of Pretoria	ZA
Sándor Szabó, Dr. Prof.	University of Pécs	HU
Sashko Martinovski, Assoc. Prof.	St. Kliment Ohridski University of Bitola	NM
Sergey Bosnyakov, Prof.	Moscow Institute of Physics and Technology	RU
Sergey Kshevetskii, Prof.	Immanuel Kant Baltic Federal University	RU
Snejana Hristova, Prof.	University of Plovdiv	BG
Svetlana Lebed, Assoc. Prof.	Brest State Technical University	BY
Tomasz Szarek, Prof.	University of Gdansk	PL
Valeriy Serov, Prof.	University of Oulu	FI
Vasily Maximov, Prof.	Saint Petersburg State University of Industrial Technologies and Design	RU
Ventsi Rumchev, Prof.	Curtin University, Perth	AU
Veronika Stoffová, Prof.	University of Trnava	SK
Veselka Pavlova, Prof.	University of National and World Economy	BG
Viorica Sudacevschi, Assoc. Prof.	Technical University of Moldova	MD
Vladimir Janković, Prof.	University of Belgrade	RS
Vladislav Holodnov, Prof.	Saint Petersburg State Institute of Technology	RU
Vyacheslav Demidov, Prof.	Saint Petersburg State University of Industrial Technologies and Design	RU
Yordan Yordanov, Assoc. Prof.	University of Sofia	BG
Yuriy Kuznetsov, Prof.	Nizhny Novgorod State University	RU
Zdenka Kolar - Begović, Prof.	University of Osijek	HR

# CONTENTS

## **COMPARISON OF THREE METHODS FOR THE PUMP ENERGY ANALYSIS**

PhD. Mrzljak Vedran, PhD. Student Lorencin Ivan, PhD. Student Anđelić Nikola, PhD. Student Baressi Šegota Sandi ..... 5

## **MULTIPURPOSE VIRTUAL MODEL OF A HUMAN BODY AND ITS UTILIZATION IN THE TRAFFIC SAFETY**

Jan Špička, Jan Vychytil, Luděk Hynčík, Tomasz Bonkowski ..... 9

## **SIMULATION OF THE MAIN COMPONENTS OF A NUCLEAR REACTOR UNDER LOAD, MADE OF ULTRAFINE-GRAINED STEEL AISI-321 IN THE NORMAL AND IRRADIATED STATE**

Abdrakhman Naizabekov, Evgeniy Panin, Andrey Tolkushkin, Daniyar Zhumagaliev ..... 13

## **INJURY PREVENTION DURING CHILDBIRTH: THE MODEL OF OBSTETRICIAN**

Jan Vychytil, Linda Havelková, Hana Čechová, Tomáš Zítka, Maximilian Melzner ..... 17

## **LINEAR SYNTHESIS OF FRAME EDDY CURRENT PROBES WITH A PLANAR EXCITATION SYSTEM**

Trembovetska R., PhD Eng., Assoc. Prof.; Halchenko V.Ya., Dr.Sc. Eng., Prof.; Tychkov V., PhD Eng., Assoc. Prof.; Bazilo C.V., Dr.Sc. Eng., Assoc. Prof. .... 20

## **NATIONAL CURRENCY DYNAMICS FORECAST AUTOMATION USING LOGISTIC FUNCTION**

Abdyraimova K. S. .... 25

## **STABILITY OF CONVECTIVE MOTION OF A FLUID WITH IMPURITY**

Prof., Dr. Dementev O., PhD. Turlakova S. .... 28

## **MOTORCYCLE ACCIDENTS RECONSTRUCTION AND SIMULATION - APPLICATION OF HYBRID HUMAN BODY MODEL**

Tomasz Bonkowski, Ludek Hyncik, Jan Spicka, Jan Vychytil ..... 32

## **INJURY PREVENTION DURING CHILDBIRTH: A MODEL OF PELVIC FLOOR**

Hana Čechová, Linda Havelková, Tomáš Zítka, Zdeněk Rušavý, Vladimír Kališ, Khaled Ismail ..... 36

## **A STUDY OF CONVERGENCE OF $\xi$ APPROXIMATIONS TRANSFORM BY REGION DEPENDED GIVEN AS DETERMINED BY $\sigma_n(t)$ FUNCTIONS ON ENTIRE COMPLEX PLANE**

Assist Prof. PhD. Işim Genç Demiriz ..... 39

## **MATHEMATICAL MODELING OF AUTOMATED PRODUCTION SYSTEMS**

Assoc. Prof. Ph.D. Sergii P.Vysloukh, Prof. Dr. Eng. Viktor S.Antonyuk, Assoc. Prof. Ph.D. Kateryna S. Barandych, Assist. Prof. Oksana V.Voloshko ..... 41





# Comparison of three methods for the pump energy analysis

Mrzljak Vedran, Lorencin Ivan, Anđelić Nikola, Baressi Šegota Sandi  
Faculty of Engineering, University of Rijeka, Vukovarska 58, 51000 Rijeka, Croatia  
E-mail: vedran.mrzljak@riteh.hr, ilorencin@riteh.hr, nandelic@riteh.hr, sbaressisegota@riteh.hr

**Abstract:** This paper presents a comparison of three methods for any pump energy analysis. Each method is used for the analysis of three different water pumps from the conventional steam thermal power plant – two feed water pumps (FWP1 and FWP2) and condensate pump (CP). For each pump three essential types of mechanical power which defines all energy analysis methods are: delivered power from power producer, real (polytropic) power and ideal (isentropic) power. Method 1 which compares delivered and real (polytropic) power show the best performances, while Method 3 which compare delivered and ideal (isentropic) power should be avoided because it results with too high energy power loss and too low energy efficiency of any pump. Method 2 which compares real (polytropic) and ideal (isentropic) pump power can be used as a good compromise for the pump energy analysis in the most of the cases – its results are similar to results of Method 1.

**KEYWORDS:** PUMP, VARIOUS ENERGY ANALYSIS METHODS, ENERGY LOSS, ENERGY EFFICIENCY

## 1. Introduction

Pumps are unavoidable components of various steam power plants [1-3], combined-cycle power plants [4, 5], cogeneration plants [6] and many different power and energy systems [7, 8].

The pumps function is the same as a function of compressors or turbocompressors – increasing of operating medium pressure [9, 10]. The only difference between pumps and compressors is in operating medium – pumps operate with liquids, while compressors and turbocompressors operate with gases, vapors and its mixtures [11, 12].

In the literature can be found pumps of various types which operate in different operating regimes [13]. Regardless of pump type or operating regime, the crucial element in energy analysis of any pump is taking into account three types of mechanical power which defines various losses – delivered mechanical power to pump from the mechanical power producer, mechanical power required for real (polytropic) pressure increase of liquid and mechanical power required for ideal (isentropic) liquid pressure increase.

The comparison of the mentioned types of mechanical power defines all the methods for any pump energy analysis. In this paper is described and presented each energy analysis method for any pump and all the methods are compared at each of three pumps from the conventional steam thermal power plant. Those pumps are two feed water pumps (FWP1 and FWP2) as well as condensate pump (CP). For each observed pump are calculated energy power losses and energy efficiencies by using each of three energy analysis methods. The obtained results are discussed in detail.

## 2. Pump description and operating characteristics

As the analysis in this paper will be performed by using three water pumps, all of the descriptions and explanations are based on the water as the operating medium for the pump (again, it must be taken into account that operating medium can be any liquid).

Operation principle of any pump is presented in Fig. 1. The pump takes liquid (water) of a lower pressure, increases its pressure and delivers liquid with a higher pressure to a higher pressure component [14]. For the liquid pressure increase, any pump uses mechanical power delivered from the mechanical power producer which are in the most of the cases electrical motors or in some situations steam or gas low-power turbines [15-17]. Mechanical power delivered to pump from mechanical power producer is the highest mechanical power related to any pump – it takes into account all the losses in shafts, bearings, pump inner losses and all the other losses which occur in power distribution.

For proper pump energy analysis (regardless of used method) are required operating parameters of liquid at pump suction side (inlet) and at the pump compression side (outlet). Those liquid operating parameters at the pump inlet and outlet are liquid pressure, temperature and mass flow rate. Therefore, pump operation can be analyzed only by measuring described liquid operating parameters at both sides of any pump. In Fig. 1, the operating points in which the measurements should be obtained are marked with yellow dots and marked as water inlet (input) and water outlet (output).

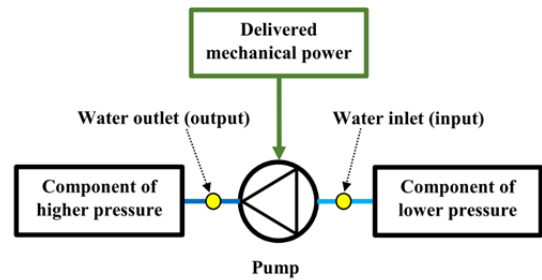


**Fig. 1.** Scheme of the pump with two operating points (marked yellow) required for the analysis

Measured operating parameters of liquid at the pump inlet (input) and at the pump outlet (output) defines real (polytropic) process of a pump, Fig. 2. This process takes into account all the losses which occur during liquid pressure increase. Losses during liquid pressure increase can be seen in liquid specific entropy increase at the pump outlet (in comparison to pump inlet). Second mechanical power related to any pump is real (polytropic) power, which is required for real (polytropic) pressure increase process. From the measured liquid operating parameters at the pump inlet and outlet can be calculated mechanical power required for the real (polytropic) process.

The third and final mechanical power of any pump is ideal (isentropic) mechanical power. This power can also be calculated from the measured liquid operating parameters at the pump inlet and from the calculated liquid operating parameters at the pump outlet. In ideal (isentropic) pump process, liquid operating parameters at the pump inlet are the same as in the real (polytropic) process. However, the difference in ideal and real pump pressure increase process can be seen in liquid operating parameters at the pump outlet. Ideal (isentropic) pressure increase process is a process between the same pressures but with assuming always the same liquid specific entropy, Fig. 2. Always the same liquid specific entropy during the pressure increase neglected any losses during such process. Any real process should be as close as possible to the ideal one, but due to losses, real process will never achieve the ideal one. By knowing the liquid specific entropy and pressure at the pump outlet can be calculated all the other liquid operating parameters in ideal process and therefore, from those parameters can be calculated ideal (isentropic) mechanical power.

Comparison of pump ideal and real pressure increase process, Fig. 2, leads to conclusion that in the real process pump will require more mechanical power (due to higher difference in liquid specific enthalpies at pump outlet and inlet). In both real and ideal pump processes, liquid mass flow rate is the same. As any pump is a mechanical power consumer, in ideal (isentropic) pressure increase process, between the same pressures as in the real process, pump will require the lowest mechanical power (in comparison to real and delivered mechanical power). From this point of view, for any pump is always valid following mechanical power relation:

$$P_{\text{delivered}} > P_{\text{real (polytropic)}} > P_{\text{ideal (isentropic)}}, \quad (1)$$

where  $P$  is mechanical power in (kW).



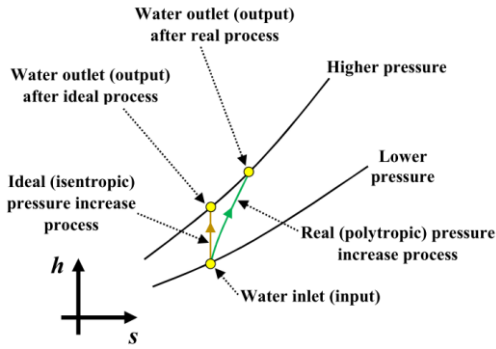


Fig. 2. A comparison of real (polytropic) and ideal (isentropic) liquid pressure increase process in specific enthalpy-specific entropy diagram

### 3. Equations for the energy analysis

#### 3.1. General energy analysis equations and balances

The first law of thermodynamics defines energy analysis of any system or a control volume [18, 19]. The general energy balance equation, disregarding potential and kinetic energies, is [20]:

$$\dot{Q}_{in} + P_{in} + \sum \dot{E}_{n,in} = \dot{Q}_{out} + P_{out} + \sum \dot{E}_{n,out}, \quad (2)$$

where  $\dot{Q}$  in (kW) is energy heat transfer, index in is related to the inlet (input) and index out is related to the outlet (output).  $\dot{E}_n$  is a total energy of operating medium flow in (kW) [21], defined by the equation:

$$\dot{E}_n = \dot{m} \cdot h, \quad (3)$$

where  $\dot{m}$  is operating medium mass flow rate in (kg/s) and  $h$  is operating medium specific enthalpy in (kJ/kg). Overall definition of the energy efficiency of any system or a control volume is [22, 23]:

$$\eta_{en} = \frac{\text{cumulative energy outlet (output)}}{\text{cumulative energy inlet (input)}}. \quad (4)$$

During the energy analysis of any system or a component usually did not occur any operating medium mass flow rate leakage, therefore it is also valid following mass flow rate balance [24]:

$$\sum \dot{m}_{in} = \sum \dot{m}_{out}. \quad (5)$$

All the general energy analysis equations and balances will be used in the following equations of three pump energy analysis methods.

#### 3.2. Equations for three energy analysis methods of the pump

All pump energy analysis methods are based on the principles and operating parameters presented in Fig. 1 and Fig. 2. It should be noted that in any method must be fulfilled pump mechanical power relation presented in Eq. 1.

##### Method 1

The first method of pump energy analysis is based on comparison of mechanical power delivered to pump from power producer and real (polytropic) power required for real pump pressure increase process. The main problem of this method in practical calculations is that for many pumps, mechanical power delivered from mechanical power producer is not known or measured [25] because in each complex process pumps are auxiliary devices. Equations for this method will be derived from [26].

Pump energy power loss by using this method is:

$$\dot{E}_{n_{PL,M1}} = \dot{m}_{in} \cdot h_{in} + P_{delivered} - \dot{m}_{out} \cdot h_{out}, \quad (6)$$

where mechanical power delivered from mechanical power producer is measured variable. Mechanical power for the real (polytropic) pump pressure increase process is derived from measured fluid operating parameters at the pump inlet and outlet:

$$P_{real \text{ (polytropic)}} = \dot{m}_{out} \cdot h_{out} - \dot{m}_{in} \cdot h_{in}, \quad (7)$$

therefore, pump energy power loss by using this method can be presented as:

$$\dot{E}_{n_{PL,M1}} = P_{delivered} - P_{real \text{ (polytropic)}}. \quad (8)$$

Pump energy efficiency by using this method is:

$$\eta_{en,M1} = \frac{\dot{m}_{out} \cdot h_{out} - \dot{m}_{in} \cdot h_{in}}{P_{delivered}} = \frac{P_{real \text{ (polytropic)}}}{P_{delivered}}. \quad (9)$$

##### Method 2

A second method of pump energy analysis is based on comparison of mechanical power which pump use in real (polytropic) pressure increase process and mechanical power which pump will use in ideal (isentropic) pressure increase process. This is the most common used method due to the highest data availability. This method, in fact, compared real pump process with the process which can be obtained in ideal situation.

Mechanical power for the ideal (isentropic) pump pressure increase process is:

$$P_{ideal \text{ (isentropic)}} = \dot{m}_{out} \cdot h_{out,IS} - \dot{m}_{in} \cdot h_{in}, \quad (10)$$

where index IS denotes isentropic process. Mechanical power for the pump real (polytropic) pressure increase process is calculated by using Eq. 7. Pump energy power loss by using this method is:

$$\dot{E}_{n_{PL,M2}} = P_{real \text{ (polytropic)}} - P_{ideal \text{ (isentropic)}}. \quad (11)$$

Pump energy efficiency by using this method is:

$$\eta_{en,M2} = \frac{P_{ideal \text{ (isentropic)}}}{P_{real \text{ (polytropic)}}}. \quad (12)$$

##### Method 3

The third method of pump energy analysis is based on comparison of delivered mechanical power from mechanical power producer and mechanical power which pump will use in the ideal (isentropic) pressure increase process. Delivered mechanical power from mechanical power producer is measured inside the power plant, while the mechanical power for the ideal (isentropic) pump pressure increase process is calculated by using Eq. 10.

Pump energy power loss by using this method is:

$$\dot{E}_{n_{PL,M3}} = P_{delivered} - P_{ideal \text{ (isentropic)}}. \quad (13)$$

Pump energy efficiency by using this method is:

$$\eta_{en,M3} = \frac{P_{ideal \text{ (isentropic)}}}{P_{delivered}}. \quad (14)$$

### 4. Water operating parameters at pump input (inlet) and output (outlet) required for the analysis

Three described pump energy analysis methods are compared at each of three water pumps which required operating parameters are found in the literature [27].

Required water operating parameters (pressure, temperature and mass flow rate) at each pump inlet and outlet are presented in Table 1. Observed pumps are two feed water pumps (FWP1 and FWP2) as well as condensate pump (CP).

Table 1. Water operating parameters at input (inlet) and output (outlet) of each pump [27]

Pump	Operating point	Water mass flow rate (kg/s)	Water temperature (K)	Water pressure (kPa)
FWP1	Inlet	59.27	452.55	1032
	Outlet	59.27	456.34	18355
FWP2	Inlet	59.98	452.55	1030
	Outlet	59.98	456.34	18359
CP	Inlet	89.91	315.12	35.28
	Outlet	89.91	316.23	1618

By using water pressure and temperature at the inlet and outlet of each pump are calculated water specific enthalpies and specific entropies by using NIST REFPROP 9.0 software [28] and presented in Table 2. Required water specific enthalpies and specific entropies are calculated for both real (polytropic) as well as for the ideal (isentropic) water pressure increase process for each pump. From Table 2 can be seen that in the ideal (isentropic) pressure increase process water specific entropy at the inlet and outlet of each pump remains the same.

**Table 2.** Water specific enthalpies and specific entropies at input (inlet) and output (outlet) of each observed pump in real (polytropic) and ideal (isentropic) pressure increase processes

Pump	Operating point	Water specific enthalpy – real (polytropic) process (kJ/kg)	Water specific entropy – real (polytropic) process (kJ/kg·K)	Water specific entropy – ideal (isentropic) process (kJ/kg·K)	Water specific enthalpy – ideal (isentropic) process (kJ/kg)
FWP1	Inlet	760.43	2.1334	2.1334	760.43
	Outlet	785.97	2.1468	2.1334	779.86
FWP2	Inlet	760.43	2.1334	2.1334	760.43
	Outlet	785.97	2.1468	2.1334	779.86
CP	Inlet	175.79	0.5986	0.5986	175.79
	Outlet	181.82	0.6127	0.5986	177.39

## 5. Results and discussion

Energy power of water, calculated for each pump at inlet (input) and outlet (output) by using Eq. 3 is presented in Fig. 3. It can clearly be seen that both feed water pumps (FWP1 and FWP2) have much higher energy power inputs and outputs in comparison to condensate pump (CP).

It should be noted that FWP1 and FWP2 operates with much higher water pressures at inlet and outlet (Table 1) in comparison to CP, which is used for the pressure increase of condensate obtained in power plant main steam condenser.

The difference between energy power of water at each pump outlet and inlet denotes required mechanical power used in each pump (regardless of mechanical power type). Therefore, FWP2 will use the highest mechanical power, followed by FWP1, while the CP will use mechanical power much lower in comparison to both feed water pumps.

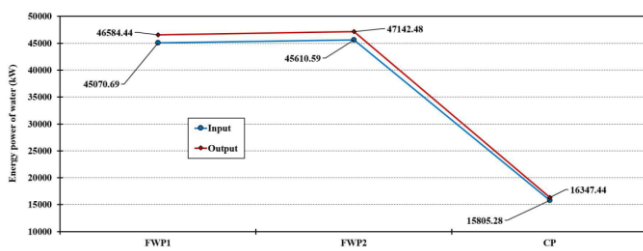


**Fig. 3.** Comparison of water energy power input and output for three observed pumps

The mechanical power relation for each pump, presented in Eq. 1 is clearly visible in Fig. 4. For each of three observed pumps delivered mechanical power is the highest one, followed by real (polytropic) power, while the lowest mechanical power is ideal (isentropic) one.

The conclusion obtained from Fig. 3 is also visible in Fig. 4 – FWP2 uses the highest mechanical power in comparison to other observed water pumps (regardless of the fact is that power delivered, real or ideal). Delivered mechanical power to FWP1, FWP2 and CP is equal to 1830 kW, 1860 kW and 850 kW, real (polytropic) power is equal to 1513.76 kW, 1531.89 kW and 542.16 kW, while ideal (isentropic) power is equal to 1151.62 kW, 1165.41 kW and 143.86 kW, respectively.

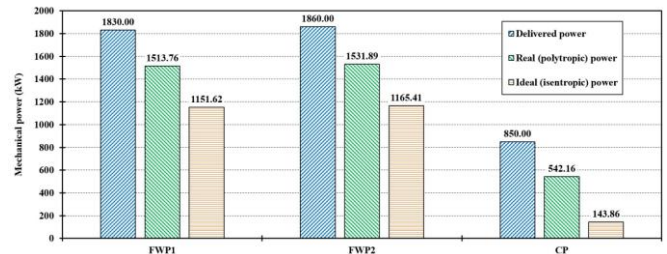


**Fig. 4.** Comparison of delivered, real (polytropic) and ideal (isentropic) mechanical power for three observed water pumps

Comparison of three methods for the pump energy analysis shows the same trends in energy power loss for each of three observed pumps, Fig. 5. The lowest energy power loss of each pump is obtained by using Method 1 (comparison of delivered and real power), followed by Method 2 (comparison of real and ideal power). It can be observed that Method 1 and Method 2 gives similar energy power loss for both feed water pumps, while the notable difference between those two methods in energy power loss can be seen only for condensate pump. Method 3 gives much higher energy power loss of each observed pump in comparison to the other two methods.

When comparing energy power loss trends between observed pumps, it can be seen that in Method 1 FWP2 has the highest, while CP has the lowest energy power loss, Fig. 5. Using Method 2 and Method 3 results with same trends in energy power loss – FWP1 has the lowest, while CP has the highest energy power loss.

A detail analysis and possible optimization of each of three observed pumps will be performed by using various artificial intelligence approaches [29-32].

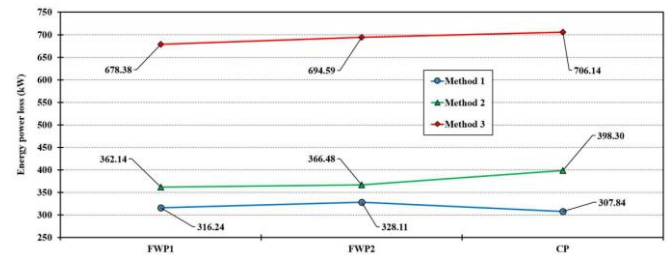


**Fig. 5.** Energy power loss obtained in all energy analysis methods for three observed water pumps

Comparison of Fig. 5 and Fig. 6 proves the fact that all of the observed pumps are components for which energy power loss and energy efficiency are reverse proportional.

Therefore, the highest energy efficiency of each observed pump will be obtained by using Method 1, while the lowest energy efficiency of each pump will be obtained by using Method 3.

Obtained energy efficiency for FWP1, FWP2 and CP is equal to 82.72%, 82.36% and 63.78% by using Method 1; 76.08%, 76.08% and 26.53% by using Method 2 and 62.93%, 62.66% and 16.92% by using Method 3, respectively, Fig. 6. Again, for both feed water pumps obtained energy efficiencies by using Method 1 and Method 2 are similar, while for the CP used energy analysis methods gives quite different results. For the CP, only Method 1 gives an acceptable energy efficiency result, while Method 2 and Method 3 gives unacceptably low energy efficiencies.

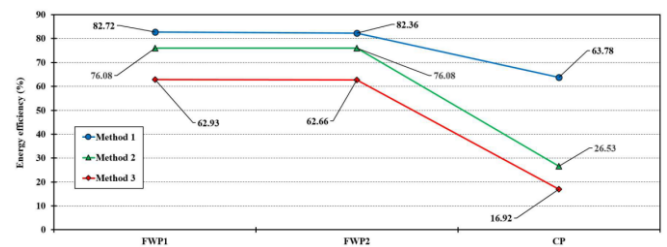


**Fig. 6.** Energy efficiency obtained in all energy analysis methods for three observed water pumps



Comparison in energy efficiency between all of the observed pumps gives as a result that the highest energy efficiency has FWP1, while the lowest energy efficiency has CP, regardless of used energy analysis method.

## 6. Conclusions

In this paper are presented three methods for any pump energy analysis. Each of observed methods is used for the analysis of three different water pumps from the conventional steam thermal power plant – two feed water pumps (FWP1 and FWP2) and condensate pump (CP). The most important conclusions are:

- The best energy analysis method for any pump is Method 1 which compare delivered and real (polytropic) mechanical power.
- Due to insufficient data (due to unknown delivered mechanical power from the mechanical power producer), Method 2 which compare real (polytropic) and ideal (isentropic) pump power can be used as a good compromise for the pump energy analysis – in the most of the cases obtained energy power loss and energy efficiency will be similar as in Method 1.
- The usage of Method 2 in the pump energy analysis can be questionable for the pumps which operate with low liquid pressure at the suction side.
- In any case, Method 3 should be avoided for the pump energy analysis, because it results with too high energy power loss and too low energy efficiency of any pump.

## 7. Acknowledgment

This research has been supported by the Croatian Science Foundation under the project IP-2018-01-3739, CEEPUS network CIII-HR-0108, European Regional Development Fund under the grant KK.01.1.1.01.0009 (DATACROSS), project CEKOM under the grant KK.01.2.2.03.0004, CEI project "COVIDAI" (305.6019-20), University of Rijeka scientific grant uniri-tehnic-18-275-1447, University of Rijeka scientific grant uniri-tehnic-18-1146 and University of Rijeka scientific grant uniri-tehnic-18-14.

## 8. References

[1] Ahmadi, G. R., Toghraie, D.: *Energy and exergy analysis of Montazeri steam power plant in Iran*, Renewable and Sustainable Energy Reviews 56, p. 454–463, 2016. (doi:10.1016/j.rser.2015.11.074)

[2] Mrzljak, V., Poljak, I.: *Energy analysis of main propulsion steam turbine from conventional LNG carrier at three different loads*, International Journal of Maritime Science & Technology "Our Sea" 66 (1), p. 10–18, 2019. (doi:10.17818/NM/2019/1.2)

[3] Naserbegi, A., Aghaie, M., Minuchehr, A., Alahyarizadeh, Gh.: *A novel exergy optimization of Bushehr nuclear power plant by gravitational search algorithm (GSA)*, Energy 148, p. 373–385, 2018. (doi:10.1016/j.energy.2018.01.119)

[4] Lorencin, I., Anđelić, N., Mrzljak, V., Car, Z.: *Genetic algorithm approach to design of multi-layer perceptron for combined cycle power plant electrical power output estimation*, Energies 12 (22), 4352, 2019. (doi:10.3390/en12224352)

[5] Adibhatla, S., Kaushik, S. C.: *Energy, exergy and economic (3E) analysis of integrated solar direct steam generation combined cycle power plant*, Sustainable Energy Technologies and Assessments 20, p. 88–97, 2017. (doi:10.1016/j.seta.2017.01.002)

[6] Burin, E. K., Vogel, T., Mulhaupt, S., Thelen, A., Oeljeklaus, G., Gorner, K., Bazzo, E.: *Thermodynamic and economic evaluation of a solar aided sugarcane bagasse cogeneration power plant*, Energy 117, Part 2, p. 416–428, 2016. (doi:10.1016/j.energy.2016.06.071)

[7] Catrini, P., Cipollina, A., Micale, G., Piacentino, A., Tamburini, A.: *Exergy analysis and thermoeconomic cost accounting of a combined heat and power steam cycle integrated with a multi effect distillation-thermal vapour compression desalination plant*, Energy Conversion and Management 149, p. 950–965, 2017. (doi:10.1016/j.enconman.2017.04.032)

[8] Hafidhi, F., Khir, T., Ben Yahya, A., Ben Brahim, A.: *Energetic and exergetic analysis of a steam turbine power plant in an existing phosphoric acid factory*, Energy Conversion and Management 106, p. 1230–1241, 2015. (doi:10.1016/j.enconman.2015.10.044)

[9] Sutton, I.: *Plant design and operations*, Elsevier Inc., 2015.

[10] Lorencin, I., Anđelić, N., Mrzljak, V., Car, Z.: *Multilayer Perceptron approach to Condition-Based Maintenance of Marine CODLAG Propulsion*

*System Components*, Scientific Journal of Maritime Research 33 (2), p. 181–190, 2019. (doi:10.31217/p.33.2.8)

[11] Koroglu, T., Sogut, O.S.: *Conventional and advanced exergy analyses of a marine steam power plant*, Energy 163, p. 392–403, 2018. (doi:10.1016/j.energy.2018.08.119)

[12] Mrzljak, V., Anđelić, N., Lorencin, I., Car, Z.: *Analysis of gas turbine operation before and after major maintenance*, Journal of Maritime & Transportation Sciences 57 (1), p. 57–70, 2019. (doi:10.18048/2019.57.04)

[13] Mrzljak, V., Prpić-Oršić, J., Poljak, I.: *Energy power losses and efficiency of low power steam turbine for the main feed water pump drive in the marine steam propulsion system*, Journal of Maritime & Transportation Sciences 54 (1), p. 37–51, 2018. (doi:10.18048/2018.54.03)

[14] Moran M., Shapiro H., Boettner, D. D., Bailey, M. B.: *Fundamentals of engineering thermodynamics*, 7<sup>th</sup> edition, John Wiley and Sons, Inc., 2011.

[15] Kostyuk, A., Frolov, V.: *Steam and gas turbines*, Mir Publishers, Moscow, 1988.

[16] Mrzljak, V., Poljak, I., Mrakovčić, T.: *Energy and exergy analysis of the turbo-generators and steam turbine for the main feed water pump drive on LNG carrier*, Energy Conversion and Management 140, p. 307–323, 2017. (doi:10.1016/j.enconman.2017.03.007)

[17] Mrzljak, V.: *Low power steam turbine energy efficiency and losses during the developed power variation*, Technical Journal 12 (3), p. 174–180, 2018. (doi:10.31803/tg-20180201002943)

[18] Kanoğlu, M., Çengel, Y.A., Dincer, I.: *Efficiency evaluation of energy systems*, Springer Briefs in Energy, Springer, 2012.

[19] Kocijel, L., Poljak, I., Mrzljak, V., Car, Z.: *Energy Loss Analysis at the Gland Seals of a Marine Turbo-Generator Steam Turbine*, Technical Journal 14 (1), p. 19–26, 2020. (doi:10.31803/tg-20191031094436)

[20] Medica-Viola, V., Baressi Šegota, S., Mrzljak, V., Štifanić, D.: *Comparison of conventional and heat balance based energy analyses of steam turbine*, Scientific Journal of Maritime Research 34 (1), p. 74–85, 2020. (doi:10.31217/p.34.1.9)

[21] Medica-Viola, V., Mrzljak, V., Anđelić, N., Jelić, M.: *Analysis of Low-Power Steam Turbine With One Extraction for Marine Applications*, International Journal of Maritime Science & Technology "Our Sea" 67 (2), p. 87–95, 2020. (doi:10.17818/NM/2020/2.1)

[22] Mrzljak, V., Blečić, P., Anđelić, N., Lorencin, I.: *Energy and exergy analyses of forced draft fan for marine steam propulsion system during load change*, Journal of Marine Science and Engineering 7 (11), 381, 2019. (doi:10.3390/jmse7110381)

[23] Taheri, M. H., Mosaffa, A. H., Garousi Farshi, L.: *Energy, exergy and economic assessments of a novel integrated biomass based multigeneration energy system with hydrogen production and LNG regasification cycle*, Energy 125, p. 162–177, 2017. (doi:10.1016/j.energy.2017.02.124)

[24] Lorencin, I., Anđelić, N., Mrzljak, V., Car, Z.: *Exergy analysis of marine steam turbine labyrinth (gland) seals*, Scientific Journal of Maritime Research 33 (1), p. 76–83, 2019. (doi:10.31217/p.33.1.8)

[25] Noroozian, A., Mohammadi, A., Bidi, M., Ahmadi, M. H.: *Energy, exergy and economic analyses of a novel system to recover waste heat and water in steam power plants*, Energy Conversion and Management 144, p. 351–360, 2017. (doi:10.1016/j.enconman.2017.04.067)

[26] Mrzljak, V., Žarković, B., Poljak, I.: *Energy and exergy analysis of sea water pump for the main condenser cooling in the LNG carrier steam propulsion system*, Proceedings of International scientific conference Mathematical Modeling 2017, p. 92–95, Borovets, Bulgaria, 2017.

[27] Uysal, C., Kurt, H., Kwak H.-Y.: *Exergetic and thermoeconomic analyses of a coal-fired power plant*, International Journal of Thermal Sciences 117, p. 106–120, 2017. (doi:10.1016/j.ijthermalsci.2017.03.010)

[28] Lemmon, E.W., Huber, M.L., McLinden, M.O.: *NIST reference fluid thermodynamic and transport properties - REFPROP*, version 9.0, User's guide, Colorado, 2010.

[29] Lorencin, I., Anđelić, N., Mrzljak, V., Car, Z.: *Marine objects recognition using convolutional neural networks*, International Journal of Maritime Science & Technology "Our Sea" 66 (3), p. 112–119, 2019. (doi:10.17818/NM/2019/3.3)

[30] Car, Z., Baressi Šegota, S., Anđelić, N., Lorencin, I., Mrzljak, V.: *Modeling the Spread of COVID-19 Infection Using a Multilayer Perceptron*, Computational and Mathematical Methods in Medicine, 2020. (doi:10.1155/2020/5714714)

[31] Lorencin, I., Anđelić, N., Španjol, J., Car, Z.: *Using multi-layer perceptron with Laplacian edge detector for bladder cancer diagnosis*, Artificial Intelligence in Medicine, 102, 101746, 2020. (doi:10.1016/j.artmed.2019.101746)

[32] Baressi Šegota, S., Lorencin, I., Ohkura, K., Car, Z.: *On the traveling salesman problem in nautical environments: an evolutionary computing approach to optimization of tourist route paths in Medulin, Croatia*, Journal of Maritime & Transportation Sciences 57 (1), p. 71–87, 2019. (doi:10.18048/2019.57.05)

# Multipurpose virtual model of a human body and its utilization in the traffic safety

Jan Špička<sup>1,2</sup>, Jan Vychytil<sup>1</sup>, Luděk Hynčík<sup>1</sup>, Tomasz Bonkowski<sup>1,2</sup>

<sup>1</sup>New Technologies – Research Centre, University of West Bohemia in Pilsen, Univerzitní 8, Pilsen, 306 14, Czech Republic

<sup>2</sup>Faculty of Applied Sciences, University of West Bohemia in Pilsen, Univerzitní 8, Pilsen, 306 14, Czech Republic

E-mail: spicka@ntc.zcu.cz, jvychytil@ntc.zcu.cz, tomasz@ntis.zcu.cz, hyncik@ntc.zcu.cz

**Abstract:** The aim of this work is the implementation of the virtual hybrid human body model Virthuman into the pedestrian traffic collision scenarios. The pedestrians are the most vulnerable traffic road users and they are exposed to a high risk and suffer with serious injuries and responsible for high number of death and injuries. The interest of the study of simulation of a car crash accident is motivated by the effort to decrease these numbers. The authors use a virtual model of the full human body called Virthuman here. This model was built based on combination of two modelling approaches, particularly multibody and finite element. Such method is call a hybrid approach and keeps advantages of both principles. The model was fully validated against published experimental data (particular body segment tests as well as full body tests) and was successfully used in the number of applications. The purpose of this paper is to present the model as a suitable tool for pedestrian collision modelling and injury risk assessment. Besides the description of the model, the examples of the application towards pedestrian safety are going to be presented here.

**KEYWORDS:** HUMAN BODY MODEL; VIRTUMAN; PEDESTRIAN SAFETY; ACCIDENT RECONSTRUCTION; INJURY RISK

## 1. Introduction

Pedestrians are the most vulnerable road users and they are exposed to a high risk in the collisions with the vehicles. The statistical data shows that pedestrians are still responsible for the second biggest number of fatalities and injuries on the road; about 2.000 in the Czech Republic [1, 2] 40.000 in the EU and 1.25 million around the globe annually, [1, 3, 4, 5].

Moreover, the recent studies in Europe indicate that the passenger cars are one of the most often involved in the collisions with the pedestrians. Figure 1 summarizes the distribution of the vehicle type participating in the pedestrian collisions in the Czech Republic in years 2009-2014 [6]

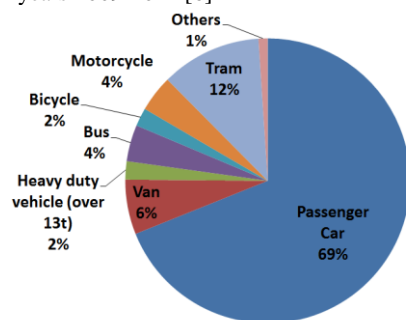


**Figure 1:** Distribution of the vehicle type involved the pedestrian accident in the Czech Republic in 2009-2014

Recently, the virtual human body models are being used more often and virtual approach in the biomechanical fields. The virtual prototyping in the automotive industry takes benefit from the numerical models of the humans. The models are mostly based on the finite element method, articulated rigid bodies (multibody) or a hybrid approach that combines advantages of both approaches. The review of the current state of biomechanical human body models is given for instance in [7, 8].

This work demonstrates the application of the virtual human body model Virthuman in various road traffic incidents including the pedestrian. Firstly, the Virthuman is described. Secondly, the model is used in the real accident reconstruction, sensitivity analysis of the gait posture during frontal car to pedestrian crash and simulation of such scenario, or development of new tram front-end design.

## 2. Methods

### 2.1. Virthuman

The Virthuman model is a hybrid model combining the two main modelling approaches, the deformable elements and rigid body segmentation within the multi-body (MBS) structure. The basic structure of the human is modelled using the multi-body and

consists of rigid segments connected via kinematic joints. The anatomical shape of the human is modelled using finite element surface segments connected via non-linear springs and dampers to the basic MBS structure. Virthuman model can be easily used as a pedestrian, driver or passenger of a car. The Virthuman model is also a fully scalable human model taking the gender, age, size and weight of the particular subject into the account [9]. The scaling algorithm implemented in the model is based on a large anthropometric database [10] measured in the Czechoslovakia in 1980's. The example of a size variable Virthuman model is demonstrated in Figure 2, where a small child, a big male and an average female are shown.

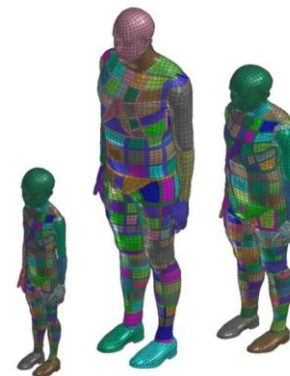


**Figure 2:** Scaled Virthuman model. 6-year-old child, 110 cm, 17 kg (left); 40-year-old male, 190 cm

The model was fully validated against a large set of validation tests and especially validated for the pedestrian impacts [11, 12]. The full-body tests as well as the detailed tests for the particular human body segments were performed to ensure the boofidelity of the Virthuman model. There is an automatic algorithm for evaluation of the specified criterion based on various mechanical quantities (e.g. contact force, acceleration, displacement, torques etc.), implemented in the model [13]. The list of the evaluated criterion is based on EuroNCAP rating and is available in [12], see Figure 3.



**Figure 3:** Example of injury risk evaluation within Virthuman model



### 3. Application example

The Virthuman model has a great benefit of the fast calculation time, a simple definition of any initial stature (position of the body), scaling algorithm (personalized subjects) and also the injury prediction. Thus, the model is very useful in the cases, where a large number of calculations is required or different postures and different occupants need to be analysed. It does not deal with the detailed injury of all tissues (hard or soft), since the model does not have any internal structures. However, it can still bring the knowledge of mechanical loading, which can be interpreted in the way of human injury. This paper presents several cases of Virthuman applications as a pedestrian.

### 3.1. Sensitivity analysis of the human gait posture on the injury

Sensitivity analysis of the frontal pedestrian-to-car collision is presented. The collision of the pedestrians with the vehicle can be divided into two phases: the primary contact (the human with the car) and the secondary contact (the human with the ground). Significant injuries can occur in both phases. The main focus of the research lays obviously on the primary contact [14, 15, 16, 17, 18, 19], since the ground contact depends on the material of the landing area, which is hardly to be improved. The research data from Yang [4] shows that a majority of the pedestrian accidents occurs while walking. In our previous work, [19], the authors were focused on the analysis of the human gait and its effect on the frontal crash with the vehicle [20]. The main effort was the analysis of the different gait postures and the walking speed of the pedestrian. The experimental measurement of the volunteer gait was used for identification of the particular body joints angles of rotation, see Figure 4.

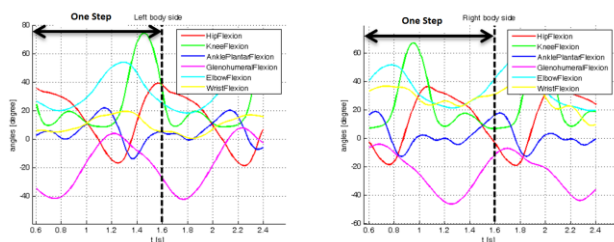


**Figure 4: Angles of rotation in the human joints, Spicka et al. (2017)**

The human gait was afterwards divided into 9 phases, see Figure 5.

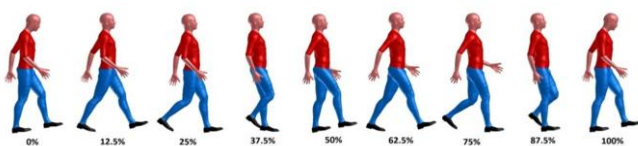


**Figure 5: Human gait phases**

Consequently, the pedestrian was also rotated around the vertical axes, to capture the effect of the different directions of impact, see Figure 7. Authors used simple multibody structure of the external car-bonnet shape ( $m = 1200$  kg,  $v_0 = 45$  km/h) with the validated virtual springs and dampers [11, 21], to preserve the calculation time as shortest as possible, see Figure 6 and Figure 7.

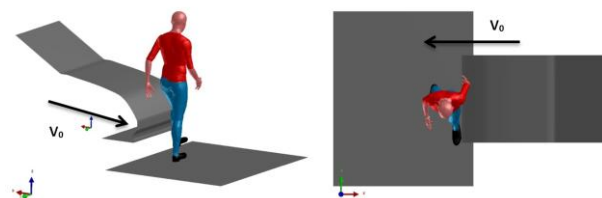


**Figure 6: Configuration of the testing collision**

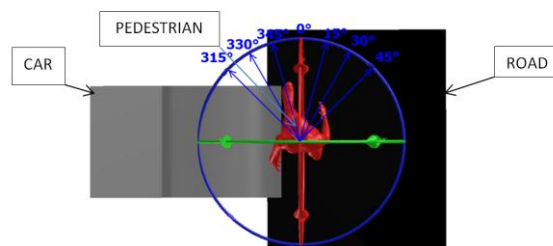


**Figure 7:** Initial posture of the pedestrian with respect to the car

Such analysis shows, how the initial posture of the pedestrian (especially position of the upper end lower extremities) can affect the overall kinematics and injury of the human.

### 3.2. Accident reconstruction

Next application example is a reconstruction of a real traffic collision between the car and the pedestrian. The specific pedestrian (defined by age, gender, size and mass) including her injury as well as the car (make and model, and the photo from the accident) were available. The accident protocol contains a description of the car damage and the injuries sustained by the pedestrian. The effort of the accident reconstruction was not only to meet the damage of the vehicle (shape and maximal bonnet intrusion), but also the pedestrian injury.

The goal was to find the initial position, that could result in such pedestrian injury and the car deformation and to test, if the available conditions could meet such results with the advantages of the numerical modelling. The defined accident involves the car Skoda Roomster 1.4 (the mass = 1205 kg, the dimensions 4.2 x 1.7 x 1.6 m and the initial velocity  $v_0 = 30$  km/h) hitting the pedestrian (female, 77 years old, mass = 70 kg, the height = 167 cm) from her left side. The injury sustained by the pedestrian is summarised as follows, together with Abbreviated Injury Score (AIS) [22], see Figure 8:



- Head contusion.
- Scapula fracture.
- Fracture of 3<sup>rd</sup> - 8<sup>th</sup> left ribs.
- Abrupton of the L1 vertebra.
- Left ankle fracture.
- Left subtalar joint fracture.
- Left knee contusion and abrasion.
- **Total injury severity score ISS = 14.**

**Figure 8: Pedestrian injury**

The image of the car was only on the frontal part, mainly the right corner of the bonnet. The deformation of the frontal part of the car, i.e. the bonnet and the bumper, as well as overall configuration of the accident are highlighted in Figure 9.



Figure 9: Deformed Skoda Roomster bonnet

The goal was the reconstruction of the real collision with respect to the given initial conditions, which requires not only the pedestrian dynamics and injuries, but also the car damage to be as close to the real collision as possible. The exact position of the pedestrian was not known. However, with the advantages of the numerical model of the car, with the proper definition of the reinforcement and the materials, the authors met the injury of the female as well as the damage of the car in the certain level of accuracy.

The calculated head injury criterion (HIC) results in value equalling to 235, which corresponds to AIS 1 - 2 (which is in agreement with the accident protocol). The maximal calculated bonnet deformation was 4 - 5 cm.

### 3.3. Tram design safe for pedestrian

Virhuman model finds its advantages also in the railway vehicles passive research. The main point of this research is to reduce the severity of the consequences of a collision between a tram and a pedestrian. The work of Špirk [23] has tended to a new tram safety system as a proposal from the pedestrian, passenger and driver points of view, and connected with the preparation of a new tram regulation [24]. Such regulation defines the shape of the front end of the tram, as well as the collision scenario (initial velocity of 20 km/h) to be tested. The position of the pedestrian with respect to the tram is also specified. For assessment of the tram geometry, it is necessary to investigate in the various shape of tram face by the numerical simulations. The tram face can be divided into the finite number of linear planes with the finite number of shapes [23]. Each flat surface has its own stiffness, damping and slope (inclination angles:  $B_{ws}$  and  $B_y$ ). Špirk in his work [25] used the definition of the segmented tram front face based on the regulation and brought a sensitivity analysis of the two main variables (the angles  $B_y$ ) on the HIC changes, see Figure 10 and Грешка! Источникът на препратката не е намерен..

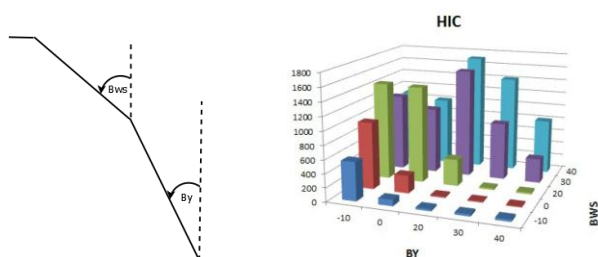


Figure 10: Profile view of the tram the angles (left) and bar plot of the two main variables of the tram shape onto HIC value (right)

During the tram design optimization, the authors were focused also on the influence of the lateral position of the pedestrian with respect to the tram, see Figure 11. The collision of the tram and pedestrian usually consists of scenario of pulling the pedestrian under the vehicle. Thus, the regulation defines the safety mechanism of the tram in the way, that the pedestrian cannot be pull under, moreover, it must be thrown latterly from the tram, not to be override after the landing.

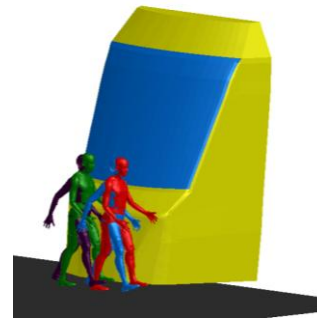


Figure 11: Pedestrian initial positions with respect to the tram

### 4. Discussion

The virtual human body model Virhuman presented in this paper shows its benefit in the road traffic field with the focused on the pedestrian. This work introduces the model in the several collision scenarios, occurring in the real world of traffic. It was shown, that the Virhuman model is a suitable and efficient tool in the modelling of the crashes between pedestrian and vehicle. The model was built based on hybrid approach, i.e. combination of finite element and multibody methods. Hence, it cannot provide detailed deformations and stress, of all the issues, as FEM can. However, with the advantage of injury prediction algorithm, it can result with the prediction of injury probability, which can be sufficient data in the numbers of applications. Moreover, with the benefit of the multibody structure, such model is easy to set-up in any initial position/posture of the human and thanks to the scaling algorithm, the variation of the population size, age and gender can be captured here.

### 5. Conclusion

This work introduced numerical model of the human called Virhuman as a useful tool for the pedestrian modelling. Such model takes advantages of the combine approach (MBS + FEM). Multibody method gives to the model benefit of scaling and positioning algorithm, while the deformable finite elements bring the local deformability to the model. The injury prediction algorithm is based EuroNCAP.

The previously described model Virhuman was used in the modelling of various road traffic scenarios consist of the pedestrian. Firstly, the model was used in the sensitivity analysis of the pedestrian gait on the collision (kinematics, dynamics and consequently the sustained injury). The second application of the Virhuman was the reconstruction of the real car to pedestrian accident, modelled based on the accident protocol only. The aim here was to use the provided data (pre-collision scenario, car make and model, the particular pedestrian, the car damage and the pedestrian injury) and numerically reconstruct the defined accident and to test, if the provided input data can meet the required output. The last example of the possible application of this model was the collision of the pedestrian with the tramway. The effort here is development of the tram front end, which could be safe for the human in case of accident.

However, the presented model is not limited only for the applications showed above. It can find the new purpose, not only in pedestrian and traffic industry. It has been successfully used also for small children modelling, which is generally taught task.

### 6. References

1. Besip, *Overview of the road accident in the EU* [online], Besip, Ministry of transportation, Available at: <http://www.ibesip.cz/cz/statistiky/statistiky-nehodovosti-v-evrope/prehled-vyvojedopravnich-nehod-v-eu>, (2016)
2. Policie ČR, *Overview of road accident in the Czech Republic in the 2014*, Directorate of Transport Police, Police Presidium



- of the Czech Republic, Praha, Available at: <http://www.policie.cz/clanek/statistika-nehodovosti-900835.aspx?Q=y2hudw09mw%3d%3d>, (2015)
3. P. Ramamurthy, M.V. Blundell, C. Bastien, Y. Zhang, *Computer simulation of real-world vehicle pedestrian impacts*, International Journal of Crashworthiness, **Vol. 16(4)**, pp: 351–363, (2011)
4. J. Yang, J. Yao, D. Otte, *Correlation of different impact conditions to the injury severity of pedestrians in real world accidents*, Proceedings of 19th International Technical Conf. Enhanced Safety of Vehicle, (2005)
5. WHO, World Health Organisation, *Global status report on road safety in 2015*, Available at [https://www.who.int/violence\\_injury\\_prevention/road\\_safety\\_status/2015/en/](https://www.who.int/violence_injury_prevention/road_safety_status/2015/en/), (2015)
6. TAČR TA04030689, *Development of active car bonnet with respect to the diversity of the human population and implementation of the biomechanical model of human body*. Intermediate report, (2015)
7. K. H. Yang, J. Hu, N. A. White, A. I. King, *Development of numerical models for injury Biomechanics research: A review of 50 years of publications in the Stapp Car Crash Conference*, No. 2006-22-0017. SAE Technical Paper, (2006)
8. S. Scataglini, P. Gunther, *DHM And Posturography*. Academic Press, (2019)
9. L. Hynčík, J. Špička, J., Mañas, J. Vychytil, *Stature Based Approach towards Vehicle Safety*, (No. 2015-26-0209), SAE Technical Paper, (2005)
10. P. Bláha, V. Šedivý, K. Čechovský, A. Kosová, *Anthropometric studies of the Czechoslovak Population from 6 to 55 years*, Czechoslovak spartakiade, **Vol. 1**, part 2, Praha, (1985)
11. J. Vychytil, J. Mañas H. Čechová, S. Špírk L. Hynčík, L. Kovář, *Scalable multi-purpose virtual Human model for future safety assessment*, (No. 2014-01-0534), SAE Technical Paper, (2014)
12. J. Vychytil, L. Hynčík, J. Mañas, P. Pavlata, R. Striegler, T., Moser, R. Valášek, R. *Prediction of Injury Risk in Pedestrian Accidents Using Virtual Human Model Virthuman: Real Case and Parametric Study*, (No. 2016-01-1511), SAE Technical Paper, (2016)
13. ESI, *Virthuman Postprocessing Manual, VPS Explicit MBS Model, Mecas ESI*, Rev, 2, (2015)
14. M. Hamacher, L. Eckstein, R. Paas, *Vehicle related influence of post-car impact pedestrian kinematics on secondary impact*, Proceedings of the International Research Council on the Biomechanics of Injury conference. **Vol. 40**. International Research Council on Biomechanics of Injury, (2012)
15. I. Han, R. M. Brach, *Throw model for frontal pedestrian collisions*, (No. 2001-01-0898), SAE Technical Paper, (2001)
16. C. K. Simms, D. P. Wood, *Effect of pre-impact pedestrian position and motion on kinematics and Injuries from vehicle and ground contact*, International Journal of Crashworthiness, Taylor & Francis, (2006)
17. Y. Suguru, T. Matsuhashi, Y. Matsuoka, *Simulation of car-pedestrian accident for evaluate car Structure*, Proceedings of the 26th Int. Tech. Conf. On the Enhanced Safety of Vehicles, Windsor (Canada), (1998)
18. D. P. Wood, C. K. Simms, D. G. Walsh, *Vehicle-pedestrian collisions: Validated models for Pedestrian impact and projection*, Proceedings of the Institution of Mechanical Engineers, Part D: Journal of Automobile Engineering, Vol 219(2), pp: 183-195, (2005)
19. J. Špička, J. Vychytil, J. Mañas, P. Pavlata, J. Motl *Modelling of Real Car-to-Pedestrian Accident: Comparison of Various Approaches in the Car Bonnet Modelling*, Proceedings of ECCOMAS Thematic Conference on Multibody Dynamics, Prague, (2017)
20. J. Špička, J. Vychytil, L. Hynčík, *Numerical analysis of a pedestrian to car collision: Effect of variations in walk*, Applied and Computational Mechanics, **Vol. 10(2)**, (2017),
21. J. R. Kerrigan, D. B. Murphy, D. C. Drinkwater, C. Y. Kam, D. Bose, J. R. Crandall, J. R. *Kinematic corridors for PMHS tested in full-scale pedestrian impact tests*, In Experimental Safety Vehicles Conference, (2005)
22. K-U. Schmitt, P. Niederer, F. Walz, *Trauma biomechanics: Introduction to accidental injury*, Springer Science & Business Media, (2004)
23. S. Špírk, *The collision of unbelted passenger with assessment of various vehicle interior*, Proceedings of Manufacturing Technology, (2017)
24. STRMTG, *Technical Agency for ropeway and Guided Transport System*, The technical guides, Tramway front end design, Version 01, (2016)
25. S. Špírk, J. Špička, *Tramway front end design safe for pedestrian*, Proceedings of Applied and Computational Mechanics, (2018)

## 7. Acknowledgement

The work was supported by the John H. and Amy Bowles Lawrence Foundation and the internal grant project SGS-2019-002.

# Simulation of the main components of a nuclear reactor under load, made of ultrafine-grained steel AISI-321 in the normal and irradiated state

Abdrakhman Naizabekov<sup>1</sup>, Evgeniy Panin<sup>2</sup>, Andrey Tolkushkin<sup>3</sup>, Daniyar Zhumagaliev<sup>1</sup>

<sup>1</sup> Rudny Industrial Institute, Rudny, Kazakhstan

<sup>2</sup> Karaganda Industrial University, Temirtau, Kazakhstan

<sup>3</sup> Ural Federal University, Yekaterinburg, Russia  
cooper802@mail.ru

**Abstract:** The creation and calculation of computer models of various products under load with the properties of UFG materials in the normal and irradiated state was performed. To model the UFG properties of non-irradiated AISI-321 steel, hardening curves were constructed based on the Hall-Petch equation for the base state of the material at a grain size of 1500 nm and for two UFG states (with grain sizes of 700 and 200 nm). To simulate the properties of irradiated AISI-321 steel, plastometric tests were performed using uniaxial compression of cylindrical samples at constant values of the strain rate of  $1 \text{ s}^{-1}$  and the temperature of  $20^\circ\text{C}$  on the "Gleeble 3800" plastometric unit. Fast neutron fluence with the following values was selected as a variable parameter:  $0.5 \cdot 10^{18} \text{ n/cm}^2$ ,  $1 \cdot 10^{18} \text{ n/cm}^2$ ,  $0.5 \cdot 10^{19} \text{ n/cm}^2$ ,  $1 \cdot 10^{19} \text{ n/cm}^2$ . The maximum operating pressure of 340 MPa was used as a static load. The simulation results showed that for both parts, the use of the material in the UFG state is the most appropriate solution.

**Keywords:** FEM, UFG STRUCTURE, IRRADIATION, STRESS

## 1. Introduction

The most important components of a nuclear reactor are the elements directly in contact with the nuclear fuel tablets: fuel assembly and fuel element.

The body of the fuel assembly is a metal structure (figure 1) containing fissionable substances and intended for generating thermal energy in a nuclear reactor by performing a controlled nuclear reaction. Usually it is a tetrahedral (PWR) or hexahedral (VVER) beam of fuel rods with a length of 2.5—3.5 m (which approximately corresponds to the height of the core) and a diameter of 30-40 cm, made of stainless steel or a zirconium alloy (to reduce neutron absorption) [1].



Figure 1 - Typical design of fuel assembly

The body of the fuel assembly has a total length of 3500 mm, there are three characteristic sections that differ not only in shape, but also in purpose. The head part is a body of rotation, the upper section of which has a conical shape, and the lower section has a cylindrical shape. It is designed for loading fuel elements, as well as fixing fuel assemblies in the overall design of the reactor. The wall thickness in this zone varies from 4 to 7 mm. The bottom part is also a cylindrical body of rotation. It is designed for loading fuel elements, as well as fixing fuel assemblies in the overall reactor structure by means of a threaded connection. The wall thickness in this zone is 4 mm. The longest central part with a length of more than 2500 mm has a hexagonal cross-section with a "turnkey" size of 96 mm and is intended for direct maintenance of fuel elements in the amount of 37 pieces. The wall thickness in this zone is 4 mm.

The geometry of the fuel element is a cylindrical body with a cavity into which uranium oxide tablets are loaded [1]. There are also three zones – head, central and bottom. But, unlike the hull, all these zones have a cylindrical shape. Wall thickness in all zones of the fuel elements is 0.45 mm.

## 2. Creation of models of UFG-materials

To create a model of AISI-321 steel in an ultrafine-grained state, it is necessary to put the values of mechanical characteristics corresponding to this state in the material database. The key parameter for this is the yield strength of the material, i.e. the mechanical characteristic of the material that characterizes the stress at which the deformations continue to grow without increasing the load. At room temperature, the yield strength is 270 MPa [2].

However, this value characterizes AISI-321 steel in the pre-deformation state, without any level of hardening. To determine the yield strength values for different grain size values, it is recommended to use the Hall-Petch ratio [3-4], which is the following relationship:

$$\sigma_Y = \sigma_0 + k d^{-1/2}, \quad (1)$$

where  $\sigma_Y$  – desired yield strength value, MPa;

$\sigma_0$  – stress impeding the dislocations movement, MPa;

$k$  – constant, depending on the properties of a particular material;

$d$  – grain size, microns.

In the course of experimental studies, a grain size range of 200–700 nm was obtained. Taking into account that when modeling properties, it is necessary to assume a uniform initial distribution of properties, we will set the limits of this range as the values used, i.e. we will create rheological models of AISI-321 steel with a grain size of 700 nm and 200 nm. For the initial grain size, we take the value of 1500 nm, corresponding to the yield strength of 270 MPa, according to equation (1). In [5], extensive studies of the Hall-Petch effect were carried out in relation to the two most used grades of austenitic stainless steels – AISI-316 and AISI-321. As a result, the following values were obtained:  $\sigma_0 = 150 \text{ MPa}$ ;  $k = 420$ . As a result, the following values of the yield strength were obtained:

–  $\sigma_Y = 652 \text{ MPa}$  (for a grain size of 700 nm);

–  $\sigma_Y = 1089 \text{ MPa}$  (for a grain size of 200 nm).

In addition, the second important characteristic required for creating a material rheology is the  $YS / TS$  parameter, i.e. the ratio of yield strength to tensile strength. This ratio is not characterized by a linear relationship, but constantly changes depending on the level of deformation and processing conditions of the material. This parameter characterizes the section of the hardening curve between the yield point and the point of failure of the sample. In [12],  $YS / TS$  values for AISI-321 steel are presented, as well as data on elongation, on the basis of which the corresponding strength limit values were obtained:

–  $\sigma_{TS} = 986 \text{ MPa}$  (for a grain size of 700 nm);

–  $\sigma_{TS} = 1194 \text{ MPa}$  (for a grain size of 200 nm).

–  $\delta = 38 \%$  (for a grain size of 700 nm);

–  $\delta = 22 \%$  (for a grain size of 200 nm).

After setting these values on the graph as points and processing with the spline function [6], the AISI-321 steel hardening curves were obtained (figure 2a).

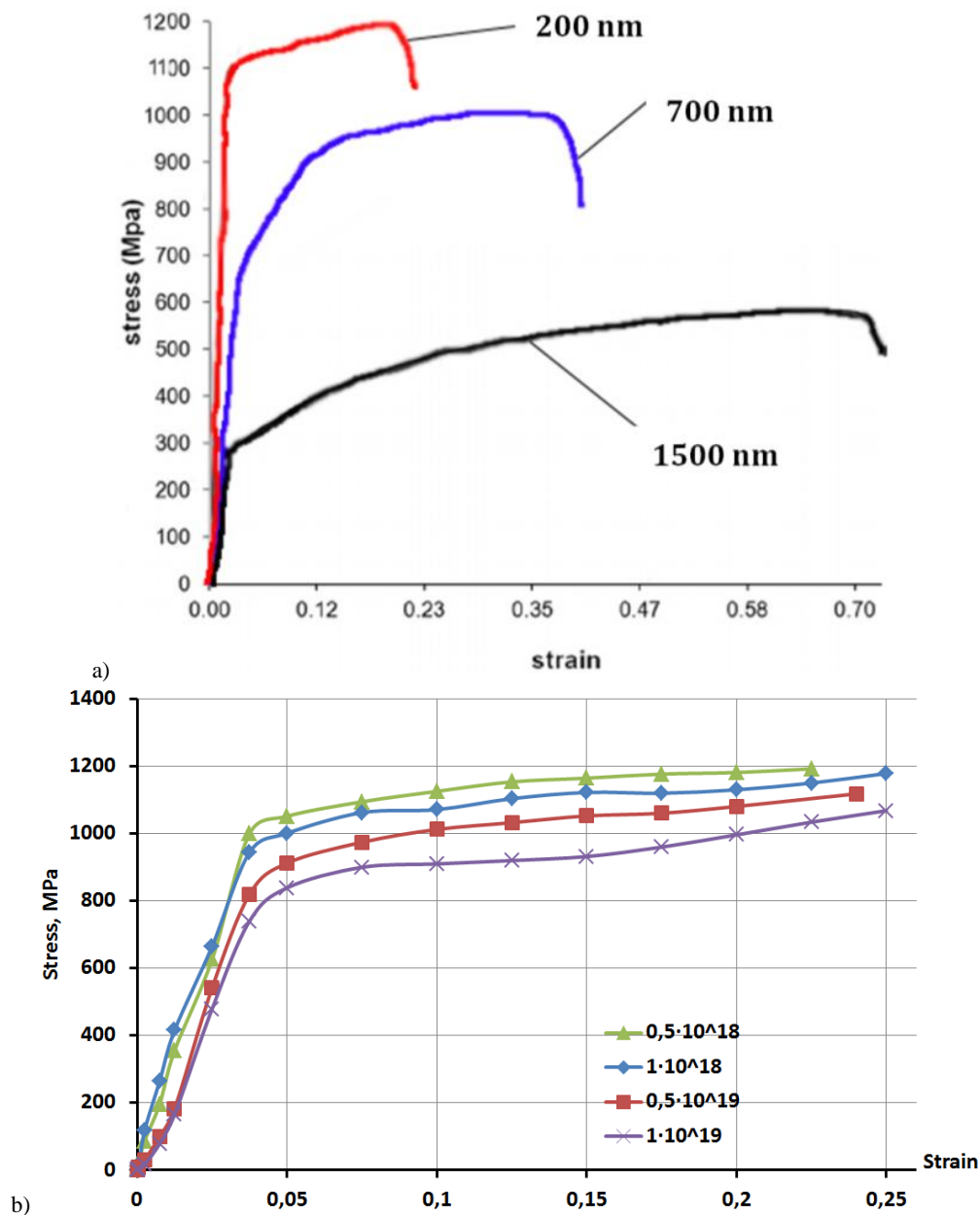


Figure 2 - AISI-321 steel hardening curves for the UFG state

When creating rheological models of irradiated material in the UFG state, the previously discussed method cannot be used. After irradiation, the metal structure is negatively affected by the fast neutron flux. As a result, a partial violation of the crystal lattice occurs at the micro level, which leads to a decrease in mechanical properties. Since it is impossible to predict the level of mechanical properties of such a material using the Hall-Petch equation due to the lack of uniformity of the structure after irradiation, the only possible way to obtain mechanical characteristics here is to conduct plastometric studies.

Plastometric tests were performed using uniaxial compression of cylindrical samples at constant values of the strain rate of  $1 \text{ s}^{-1}$  and a temperature of  $20^\circ\text{C}$ . As a variable parameter, the fast neutron fluence was chosen with the following values:  $0.5 \cdot 10^{18} \text{ n/cm}^2$ ,  $1 \cdot 10^{18} \text{ n/cm}^2$ ,  $0.5 \cdot 10^{19} \text{ n/cm}^2$ ,  $1 \cdot 10^{19} \text{ n/cm}^2$ . The tests were carried out under continuous loading on a Gleeble 3800 plastometric unit using Pocket Jaw module. Based on the test results, graphs of stress-strain flow curves were obtained (figure 2b). The results show that with an increase in the value of fast neutron fluence from  $0.5 \cdot 10^{18} \text{ n/cm}^2$  to  $1 \cdot 10^{19} \text{ n/cm}^2$ , the deformation resistance decreases by about ~20%, which allows us to conclude that the irradiation has a negligible effect on the properties of AISI-321 steel in UFG state. It should be noted that the deformation resistance of a sample with a

maximum radiation dose of  $1 \cdot 10^{19} \text{ n/cm}^2$  is higher than the properties of a homogeneous UFG material with a grain size of 700 nm. This fact allows us to conclude that, despite the known data on the significant negative impact of radiation on the structure of metals in the usual coarse-grained state, when using materials in the UFG state, the effect of radiation on the structure is significantly reduced.

### 3. Results and discussion

When determining the static load value, the value of 340 MPa was set as the maximum pressure in the core, according to the technical characteristics [1]. The main area of impact of the load on both parts is the central part, while the head and bottom parts serve as retainers. In accordance with this principle, the head and bottom parts were fixed in space on all three axes. After calculating the static load of the fuel Assembly housing, the following results were obtained (figure 3). When analyzing all three models of materials, a similar distribution of stress along the length of the central part of the body of the fuel assembly was noted. Despite the given uniform pressure distribution, the nature of the stress action along the length is uneven and shifted towards the head part.



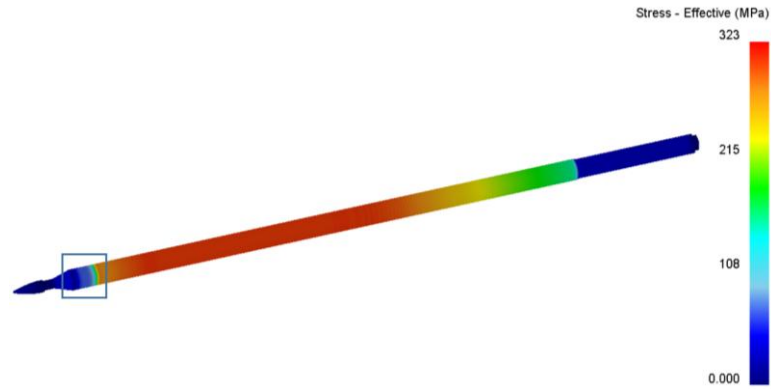


**Figure 3** - Results of calculating the static load of the fuel assembly with a grain size of 1500 nm

Also here, in the area of the junction of the head and central part (in figure 3 this zone is highlighted by a frame), the effect of residual stresses is traced. This phenomenon is a consequence of the design features of the fuel assembly - the head and bottom parts have different lengths, as a result of which different levels of elastic deformation occur in them under static load. The maximum stress value recorded in this model is 274 MPa. According to this value, you can determine the safety margin in the most loaded areas under the specified operating conditions:  $340 \text{ MPa} / 274 \text{ MPa} = 1.24$ .

For the other two models, the following results were obtained: stress in the model with a grain size of 700 nm – 238 MPa; stress in the model with a grain size of 200 nm – 186 MPa; safety margin in the model with a grain size of 700 nm  $\rightarrow 340 \text{ MPa} / 238 \text{ MPa} = 1.43$ ; safety margin in the model with a grain size of 200 nm  $\rightarrow 340 \text{ MPa} / 186 \text{ MPa} = 1.83$ . Thus, when using AISI-321 steel in the UFG state as the fuel assembly material, it is possible to increase the safety margin by 15–47%, depending on the resulting grain size.

After calculating the static load of the fuel element, the following results were obtained (figure 4).

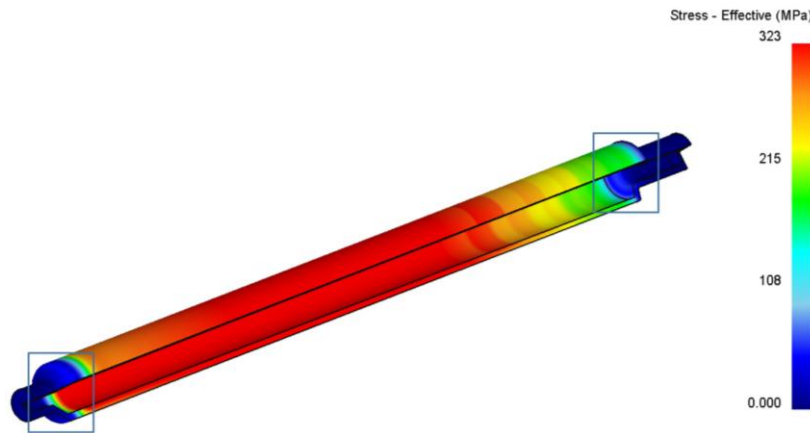


**Figure 4** - Results of calculating the static load of a fuel element with a grain size of 1500 nm

The nature of the stress distribution here is similar to the distribution on the fuel assembly – there is an uneven spread along the length of the central part, with a shift to the head part. However, in contrast to the previously discussed case, in this part, under static load, there are already two centers of action of residual stresses in the areas of the junction of the head and bottom parts with the central one (in figure 4, these zones are highlighted by frames). The presence of such zones at both ends of the central part is a consequence of the fact that the length of the head and bottom parts in the design of the fuel element is not so different as in the case of the fuel assembly.

The maximum values of stresses recorded in these models are as follows: the stress in the model with a grain size of 1500 nm – 313 MPa; the stress in the model with a grain size of 700 nm – 269 MPa; the stress in the model with a grain size of 200 nm – 224 MPa. According to these values, it is possible to determine the safety margin in the most loaded areas for all three materials under the specified operating conditions: the safety margin in the model with a grain size of 1500 nm  $\rightarrow 340 \text{ MPa} / 313 \text{ MPa} = 1.08$ ; the safety margin in the model with a grain size of 700 nm  $\rightarrow 340 \text{ MPa} / 269 \text{ MPa} = 1.26$ ; safety margin in a model with a grain size of 200 nm  $\rightarrow 340 \text{ MPa} / 224 \text{ MPa} = 1.51$ . Thus, when using AISI-321 steel in the UFG state as the material of the body of the fuel element, it is possible to increase the safety margin by 17–40%, depending on the resulting grain size. At the same time, it is necessary to note a decrease in the overall level of safety margin at a constant level of

static load. This phenomenon is directly related to the design features of both parts. In particular, this occurs due to the different wall thickness in the central part – if the wall thickness in the fuel assembly is 4 mm, then in the fuel element it is almost an order of magnitude less – 0.45 mm.

When modeling the behavior of the studied parts made of AISI-321 irradiated UFG steel under static load, the same criteria were used that would be accepted for modeling homogeneous materials. After calculating the static load of the fuel assembly, the following results were obtained:

Maximum stress values:

- in the model after irradiation at  $0.5 \cdot 10^{18} \text{ n/cm}^2$  – 192 MPa;
- in the model after irradiation at  $1 \cdot 10^{18} \text{ n/cm}^2$  – 198 MPa;
- in the model after irradiation at  $0.5 \cdot 10^{19} \text{ n/cm}^2$  – 209 MPa;
- in the model after irradiation at  $1 \cdot 10^{19} \text{ n/cm}^2$  – 227 MPa.

Safety margin for all four irradiated materials under specified operating conditions:

- in the model after irradiation at  $0.5 \cdot 10^{18} \text{ n/cm}^2 \rightarrow 340 \text{ MPa} / 192 \text{ MPa} = 1.77$ ;
- in the model after irradiation at  $1 \cdot 10^{18} \text{ n/cm}^2 \rightarrow 340 \text{ MPa} / 198 \text{ MPa} = 1.71$ ;
- in the model after irradiation at  $0.5 \cdot 10^{19} \text{ n/cm}^2 \rightarrow 340 \text{ MPa} / 209 \text{ MPa} = 1.62$ ;
- in the model after irradiation at  $1 \cdot 10^{19} \text{ n/cm}^2 \rightarrow 340 \text{ MPa} / 227 \text{ MPa} = 1.49$ .

After calculating the static load of the fuel element, the following results were obtained.

Maximum stress values:

- in the model after irradiation at  $0.5 \cdot 10^{18}$  n/cm<sup>2</sup> - 233 MPa;
- in the model after irradiation at  $1 \cdot 10^{18}$  n/cm<sup>2</sup> - 241 MPa;
- in the model after irradiation at  $0.5 \cdot 10^{19}$  n/cm<sup>2</sup> - 249 MPa;
- in the model after irradiation at  $1 \cdot 10^{19}$  n/cm<sup>2</sup> - 258 MPa.

Safety margin:

- in the model after irradiation at  $0.5 \cdot 10^{18}$  n/cm<sup>2</sup> → 340 MPa / 233 MPa = 1.46;

- in the model after irradiation at  $1 \cdot 10^{18}$  n/cm<sup>2</sup> → 340 MPa / 241 MPa = 1.42;

- in the model after irradiation at  $0.5 \cdot 10^{19}$  n/cm<sup>2</sup> → 340 MPa / 249 MPa = 1.37;

- in the model after irradiation at  $1 \cdot 10^{19}$  n/cm<sup>2</sup> → 340 MPa / 258 MPa = 1.31.

Figure 5 shows a summary diagram of the safety factor for the fuel assembly and fuel element when using conventional and irradiated variations of AISI-321 steel in UFG state.

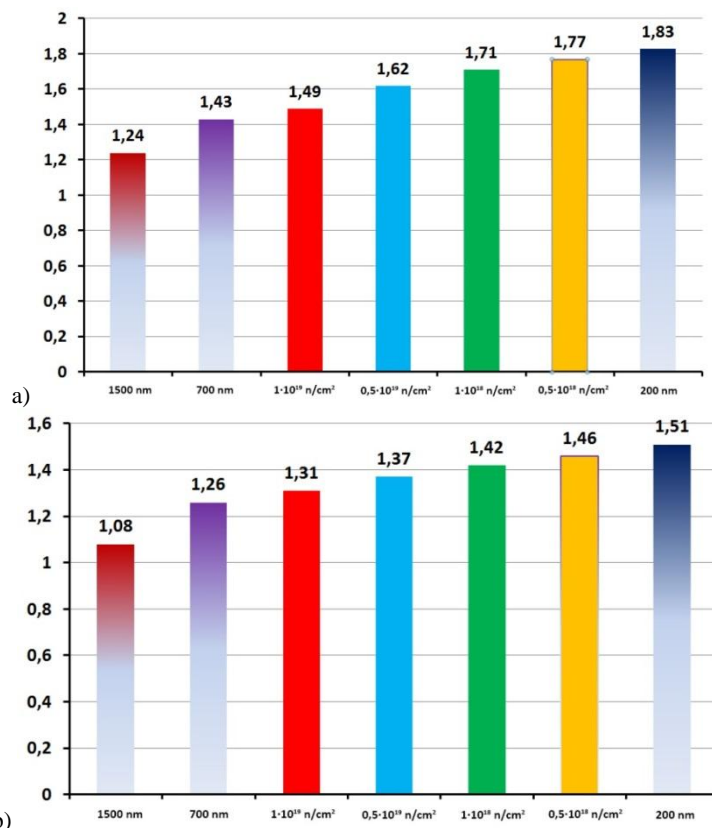


Figure 5 - Diagrams of the safety factor of the fuel assembly (a) and fuel element (b)

Thus, when using AISI-321 steel in the UFG irradiated state as the material both for fuel assembly and fuel element, the margin of safety increases with a decrease in the level of radiation dose. At the same time, it was noted that even at maximum irradiation, the margin of safety in both parts does not reach the lower limit of the UFG structure of 700 nm.

## Conclusions

The creation and calculation of computer models of various products under load with the properties of UFG materials in the normal and irradiated state was carried out. As the products under consideration, the fuel assembly and the fuel element were selected as the most suitable reactor parts in terms of size. To model the properties of UFG non-irradiated AISI-321 steel, the Hall-Petch equation was used to construct hardening curves for the base state of the material at a grain size of 1500 nm and for two UFG states (with grain sizes of 700 and 200 nm). To simulate the properties of UFG irradiated AISI-321 steel, plastometric tests were performed using uniaxial compression of cylindrical samples at constant values of the strain rate of  $1 \text{ s}^{-1}$  and a temperature of 20°C on the "Gleeble 3800" plastometric unit. As a variable parameter, the fast neutron fluence was chosen with the following values:  $0.5 \cdot 10^{18}$  n/cm<sup>2</sup>,  $1 \cdot 10^{18}$  n/cm<sup>2</sup>,  $0.5 \cdot 10^{19}$  n/cm<sup>2</sup>,  $1 \cdot 10^{19}$  n/cm<sup>2</sup>. The maximum operating pressure of 340 MPa was used as a static load. The simulation results showed that for both parts, the use of material in the UFG state is the most appropriate solution, since in this case the margin of safety even

at maximum irradiation in both parts does not reach the lower limit of the UFG structure.

## Acknowledgements

This work was carried out within the framework of the theme № AP05131382 "Development and research of technology for obtaining ultrafine materials with improved mechanical properties and increased radiation resistance for use as materials of the first wall of thermonuclear reactors and in nuclear power" under the grant funding program for scientific and (or) scientific and technical projects for 2018-2020 in the Republic of Kazakhstan.

## References

1. Шмелев В.Д., Драгунов Ю.Г., Денисов В.П., Васильченко И.Н. *Активные зоны ВВЭР для атомных электростанций* (Академкнига, 2004).
2. Shakhova I., Dudko V., Belyakov A., Tsuzaki K., Kaibyshev R. *Mater. Sci. Eng. A* **545** (2012) 176–186.
3. Petch N.J., *J. Iron Steel Inst.* **174** (1953) 25–28.
4. Hall E.O. *Proc. Phys. Soc. Lond. B.* **64** (1951) 747–753.
5. Astafurov S.V., Maier G.G., Melnikov E.V., Moskvina V.A., Panchenko M.Yu., Astafurova E.G. *Mater. Sci. Eng. A* **756** (2019) 365–372.
6. Craven P., Wahba G. *Numerische Mathematik* **31** (1979) 377–403.

# Injury prevention during childbirth: The model of obstetrician

Jan Vychytil<sup>1,\*</sup>, Linda Havelková<sup>1</sup>, Hana Čechová<sup>1</sup>, Tomáš Zítka<sup>1</sup>, Maximilian Melzner<sup>2</sup>  
 University of West Bohemia in Pilsen, Pilsen, Czech Republic<sup>1</sup>  
 Ostbayerische Technische Hochschule, Regensburg, Germany<sup>2</sup>  
 jvychyti@ntc.zcu.cz

**Abstract:** During childbirth, a technique called manual perineal protection (MPP) is often used to prevent injuries of relevant tissues. The obstetrician uses his (or her) hand to apply certain forces at the perineum in order to decrease its excessive loading during child delivery. Amount of applied forces as well as the correct posture of the obstetrician during the MPP technique are based so far on the experiences and approach of the obstetrician himself (or herself). In order to assess the role of obstetrician and in order to optimize the MPP technique, mathematical models may be of use. This work presents a combination of both experimental measurement and mathematical modeling. In the experimental part, a unique device is developed to measure forces applied by obstetrician during real child delivery. In the modeling part, the obstetrician is represented with an active musculoskeletal human body model in an AnyBody Modeling System software. Providing forces and muscle activities of the model may lead to the assessment and optimization of the MPP technique.

**Keywords:** VAGINAL DELIVERY, MANUAL PERINEAL PROTECTION, ANYBODY MODELING SYSTEM

## 1. Introduction

During a vaginal delivery, injuries of relevant tissues may occur such as ruptures of perineum, levator ani muscle and the obturator muscle [1]. In fact, only 9.6 % and 31.2 % of women deliver with an intact perineum at their first and second births respectively [2]. These injuries may have consequences in future in terms of female pelvic floor dysfunctions (perineal pain, anal incontinency, dyspareunia) [3].

In order to prevent injuries during childbirth, a technique called manual perineal protection (MPP) is often used [4]. The obstetrician uses his (or her) hand and fingers to apply certain forces at the perineum in order to decrease its excessive loading during child delivery. Amount of applied forces as well as the correct posture of the obstetrician during the MPP technique are based so far on the experiences and approach of the obstetrician himself (or herself). Still, proper execution of the MPP technique is a complex problem with lots of obstetrics variables [5].

In order to assess the role of obstetrician and in order to optimize the MPP technique, mathematical models may be of use. Here, we present a combination of both experimental measurement and mathematical modeling. At first, it is essential to determine forces applied by the obstetrician hand and fingers during the MPP technique. Although there are existing devices on the market (see e.g. [6]), these are not suitable for our application. Therefore, we develop our own experimental measurement system in a form of a glove for obstetrician. It records forces that are exerted by the obstetrician hand during a real delivery.

These data are used in the mathematical modeling of child delivery. The obstetrician is represented with a musculoskeletal model in the AnyBody Modeling System (AMS, Aalborg, Denmark, Version 7.2, AMMR 2.2.2) [7]. Here, human body is formed of rigid bones that are interconnected via joints based on real anatomy [8]. Muscles, tendons and ligaments are considered using models that enables active motion of the whole body model [9]. Kinematics of the AMS model is prescribed here using the data from the motion capture system during a delivery with physical model, see e.g. [10]. Finally, the results in terms of muscle activities of individual muscles are obtained.

## 2. Experimental measurement device

In the MPP technique used in this study, the obstetrician applies the force of his (or her) dominant hand at the perineum via thumb, index finger and the middle finger. The thumb and the middle finger press anterolaterally to the fourchette to reduce midline perineal strain. The flexed middle finger is used to apply pressure against the perineal body to facilitate the process of the fetal head extension. The non-dominant hand controls the speed of the fetal head expulsion and facilitates the fetal head extension [11].

To record these forces during this particular technique, we develop our own measurement glove. It must be 100% safe for child and the mother, it needs to measure forces acting at three defined points, it must be very simple to use and finally it must be durable for repeated use. The proposed prototype is depicted in Fig. 1.

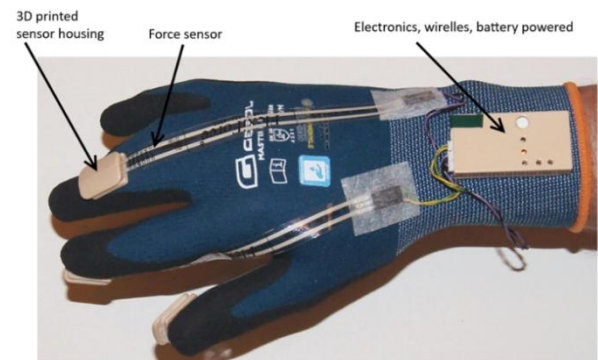


Fig. 1 Measurement glove with force sensors.

As force sensors, three force sensitive resistors Tekscan FlexiForce A201 are used. The device is powered with 3V coin battery and its rate is 100 samples per second. To achieve maximum safety, the glove is wireless and its electronics is isolated from obstetrician and touched surface. For each use, that is, for each child delivery, the glove is covered with new sterile surgical glove.

Experimental measurement includes real deliveries of 20 volunteers, see [11]. The forces are measured at the moment of the head expulsion. The example of measured data are depicted in Fig. 2. Here, evolution of forces in time for all the fingers are displayed for one particular volunteer.

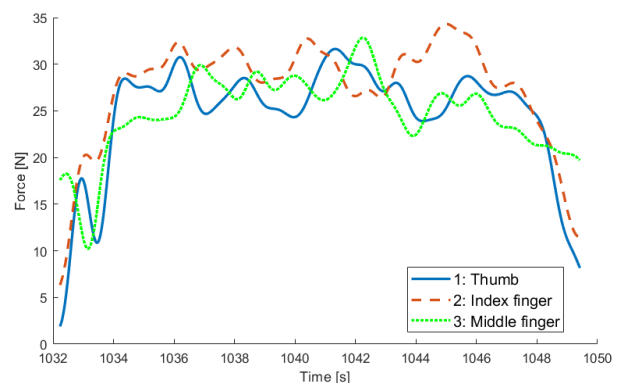


Fig. 2 Measured time-force dependencies of fingers during MPP. The curve no. 1 (blue) denotes thumb, no. 2 (dashed red) denotes index finger and no. 3 (green) the middle finger.



### 3. Obstetrician model

To represent the obstetrician, the AnyBody Modeling System is used. Here, human body is represented with rigid bones interconnected via joints. Active motion of the model is enabled by considering muscles, ligaments and tendons as type of simple models within AMS. Particular focus is given to the model of hand. In order to simulate the MPP technique properly, it is necessary to prepare the hand model in a great detail. Special attention is paid to the muscle attachment sites. Their proper definition allows us to determine exactly the positions and trajectories of individual muscles and hence to capture realistic moment arms and muscle activity during the MPP within the musculoskeletal model.

We use the MRI scans of real hand to obtain locations of muscle attachments. In AnyBody Modeling System individual muscles are replaced with user defined number of action lines or virtual muscle elements. These elements need to be placed within muscle volume in a way that respects anatomy of the muscle. Therefore, two tasks are to be solved in the mathematical modeling: placing required number of endpoints onto attachment surfaces and then pairing these endpoints in order to specify individual elements.

For the first task we use modified k-means algorithm. Given a finite set of points  $\omega \subset \mathbb{R}^N$ ,  $N \in \mathbb{N}$  and number  $k \in \mathbb{N}$ , original k-means method iteratively tries to approximate solution to k-partition problem. That is to partition set  $\omega$  into  $k$  classes  $\omega_1, \dots, \omega_k$  each corresponding with point  $c_i \in \mathbb{R}^N$ ,  $i = 1 \dots k$  called centroid, in such way that

$$\sum_{i=0}^k \sum_{x \in \omega_i} \|c_i - x\|^2$$

is minimal. In our setting, we use set of centres of gravity of the triangles in the mesh as a set  $\omega$ . We modify the basic k-means method to ensure that the partition does not depend on density of points of the mesh [12].

The second task (pairing of the endpoints) is based on Euclidean matching problem in two dimensions. It can be proven that the minimality of total pairing distance ensures that no two line segments connecting paired points intersect. The minimal pairing is obtained by Hungarian algorithm which finds minimal matching in weighted bipartite graph [12]. The resulting minimal matching with pairs connected by lines can be seen in Fig. 3.

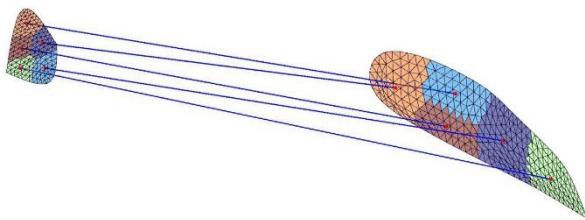


Fig. 3 *Opponens pollicis* connectivity with five muscle elements.

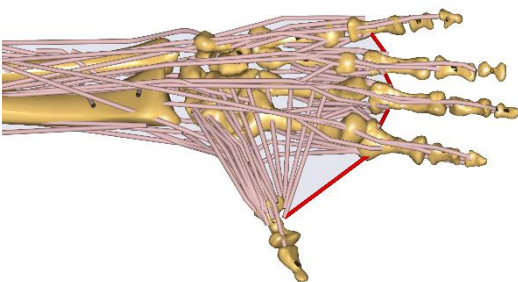


Fig. 4 Detailed hand model in AMS software.

The results from the k-means method are used to represent muscle attachment sites and muscle lines in the AMS model of the obstetrician hand. Individual muscles and tendons are represented with a type of simple muscle model [9] that includes contractile elements as well, see Fig. 4. Hence, both elasticity and muscle activity are included in the model. The geometry of the completed detailed hand model is depicted in Fig. 4. Finally, the hand model is embedded in the musculoskeletal model of whole human body within the AMS software to obtain the model representation of an obstetrician.

### 4. Simulation of the MPP and results

The AMS model of the obstetrician is employed for the simulation of the MPP technique. Here, the inverse dynamics method is used. It means that the motion of the obstetrician is prescribed and muscle activities and forces that correspond to that particular motion are calculated. To do that, an optimization algorithm is embedded in default in the AMS software. Typically, an objective function of a form

$$G = \sum_i \left( \frac{f_i}{N_i} \right)^p$$

is defined, where  $f_i$  is a force in an individual muscle,  $N_i$  is a normalization factor and  $p$  is a number ( $p = 3$  by default). The objective function thus represents a higher order sum of muscle activities. Minimization of this objective function for prescribed motion leads to the solution in terms of resulting muscle forces and activities.

In this particular application, the kinematics data of the obstetrician performing the MPP technique are obtained using the motion capture system XSens that uses the IMU sensors instead of markers. Employing this device, the obstetrician performs the MPP protection technique during the child delivery with the physical model, see Fig. 5. While the right hand is used for the MPP technique itself, the left hand is used to support the head of the child model.

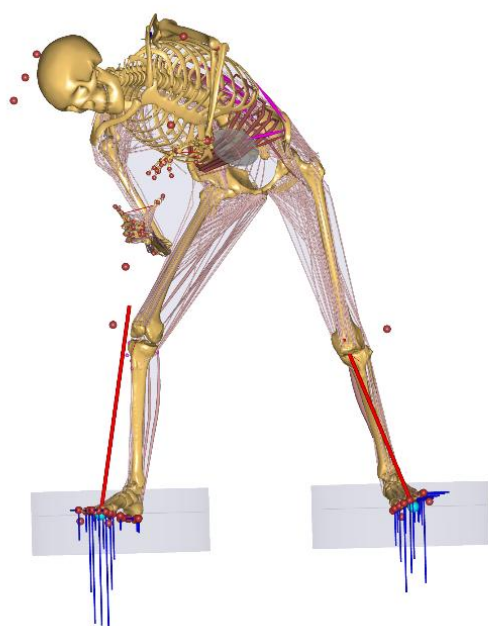


Fig. 5 Obstetrician performing MPP technique with physical model for kinematics data recording using XSens motion capture system.

Finally, all the experimental data gathered include forces exerted by hand of the obstetrician during a real delivery and the kinematics of the obstetrician during the MPP technique with the physical model. These are used as input data for the simulation of

MPP technique with musculoskeletal model of the obstetrician within the AMS software. The method of inverse dynamics is applied.

In fact, the MPP technique are simulated considering various postures of two obstetricians. The reason is to assess the MPP technique under varying conditions for its optimization. The example of the results is provided in Fig. 6. The musculoskeletal AMS model of the obstetrician performing the MPP technique in standing position is displayed. Colouring of individual muscles corresponds to the level of their activities calculated in the model. Namely, there is an increased muscle activity on the lower back due to the bent posture. This leads to increased joint reaction forces and hence it may cause increased problems within this body part.



**Fig. 6** Simulation of the MPP technique in the AMS software with the musculoskeletal model of the obstetrician. Coloured muscles correspond to their muscle activity.

## 5. Conclusion

The aim of this study is to present the abilities of mathematical modeling for improvements in medical field. Namely, the aim is to contribute to the knowledge regarding the manual perineal protection, i.e. the technique performed by obstetricians to prevent injuries of tissues during vaginal delivery.

The musculoskeletal model of hand is developed in great detail and embedded with the whole human body model in the AnyBody Modeling System software. To perform simulation of an obstetrician performing MPP technique, experimental data are necessary to gather as model input. Hence, unique measurement device is developed to record forces exerted by the hand of obstetrician during the delivery. Second, kinematics of the obstetrician is obtained during the delivery with physical model using the motion capture system.

The results of the mathematical modelling are obtained in terms of individual muscle activities and forces of the obstetrician. Hence, the MPP technique may be assessed and optimized from the perspective of the obstetrician and possible overloading of his or her body parts. In the example presented in this study, increased activity of the lower back muscles is obtained due to the bent postures. This indicates possible problems within this body part.

## 6. References

1. J. O. DeLancey, R. Kearney, *Obstet Gynecol.* 2003; 101: 46-53.
2. L.A. Smith, N. Price, V. Simonite, E.E. Burns, *BMC Pregnancy Childbirth*, 7 (2013).
3. J. Mant, R. Painter, M. Vessey, *Brit J Obstet Gynecol.* 1997; 104 (5):579-585.
4. K. Laine, F.E. Skjeldestad, L. Sandvik, Staff AC, *ISRN Obstet Gynecol* (2013).
5. H. Kleprikova, V. Kalis, M. Lucovnik, Z. Rusavy, M. Blaganje, R. Thakar, et al, *Acta Obstet Gynecol Scand*, 99, 4 (2020).
6. S. Rahayu, M. Firdaus, K. Husain, *AJBAS*, 19, 9 (2015).
7. M. E. Lund, S. Torholm, C. M. Dzialo, B. K. Jensen, *The AnyBody Managed Model Repository*, AMMR, Zenodo.
8. V. Bouskova, Diploma thesis, University of West Bohemia in Pilsen, 2018.
9. [https://anyscript.org/tutorials/Muscle\\_modeling/lesson5.html](https://anyscript.org/tutorials/Muscle_modeling/lesson5.html)
10. D. Roetenberg, H. Luinge, P. Slycke, *Xsens Motion Technol. BV Tech. Rep. 3* (2009).
11. V. Kalis, Z. Rusavy, L. Havelkova, T. Zitka, D. Tolar, K.M. Ismail, *BMC Pregnancy Childbirth*, 20 (2020).
12. T. Zítka, L. Havelková, R. Tupý, *Proceedings of Computational Mechanics 2018, Czech Republic* (2018).

## Acknowledgements

This work was supported by the project n. 182 "Obstetrics 2.0 – Virtual models for the prevention of injuries during childbirth" realised within the frame of the Program INTERREG V-A: Cross-border cooperation between the Czech Republic and the Federal State of Germany Bavaria, Aim European Cross-border cooperation 2014-2020. The realisation is supported by financial means of the European Regional Development Fund (85% of the costs) and the state budget of the Czech Republic (5%).

# Linear synthesis of frame eddy current probes with a planar excitation system

Trembovetska R., PhD Eng., Assoc. Prof. ; Halchenko V.Ya., Dr.Sc. Eng., Prof. ; Tychkov V., PhD Eng., Assoc. Prof. ;  
Bazilo C.V., Dr.Sc. Eng., Assoc. Prof.

Faculty of Electronic Technologies and Robotics – Cherkasy State Technological University, Ukraine

r.trembovetska@chdtu.edu.ua

**Abstract:** A mathematical method of linear surrogate parametric synthesis of frame surface non-coaxial eddy current probes with a uniform eddy current density distribution in the testing object's zone is proposed. The metamodel of a frame eddy current probe with a planar structure of the excitation system is constructed. Acceptable accuracy of the created metamodel is obtained by using the decomposition of the extremum search space and using associative neural networks. Examples of the synthesis of such excitation systems using modern metaheuristic stochastic algorithms for finding the global extremum are considered. The numerical results of the obtained solution and graphic illustrative material of the density distribution of the eddy currents on the surface in the testing object's zone are given.

**Keywords:** FRAME EDDY CURRENT PROBE, PLANAR STRUCTURE OF THE EXCITATION SYSTEM, EDDY CURRENTS DENSITY, UNIFORM SENSITIVITY, NEURAL NETWORKS

## 1. Introduction

Creation of favorable conditions for reliable detection of defects and determination of their geometrical parameters by means of eddy current testing is an urgent and at the same time complex problem. A wide range of scientists is engaged in research on the problem of creating a homogeneous and tangential field of probes excitation. The authors propose the creation of electromagnetic field (EMF) with a predetermined topology, which makes it possible to improve the selectivity and sensitivity of surface eddy current probes (SECP) [1-5]. The solutions usually proposed by them on the a priori given properties of the EMF are based on the creation of an uneven distribution of the excitation current in the generator coil of the SECP or on the use of a special geometry of the excitation winding. A detailed review of scientific and technical information on the use of EMF excitation with specified properties is given in [6]. Namely, a number of works, which reflect the results of studies where a uniform distribution of EMF on the surface of an immobile testing object (TO) is achieved by linear or nonlinear synthesis, is considered. Also in [6], ECP designs, in which a uniform excitation field is created by rectangular tangential and normal coils and due to the rotational excitation field, are analyzed.

As a result of the review, it was found that research on the creation of mobile ECPs, which provide uniform sensitivity in the testing zone, were not carried out according to the information available to the authors.

## 2. Background and the means for solving the problem

Linear and nonlinear synthesis of mobile circular SECP with a planar structure of the excitation system (ES) are described in a number of works by the authors [7-9]. In this case, options for the uniform and uneven placement of the coil sections along the radius, that located at the same height  $z_0$  above the TO, are considered. The response surface is described by the dependence of the eddy currents density (ECD) distribution on several parameters  $J = f(x, y, r)$ , namely, the spatial coordinates  $x, y$  of the testing zone on the TO surface and the radius  $r$  of the excitation coil sections. The sought parameters for the linear synthesis procedure are the MMF  $Iw$  of each coil, and for the nonlinear one they are the coil radii and MMF. For such structure of ES the value of the reduced error of the homogeneity of the ECD in the testing zone is obtained from 9 to 12%, which is a satisfactory result.

The authors have also carried out a number of studies of circular SECP [10]. The probes had a volumetric homogeneous ES structure both with a uniform arrangement of sections  $\Delta r = \text{const}$ ,  $\Delta z = \text{const}$ , and with an uneven one –  $\Delta r = \text{var}$ ,  $\Delta z = \text{var}$ , where  $\Delta$  is a parameter increment. To solve such a synthesis problem, a multiparametric ECP metamodel  $J = (x, y, r, z_0)$  was previously created, the construction features of which are considered in [10].

The obtained results of numerical experiments demonstrate the advantages of the synthesized volumetric ES structures in comparison with planar ones to ensure the requirements of uniformity.

At the same time, in addition to the considered ES structures with circular turns, there are also ESs in the form of rectangular frames with different positions relative to the TO, for example, parallel to the TO or perpendicular to it. Therefore, it is advisable to investigate a frame probe with a planar ES structure, consisting of a set of normal coils (see Fig. 1).

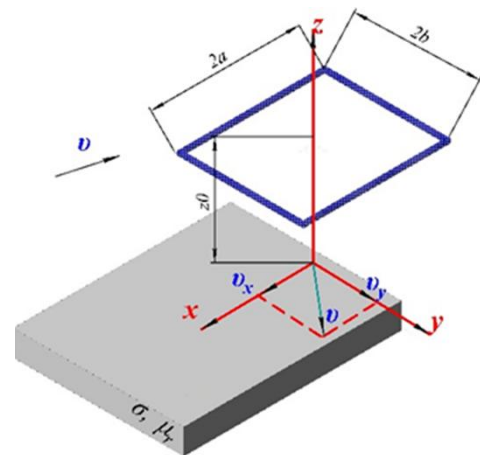


Fig. 1 The source of the exciting field in the form of a rectangular turn.

## 3. Solution of the problem

The purpose of the work is to create a method for linear surrogate synthesis of a frame non-coaxial ECP with a planar structure of the ES and uniform sensitivity in the testing zone. The method is provided by using a stochastic extremum search algorithm.

Before considering the SECP of a planar structure with a frame ES, let us first dwell on an EMF excitation source in the form of a single rectangular turn, which is a constituent element of such a structure. A rectangular turn with dimensions  $a \times b$  is supplied with alternating current  $I$  and frequency  $\omega$  and is located at a height  $z_0$  above the TO of thickness  $d$  with constant specific electrical conductivity  $\sigma$  and magnetic permeability  $\mu_r$  (see Fig. 1). The medium is considered linear, isotropic and homogeneous one. The velocity of the coil movement  $\vec{v} = (v_x, v_y, 0)$  relative to the TO is constant.

The interaction of the field source in the form of a single turn with the TO is determined by the ratios of the complex components of the magnetic induction along the spatial coordinates  $B_x, B_y, B_z$ . They are obtained as a result of solving Maxwell's differential



equations [11, 12] under the condition of continuity of tangential  $H_{1t} = H_{2t}$  and normal  $B_{1n} = B_{2n}$  components of the field at the interface between media 1 (air) and 2 (TO medium):

$$B_x = -j \frac{\mu_0 \cdot \mu_r \cdot I}{2 \cdot \pi^2} \cdot \int_{-\infty}^{\infty} \int_{-\infty}^{\infty} \frac{\sin(a \cdot \xi) \cdot \sin(b \cdot \eta)}{\eta \cdot (1 - e^{-2 \cdot \gamma \cdot d})} \times$$

$$\times \left[ \left( - (1 + \lambda_0) \cdot e^{-2 \cdot \gamma \cdot d} + \nu_0 \cdot e^{\left( \gamma \cdot \sqrt{\xi^2 + \eta^2} \right) \cdot d} \right) \cdot e^{\gamma \cdot z} + \right.$$

$$\left. + \left( 1 + \lambda_0 - \nu_0 \cdot e^{\left( \gamma \cdot \sqrt{\xi^2 + \eta^2} \right) \cdot d} \right) \cdot e^{-\gamma \cdot z} \right] \times$$

$$\times e^{-z \cdot 0 \cdot \sqrt{\xi^2 + \eta^2}} \cdot e^{-j(x \cdot \xi + y \cdot \eta)} d\xi d\eta \quad (1)$$

$$B_y = -j \frac{\mu_0 \cdot \mu_r \cdot I}{2 \cdot \pi^2} \cdot \int_{-\infty}^{\infty} \int_{-\infty}^{\infty} \frac{\sin(a \cdot \xi) \cdot \sin(b \cdot \eta)}{\xi \cdot (1 - e^{-2 \cdot \gamma \cdot d})} \times$$

$$\times \left[ \left( - (1 + \lambda_0) \cdot e^{-2 \cdot \gamma \cdot d} + \nu_0 \cdot e^{\left( \gamma \cdot \sqrt{\xi^2 + \eta^2} \right) \cdot d} \right) \cdot e^{\gamma \cdot z} + \right.$$

$$\left. + \left( 1 + \lambda_0 - \nu_0 \cdot e^{\left( \gamma \cdot \sqrt{\xi^2 + \eta^2} \right) \cdot d} \right) \cdot e^{-\gamma \cdot z} \right] \times$$

$$\times e^{-z \cdot 0 \cdot \sqrt{\xi^2 + \eta^2}} \cdot e^{-j(x \cdot \xi + y \cdot \eta)} d\xi d\eta \quad (2)$$

$$B_z = \frac{\mu_0 \cdot \mu_r \cdot I}{2 \cdot \pi^2} \cdot \int_{-\infty}^{\infty} \int_{-\infty}^{\infty} \frac{(\xi^2 + \eta^2) \cdot \sin(a \cdot \xi) \cdot \sin(b \cdot \eta)}{\xi \cdot \eta \cdot \gamma \cdot (1 - e^{-2 \cdot \gamma \cdot d})} \times$$

$$\times \left[ \left( - (1 + \lambda_0) \cdot e^{-2 \cdot \gamma \cdot d} + \nu_0 \cdot e^{\left( \gamma \cdot \sqrt{\xi^2 + \eta^2} \right) \cdot d} \right) \cdot e^{\gamma \cdot z} - \right.$$

$$\left. - \left( 1 + \lambda_0 - \nu_0 \cdot e^{\left( \gamma \cdot \sqrt{\xi^2 + \eta^2} \right) \cdot d} \right) \cdot e^{-\gamma \cdot z} \right] \times$$

$$\times e^{-z \cdot 0 \cdot \sqrt{\xi^2 + \eta^2}} \cdot e^{-j(x \cdot \xi + y \cdot \eta)} d\xi d\eta \quad (3)$$

where  $\gamma = \sqrt{\xi^2 + \eta^2 - j \times \sigma \times \mu_0 \times \mu_r \times (v_x \times \xi + v_y \times \eta) + j \times \omega \times \sigma \times \mu_0 \times \mu_r}$ ;

$$\lambda_0 = \frac{\left\{ \gamma^2 - \mu_r^2 \cdot (\xi^2 + \eta^2) \right\} \cdot (1 - e^{-2 \cdot \gamma \cdot d})}{\left( \gamma + \mu_r \cdot \sqrt{\xi^2 + \eta^2} \right)^2 - \left( \gamma - \mu_r \cdot \sqrt{\xi^2 + \eta^2} \right)^2 \cdot e^{-2 \cdot \gamma \cdot d}}$$

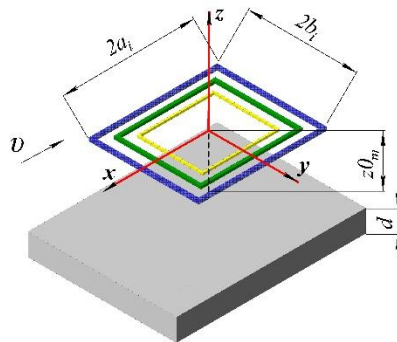


Fig. 3 Planar structure of ES of rectangular shape.

The synthesis problem of a rectangular coils system is formulated in an optimization formulation by minimizing a quadratic functional [7]. The analytical mathematical model for calculating the ECD distribution, which is created by a real system of coils, taking into account their transverse section, is cumbersome

$$\nu_0 = \frac{4 \times \mu_r \times \gamma \times \sqrt{\xi^2 + \eta^2} \times e^{\left( \sqrt{\xi^2 + \eta^2} - \gamma \right) \times d}}{\left( \gamma + \mu_r \times \sqrt{\xi^2 + \eta^2} \right)^2 - \left( \gamma - \mu_r \times \sqrt{\xi^2 + \eta^2} \right)^2 \times e^{-2 \times \gamma \times d}};$$

$\mu_0 = 4 \cdot \pi \cdot 10^{-7}$  H/m – the magnetic constant in vacuum;  $j = \sqrt{-1}$ ;  
 $\xi, \eta$  – variables of integration.

The mathematical model of the ECD distribution on the TO surface is determined through the partial derivatives of the magnetic induction components (1) - (3) with respect to spatial coordinates. Fig. 2 shows the ECD distribution obtained using a mathematical model for a single frame turn of 15 x 15 mm. The ECD distribution has a substantially non-linear characteristic in the testing area. It is possible to improve the distribution, namely to bring it closer to the desired uniform one (see Fig. 2), using a system of coils of various ES structures, as it is shown by the authors using the example of circular ECPs [7-10].

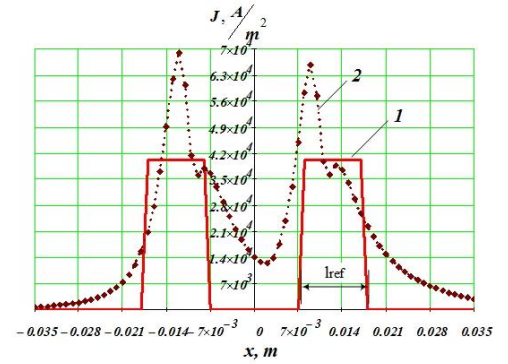


Fig. 2 ECD distribution on the TO surface: 1 - desirable; 2 - created by a single turn of rectangular shape.

The planar structure of the ES of a rectangular shape is a set of sectional coils connected in series with the dimensions of the sides  $a_i \times b_i$  and a rectangular section, the width and height of which for each coil is individual  $q_i \times \tau_i$  (see Fig. 3). The coils are switched on oppositely or matched "across the field" and are located at the same average height  $z_{0m}$  above the TO. In this case, each  $i$ -th from  $M$  excitation coils ( $i = 1, \dots, M$ ) is located in space uniformly  $\Delta a = \text{const}$ ,  $\Delta b = \text{const}$  (see Fig. 3).

computations. The main stages of the technology are described in [7, 8, 13].

According to the surrogate optimization algorithm, the first stage is the construction of an ECP metamodel based on a computer experiment design. Since the topology of the response hypersurface is complex, the computer experiment design for the multidimensional plan is based on a combination of Sobol's  $LP_{\tau}$ -sequences. These sequences have the best indicators of centered and cyclic divergence, namely sequences  $(\xi_6, \xi_7, \xi_{12})$  [14].

Among a wide class of methods for constructing metamodels [15], taking into account their advantages and disadvantages for the approximation of multidimensional response surfaces, a heuristic method based on artificial neural networks (NN) was chosen, namely RBF - neural networks with a nuclear Gaussian activation function. At the same time, as has been repeatedly demonstrated in a number of works [7-9], it is inappropriate to use a single RBF-neural network given the large error of the metamodel obtained in this way. Therefore, the study uses a hybrid approach with the simultaneous use of search area decomposition and associative techniques of NN [7, 15]. Thus, metamodels for each subdomain using additive NN regression were obtained [15, 16]. At the same time, to improve the accuracy, a bagging-procedure for forming subsamples was used. For the formation of the NN committee, the best networks were selected according to the indicators of the coefficient of determination  $R^2$ , the ratio of standard deviations  $S.D.ratio$ , mean absolute percentage error  $MAPE, \%$ . Then the output of each NN stage is formed by averaging over an ensemble of NNs with a performance of more than 90% [7, 9, 15].

In what follows, we restrict ourselves to considering the particular case of a rectangular frame, namely a square frame, when the average dimensions are equal to  $a_{mi} = b_{mi}$  and, respectively, the increment  $\Delta$  of the parameter is constant  $\Delta a = \Delta b = \text{const}$ . The metamodel, as a function of three parameters  $\hat{J} = f(x, y, a_m)$ , is constructed for the movable structure of the ES in the form of a complex of square-shaped ampere-turns. To construct a metamodel, the ranges of variation of the variables are as follows: spatial coordinates of the testing zone  $x = -35 \dots 35$  mm;  $y = 0 \dots 25$  mm; dimensions of ES coils  $a_m = 3 - 15$  mm. In this case, according to the size of the coil am, the search area is divided into six subregions  $I_a$  ( $3 \leq a < 5$  mm),  $II_a$  ( $5 \leq a < 7$  mm),  $III_a$  ( $7 \leq a < 9$  mm),  $IV_a$  ( $9 \leq a < 11$  mm),  $V_a$  ( $11 \leq a < 13$  mm),  $VI_a$  ( $13 \leq a \leq 15$  mm). All other parameters are constant and amounted to:  $d = 10$  mm,  $z_m = 3$  mm,  $\vec{v} = (40, 0, 0)$  m/s, frequency of the excitation current  $f = 1$  kHz, electrophysical parameters of the TO material, respectively,  $\sigma = 3.745 \cdot 10^7$  S/m and  $\mu_r = 1$ .

As a result, metamodels, for which the value of  $MAPE, \%$  for different subranges is from 7.38 % to 14.91 % when teaching NN and, respectively, from 7.97 % to 14.24 % when reproducing the response surface using NN, were obtained. The reproduction of the response surface was performed on the number of reproduction points  $N_{reproduction}$  that is larger than number of training points  $N_{training}$  using a formula describing the output of an RBF-neural network [10].

Next, the problem of linear optimal synthesis was solved. In the objective function formula, the obtained RBF-metamodel of ECP was used instead of the "exact" mathematical model.

At the same time, the desired ECD distribution, which must be obtained as a result of solving the problem, was set, namely, the U-shaped distribution of ECD with intensity  $J_{reference} = 40000$  A/m<sup>2</sup> in the testing zone ( $7 \leq x \leq 17$ ) mm (see Fig. 2 graph 2).

To solve nonlinear inverse problems, it is advisable to apply stochastic algorithms for finding the global extremum [17]. In this research, the solution using several algorithms is obtained. First of them is a hybrid algorithm based on the genetic one with local search using the Nelder-Mead simplex method. The second is a swarm of PSO-RND particles with a random link topology strategy. In addition, the next one is a population metaheuristic optimization algorithm by a swarm of particles with evolutionary formation of the swarm composition. It is a low-level hybridization of the genetic algorithm and the PSO algorithm. As a result of the solution of the nonlinear inverse problem, the MMF Iwi of each ES coil was determined, which together provide an approximation of the created ECD distribution to the specified on the TO surface in the testing zone.

#### 4. Results and discussion

For numerical simulation, the variants of ES structures with a different number of square coils  $M = 3 - 5$  were specified, the distance between which is uniform  $\Delta a = \text{const}$  (see Fig. 3). A preliminary analysis of the synthesis results allows one to select several ES structures. They have the best approximations to a uniform U-shaped ECD distribution, the width of which in the testing zone is  $l_{ref} = 10$  mm. The numerical results of solving the synthesis problem are presented in Table 3.

**Table 3:** Results of linear synthesis of the ES frame probe with different structures

№	Synthesized excitation systems					
	$M=3$		$M=4$			
	$a$ , mm	$Iw$ , A×turns	variant 1		variant 2	
	$a$ , mm	$Iw$ , A×turns	$a$ , mm	$Iw$ , A×turns	$a$ , mm	$Iw$ , A×turns
1	6.5	-0.656	4.5	-0.421	6.5	-0.898
2	10.5	1.5	7.5	0	9.16	1.24
3	14.5	0.75	10.5	1.01	11.82	0.503
4			14.5	0.364	14.48	0.343

In table 3 the sign "-" for MMF means the opposite connection of the coil.

For synthesized ESs, according to "exact" mathematical expressions (1) - (3), the results of the ECD distribution along the Ox axis were obtained, as shown in Fig. 4, 5 (graph 1). In these figures, graph 2 is a given desired ECD distribution in the testing zone. Also, for comparison, these graphs show the ECD distribution created by a single rectangular turn (graph 3).

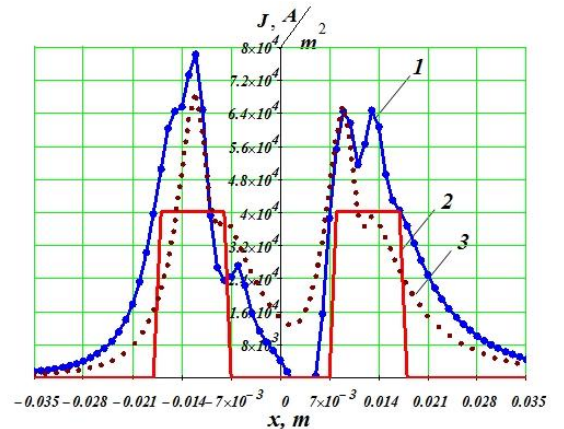


**Fig. 4** ECD distribution created by the ES structure of three coils.

For clarity, the results of numerical experiments obtained as a result of linear synthesis of SECP are shown in Fig. 6 by the lines of the ECD level.

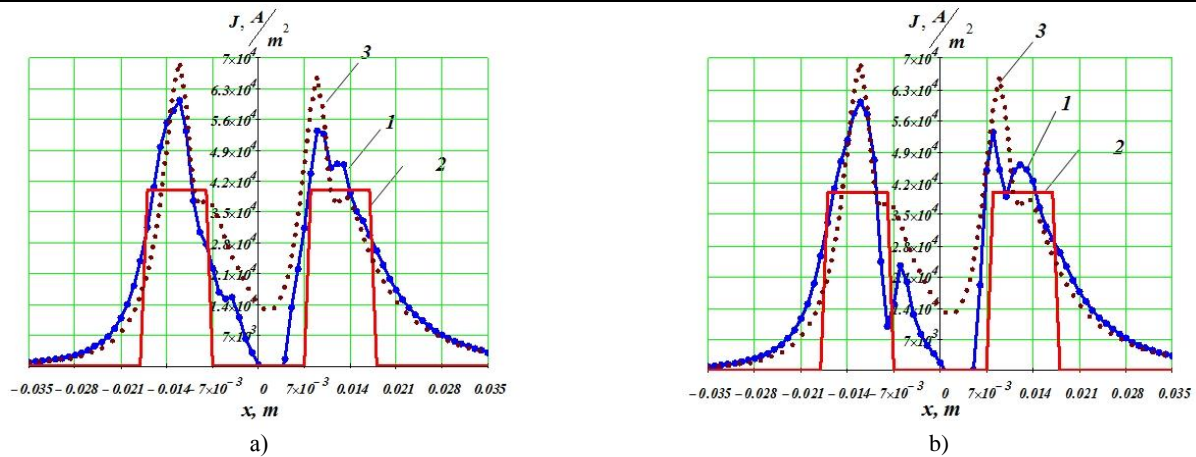


Fig. 5 ECD distribution, created by the ES structure of four coils: a) option 1; b) option 2.

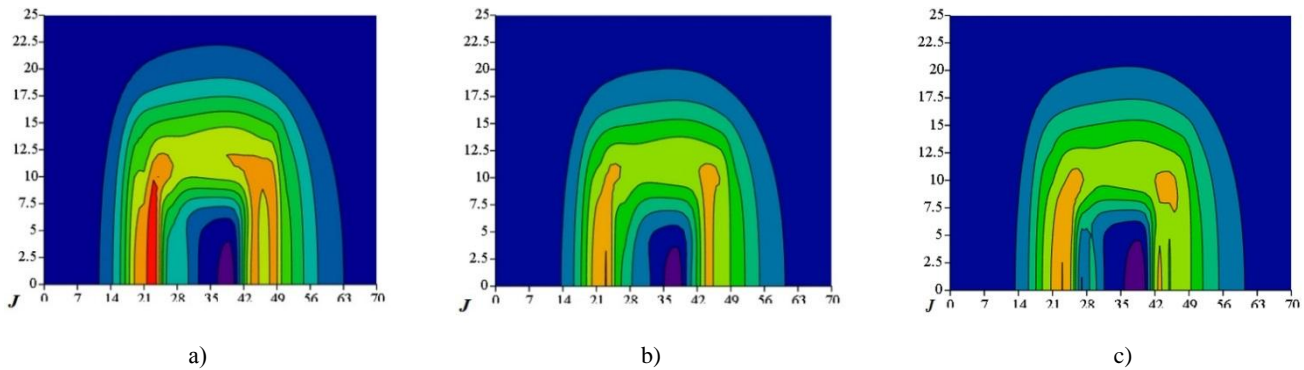


Fig. 6 ECD distribution in the form of level lines, obtained as a result of linear synthesis of ES structures: a) for three coils; b) for four coils, option 1; c) for four coils, option 2.

Comparative visual analysis of the width of the uniform ECD distribution of the obtained ES structures with a different number of coils shows almost the same result. However, the preference must be given to a structure that provides it with their smaller number, that is,  $M = 3$ .

If the synthesized ES structure is compared with a single rectangular turn in the sense of the uniform ECD distribution created by them, then, undoubtedly, the best results were obtained for the planar ES, which is illustrated by the graphs in Figs. 4, 5

Thus, in the research by numerical experiments, the efficiency of solving the problem of linear synthesis of a frame ECP with a planar structure of the ES is shown.

Analysis of the results of linear synthesis indicated that it makes sense to carry out additional studies using nonlinear synthesis in order to clarify the geometric dimensions of the sectional coils.

## 5. References

- [1] Rosado L.S., Gonzalez J.C., Santos T.G., Ramos P.M., Piedade M. Geometric optimization of a differential planar eddy currents probe for non-destructive testing. *Sensors and Actuators A: Physical*. - 2013. - V. 197. - P. 96-105. <https://doi.org/10.1016/j.sna.2013.04.010>
- [2] Su Z., Efremov A., Safdarnejad M., Tamburrino A., Udpa L., Udpa S. Optimization of coil design for near uniform interrogating field generation / *Z. AIP Conference Proceedings*. - 2015. - V. 1650. - P. 405-413. <https://doi.org/10.1063/1.4914636>
- [3] Su Z., Ye C., Tamburrino A., Udpa L., Udpa S. Optimization of coil design for eddy current testing of multi-layer structures. *International Journal of Applied Electromagnetics and Mechanics*. - 2016. - V. 52. - № 1-2. - P. 315-322. <https://doi.org/10.3233/JAE-162030>
- [4] Repelianto A.S., Kasai N., Sekino K., Matsunaga M. A Uniform Eddy Current Probe with a Double-Excitation Coil for Flaw Detection on Aluminium Plates. *Metals*. - 2019. - № 9. - Article № 1116. <https://doi.org/10.3390/met9101116>
- [5] Liu Z., Yao J., He C., Li Z., Liu X., Wu B. Development of a bidirectional-excitation eddy-current sensor with magnetic shielding: Detection of subsurface defects in stainless steel. *IEEE Sensors J.* - 2018. - V. 18. - № 15. - P. 6203-6216. <https://doi.org/10.1109/JSEN.2018.2844957>
- [6] Halchenko V.Ya., Trembovetskaya R.V., Tychkov V.V. Surface eddy current probes: excitation systems of the optimal electromagnetic field (review). *Devices and Methods of Measurements*. 2020. № 1 (11). P. 42-52. <https://doi.org/10.21122/2220-9506-2020-11-2-91-104>
- [7] Halchenko V.Ya., Trembovetska R.V., Tychkov V.V., Storchak A.V. Nonlinear surrogate synthesis of the surface circular eddy current probes. *Przeglad elektrotechniczny*. - 2019. - № 9. - P. 76-82. <https://doi.org/10.15199/48.2019.09.15>
- [8] Trembovetska R.V., Halchenko V.Ya., Tychkov V.V. Optimal surrogate parametric synthesis of surface circular non-axial eddy current probes with uniform sensitivity in the testing zone // *Bulletin of the Kherson National Technical University*. - 2019. - № 2(69). - Part 2. - P. 118-125. <https://mkmm.org.ua/upload/%D0%92%D1%96%D1%81%D0%BD%D0%B8%D0%BA%20%D0%A5%D0%9D%D0%A2%D0%A3%20%D1%87%D0%B0%D1%81%D1%82%D0%B8%D0%BD%D0%B0%202.pdf>
- [9] Halchenko V.Ya., Trembovetska R.V., Tychkov V.V. Linear synthesis of non-axial surface eddy current probes. *International Journal "NDT Days"*. - 2019. - Vol. 2. - Issue. 3. - P. 259-268. <https://www.ndt.net/article/NDTDays2019/papers/JNDTD-v2-n3-a03.pdf>
- [10] Trembovetska R.V., Halchenko V.Y., Tychkov V.V. Multiparameter hybrid neural network metamodel of eddy



- current probes with volumetric structure of excitation system. International Scientific Journal «Mathematical Modeling». 2019. № 4 (3) P. 113-116.  
<https://stumejournals.com/journals/mm/2019/4/113>
- [11] Itaya T., Ishida K., Kubota Y., Tanaka A., Takehira N. Visualization of Eddy Current Distributions for Arbitrarily Shaped Coils Parallel to a Moving Conductor Slab. Progress in Electromagnetics Research M. 2016. Vol. 47. Pp. 1-12.  
<https://doi.org/10.2528/PIERM16011204>
- [12] Trembovetska R.V., Halchenko V.Ya., Tychkov V.V. Studying the computational resource demands of mathematical models for moving surface eddy current probes for synthesis problems. Eastern-European Journal of Enterprise Technologies. – 2018. - № 5/5 (95). - P. 39-46.  
<https://doi.org/10.15587/1729-4061.2018.143309>
- [13] Halchenko V.Ya., Trembovetskaya R.V., Tychkov V.V. Development of excitation structure RBF-metamodels of moving concentric eddy current probe. Electrical Engineering & Electromechanics. - 2019. - No 1. - P. 28-38.  
<https://doi.org/10.20998/2074-272X.2019.2.05>
- [14] Halchenko V.Ya., Trembovetska R.V., Tychkov V.V., Storchak A.V. The Construction of Effective Multidimensional Computer Designs of Experiments Based on a Quasi-random Additive Recursive Rd-sequence. Applied Computer Systems. 2020. Vol. 25, No. 1. Pp. 70-76.  
<https://doi.org/10.2478/acss-2020-0009>
- [15] Halchenko V.Ya., Trembovetska R.V., Tychkov V.V., Storchak A.V. Methods for creating metamodels: state of the question. Bulletin of Vinnitsa Polytechnic Institute. - 2020. - No. 4 (151). - P. 74 - 88.  
<https://doi.org/10.31649/1997-9266-2020-151-4-74-88>
- [16] Géron A. Hands-On Machine Learning with Scikit-Learn, Keras and TensorFlow: Concepts, Tools, and Techniques to Build Intelligent Systems. 2nd Edition. O'Reilly Media, Inc. 2019. 856 p.  
ISBN-10: 1492032646.
- [17] Halchenko V.Ya., Yakimov A.N. Population Metaheuristic Optimization Algorithms by a Particles Swarm: A Study Guide. Cherkasy. Publ. by Tretyakov A.N., 2015.160 p.  
ISBN 978-617-7318-06-3.

# АВТОМАТИЗАЦИЯ ПРОГНОЗА ДИНАМИКИ КУРСА НАЦИОНАЛЬНОЙ ВАЛЮТЫ С ПОМОЩЬЮ ЛОГИСТИЧЕСКОЙ ФУНКЦИИ

## NATIONAL CURRENCY DYNAMICS FORECAST AUTOMATION USING LOGISTIC FUNCTION

Абдыраимова К.С.

Кыргызский Государственный Университет строительства, транспорта и архитектуры им. Н. Исанова,  
Кыргызстан  
e-mail: kairgul\_ac@mail.ru

**Аннотация:** Исследована динамика курса национальных валют России, Казахстана и Кыргызстана с 2012 по 2016 гг. В качестве математического метода аппроксимации переходного процесса курса валют из одного квазистационарного состояния в другое использована  $S$  - функция. Для автоматизации вычислительного процесса установлены границы итерационной сходимости при определении параметров кривой Перла-Рида.

**КЛЮЧЕВЫЕ СЛОВА:** МАТЕМАТИЧЕСКОЕ МОДЕЛИРОВАНИЕ, ПРОГНОЗИРОВАНИЕ, ВАЛЮТНЫЕ РИСКИ, ЛОГИСТИЧЕСКАЯ ФУНКЦИЯ, ЭКСПОНЕНЦИАЛЬНЫЙ РОСТ, ИНТЕРПОЛЯЦИЯ, АСИМПТОТИКА

**Abstract:** The dynamics of the exchange rate of national currencies of Russia, Kazakhstan and Kyrgyzstan from 2012 to 2016 is studied. As a mathematical method for approximating the transition process of the exchange rate from one quasi-stationary state to another, the  $S$  - function is used. To automate the computational process, iterative convergence limits are established when determining the parameters of the Pearl-Read curve.

**KEYWORDS:** MATHEMATICAL MODELING, FORECASTING, CURRENCY RISKS, LOGISTIC FUNCTION, EXPONENTIAL GROWTH, INTERPOLATION, ASYMPTOTICS

### 1. Введение

В современных рыночных условиях хозяйствования, особенно в нынешний кризисный период, Национальный валютный рынок характеризуется колебанием курсов валют, оказывающим негативное влияние на экономику страны. В качестве показателя неопределенности валютных сделок и неблагоприятных, непредсказуемых спекулятивных колебаний курсов валют выступают валютные риски. При этом, в экономике предприятий усиливается влияние рисков, т.е. увеличивается опасность непредвиденных потерь от управления экономическими ресурсами предприятия. Особенно велико влияние валютных рисков для предприятий, ведущих экономический обмен с другими странами. Валютные риски вносят дополнительную неопределенность планирования бюджета предприятий, обеспечения контроля и учета расхода денежных средств, а также увеличивают временные и трудовые ресурсы на обслуживание валютных сделок. Кроме того, на валютный климат страны сильно влияет поток денежных переводов трудовых мигрантов.

Необходимость решения проблемы управления валютными рисками в предприятиях республики стала особенно актуальна в последнее время в связи с увеличением количества, заключенных долгосрочных валютных сделок, с изменением структуры валютного рынка в СНГ, появлением новых финансовых инструментов управления валютными сделками. В настоящее время для принятия решения о заключении долгосрочной валютной сделки в отечественных предприятиях приходится использовать прогнозы динамики валютного рынка Кыргызстана, публикуемые аналитиками НБКР или другими независимыми экспертами. Однако, эти прогнозы не позволяют получить точного прогноза валютных рисков для долгосрочных валютных сделок и не учитывают сильное влияние слабо формализованных факторов: политических, психологических, ожидаемых и структурных. Такой подход к проблеме управления долгосрочными валютными сделками не позволяет избежать

банкротства или минимизировать расходы на обслуживание долгосрочных валютных сделок, выбрать наиболее благоприятные периоды расчета по сделке или своевременно применить финансовый инструмент для страхования сделки и фиксации её цены.

Валютному менеджеру, обслуживающему валютные сделки, при отсутствии математической прогнозирующей модели, трудно оперативно дать аналитическую оценку перспективности заключаемой сделки из-за отсутствия оптимального финансового инструмента страхования, реализующего количественную и качественную оценку вероятности валютного риска на базе долгосрочного прогноза валютного рынка.

Тем более, что в современных рыночных условиях оперативность выбора благоприятных условий валютной сделки является одним из ключевых моментов, позволяющих предприятию усилить свои экономические позиции на рынке.

Проблема управления валютными рисками также актуальна для предприятий, которые могут компенсировать потери по одним валютам за счет прибыли по другим. Однако, такая позиция предприятий не учитывает возможности изменения курса одной валюты по отношению ко всем другим валютам, взятым в совокупности.

Таким образом, для управления валютными рисками при заключении долгосрочных валютных сделок необходимо внедрить новые информационные технологии, которые обеспечили бы прогнозирование в реальном масштабе времени и позволили бы проводить оценку вероятности валютного риска. Следовательно, разработка нового подхода к управлению валютными рисками и их оценка на кратко- и среднесрочный период является актуальной научной и практической задачей, обеспечивающей достижение стабильного роста прибыли [1-4].

## 2. Цель работы

Цель работы заключается в разработке нового инструмента на основе метода логистической функции для математического моделирования и прогнозирования валютных рисков, позволяющего осуществить в реальном масштабе времени оценку с учетом экономического потенциала предприятия, и минимизация времени принятия решения.

## 3. Алгоритм определения вида логистической функции

Общий вид логистической функции (S – функция)

$$y = \frac{\alpha}{1 + \exp(\beta + \gamma \cdot x)} \quad (1)$$

S функция имеет три параметра:  $\alpha, \beta, \gamma$  [5-7]

Для определения  $\alpha, \beta, \gamma$  используем три эмпирические точки  $A(x_1, y_1), B(x_2, y_2), C(x_3, y_3)$

Распишем (1) для этих точек A,B,C

$$\begin{cases} y_1 = \frac{\alpha}{1 + \exp(\beta + \gamma \cdot x_1)} \\ y_2 = \frac{\alpha}{1 + \exp(\beta + \gamma \cdot x_2)} \\ y_3 = \frac{\alpha}{1 + \exp(\beta + \gamma \cdot x_3)} \end{cases} \quad (2)$$

Приведем (2) к виду

$$\begin{cases} \beta + \gamma \cdot x_1 = \ln\left(\frac{\alpha}{y_1} - 1\right) \\ \beta + \gamma \cdot x_2 = \ln\left(\frac{\alpha}{y_2} - 1\right) \\ \beta + \gamma \cdot x_3 = \ln\left(\frac{\alpha}{y_3} - 1\right) \end{cases} \quad (3)$$

Первое уравнение системы (3) напомним в виде

$$\beta = \ln\left(\frac{\alpha}{y_1} - 1\right) - \gamma \cdot x_1 \quad (4)$$

Исключив  $\beta$  во втором и третьем уравнении системы (3), получим

$$\begin{cases} \gamma = \frac{1}{(x_2 - x_1)} \ln\left(\frac{\frac{\alpha}{y_2} - 1}{\frac{\alpha}{y_1} - 1}\right) \\ \gamma = \frac{1}{(x_3 - x_1)} \ln\left(\frac{\frac{\alpha}{y_3} - 1}{\frac{\alpha}{y_1} - 1}\right) \end{cases} \quad (5)$$

Вычитая уравнения системы (5), исключим  $\gamma$

$$(x_3 - x_1) \cdot \ln\left(\frac{y_1(\alpha - y_2)}{y_2(\alpha - y_1)}\right) = (x_2 - x_1) \cdot \ln\left(\frac{y_1(\alpha - y_3)}{y_3(\alpha - y_1)}\right) \quad (6)$$

Преобразуем (6) к виду

$$\frac{y_1(\alpha - y_3)}{y_3(\alpha - y_1)} = \left[ \frac{y_1(\alpha - y_2)}{y_2(\alpha - y_1)} \right]^{\frac{x_3 - x_1}{x_2 - x_1}} \quad (7)$$

Откуда получим нелинейное соотношение для расчета  $\alpha$

$$\alpha = y_1 y_3 \left\{ \frac{[y_2(\alpha - y_1)]^{\frac{x_3 - x_1}{x_2 - x_1}} - [y_1(\alpha - y_2)]^{\frac{x_3 - x_1}{x_2 - x_1}}}{y_1[y_2(\alpha - y_1)]^{\frac{x_3 - x_1}{x_2 - x_1}} - y_3[y_1(\alpha - y_2)]^{\frac{x_3 - x_1}{x_2 - x_1}}} \right\} \quad (8)$$

Для использования итерационных методов при решении (8) требуется указать начальное приближение  $\alpha = \alpha_0$

Критерием сходимости выберем соотношение

$$\left| \frac{\alpha_{i+1} - \alpha_i}{\alpha_i} \right| < \varepsilon \quad (9)$$

где  $\varepsilon = 0.001$ .

Значение  $\beta$  находим из (4), а параметр  $\gamma$  вычислим из выражения

$$\gamma = \frac{1}{x_2 - x_1} \cdot \ln\left(\frac{\frac{\alpha}{y_2} - 1}{\frac{\alpha}{y_1} - 1}\right) \quad (10)$$

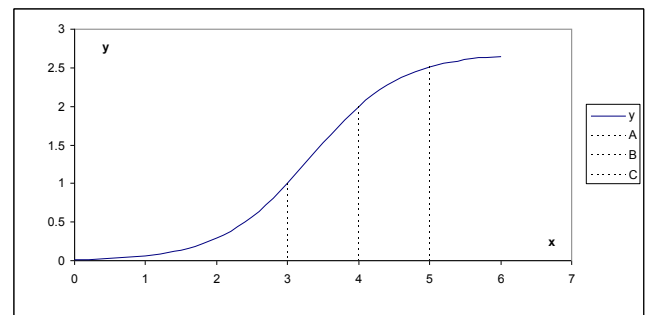


Рис.1. Схема кривой Перла-Рида

$A - x_1, y_1$ ;  $B - x_2, y_2$   $C - x_3, y_3$



Расчетная формула имеет вид

$$y = \frac{\alpha}{1 + \exp(\beta + \gamma \cdot x)} + \bar{y} \quad (11)$$

В (11) поправка  $\bar{y}$  указывает на уровень курса валюты в квазистационарном стадии [5-7].

#### 4. Анализ результатов

Обработаны и сопоставлены данные национальных валют России, Казахстана и Кыргызстана с 2012 г. по 2016 годы. Анализ динамики развития курса рубля и сома показывает наличие одной S – функции, а колебание курса тенге имеет два выраженных S – функций.



Рис. 2. Аппроксимация курса национальной валюты России  
 $\bar{y} = 31.29$ ;  $\alpha = 32.38$ ;  $\beta = -0.0216$ ;  $\gamma = 1048$

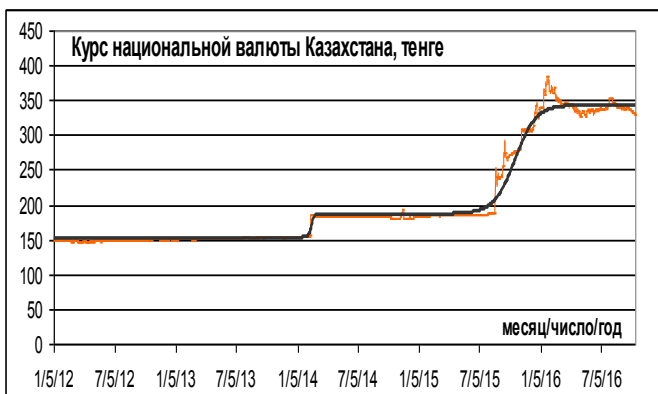


Рис. 3. Аппроксимация курса национальной валюты Казахстана

$$\bar{y}_1 = 153; \alpha_1 = 34; \beta_1 = -0.2435; \gamma_1 = 774$$

$$\bar{y}_2 = 187; \alpha_2 = 155.86; \beta_2 = -0.0317; \gamma_2 = 1385$$



Рис. 4. Аппроксимация курса национальной валюты Кыргызстана

$$\bar{y} = 46.85; \alpha = 22.13; \beta = -0.007; \gamma = 1048$$

#### 5. Заключение

Исследование специфики, условий и принципов управления валютными рисками в Кыргызстане и изучение состояния валютного рынка КР и анализ базы данных курса валют установило три характерных переходных процесса.

Экспоненциальный рост функции – слабое изменение курсов валют. Трудность определения  $\alpha, \beta, \gamma$  показателей S – функции состояла в неопределенности исходных данных из-за их малых возмущений. Решение нелинейного уравнения (10) имеет ограничение для задания разности эмпирических точек

$$\delta = \frac{(y_3 - y_2) / (x_3 - x_2)}{(y_2 - y_1) / (x_2 - x_1)}$$

На этом этапе рекомендуется метод, предложенный Ф.Фостером и А. Стюартом, который позволяет обнаружить тренд в стохастическом ряду.

Рост функции с выходом на плато квазистационарного режима. В этом режиме трудности с определением не возникали. Картина переходного процесса устойчива. Параметры кривой Перла-Рида определены из (4), (8), (10).

Интерполяция кривой с выходом на асимптотику. Трудности вычисления зависели от крутизны роста курса валют. При этом соотношение  $\delta$  не должен превышать  $\delta \leq 3$ .

#### 6. Литература

- 1.Акаев А.А. От Великой дивергенции к эпохе Великой конвергенции: Математическое моделирование и прогнозирование долгосрочного технологического и экономического развития мировой экономики. – М.: ЛЕНАНД, 2015г.
2. Акаев А.А., Акаева Б.А. Кыргызстан в эпоху цифровой экономики на новом шелковом пути. М.:2019г.
- 3.Мачуева Д.А. Модели и методика информационного управления социальными системами на основе мультиагентного подхода. Спец-ть: 05.13.10 «Управление в социальных и экономических системах» автореферат диссертации на соискание ученой степени к. т.н. Астрахань:2019г.
- 4.Кожухова В. Н. Разработка и исследование комплекса моделей логистической динамики социально-экономических показателей 08.00.13 – Математические и инструментальные методы экономики. 08.00.13 – Математические и инструментальные методы экономики Автореферат диссертации на соискание ученой степени к. э. н. Оренбург:2013г.
- 5.Четыркин Е.М. Статистические методы прогнозирования. М., «Статистика», 1975г.
- 6.Абдыраимова К.С. Анализ обменного курса национальной валюты Кыргызстана на основе S-образной модели. Вестник КГУСТА. 2017. № 2 (56). С. 185-189. URL: <https://elibrary.ru/item.asp?id=32294990>
- 7.Абдыраимова К.С., Укуев Б.Т. «Алгоритм нахождения аппроксимирующих параметров логистической функции для прогнозирования финансовой политики в строительном бизнесе». Вестник КГУСТА 1(63), 2019г., стр.35-40 UML: <https://elibrary.ru/item.asp?id=41132097>

# Stability of convective motion of a fluid with impurity

Устойчивость конвективного течения жидкости с примесью

Prof., Dr. Dementev O.<sup>1</sup>, PhD. Turlakova S.<sup>2</sup>

Chelyabinsk State University, Chelyabinsk, Russia<sup>1</sup>, South Ural National Research University, Chelyabinsk, Russia<sup>2</sup>  
e-mail: dement@csu.ru<sup>1</sup>, turlakovasu@susu.ru<sup>2</sup>

**Abstract:** The problem of convective stability in a medium containing settling heavy solid particles are discussed. A study is made of the stability of steady convective flow of a medium containing an additive between vertical plates heated to different temperatures. It is shown that the presence of settling solid particles has a significant stabilizing effect on convective stability.

**Keywords:** STEADY-STATE CONVECTIVE FLOW, STABILITY, LIQUID, HEAVY IMPURITY

1. The transporting medium and the additive were considered as interpenetrating and interacting continuous media; interaction between particles was neglected. A formulation of the problem of flow stability based on these concepts was first given in [1] where stability of motion in a plane vertical channel was considered for a fluid containing an additive. The stability of convective motion of a medium transporting a solid additive in a layer between vertical plates heated to different temperatures was studied in [5] where the settling of the particles was neglected, as was the case in [2-4].

Particle setting and the displacement force acting on the particles were neglected. The existence of thermal equilibrium between particles and gas was assumed, i.e., the simple limiting case of an infinitely short temperature relaxation time  $\tau_t$  was considered. Under the assumptions described, the effect of the particles present in a layer reduced to a mere renormalization of the heat capacity of the gas and so to a trivial renormalization of the Rayleigh number also. A study is made of the effect on convective of all factors characterizing the added particles: the rate of particle settling  $u_s$ , the velocity and temperature relaxation times for the particles (or, which comes to the same thing, their size, density, and heat capacity), and the mass concentration of the additive.

2. We consider a viscous incompressible fluid containing a cloud of spherical nondeformable solid particles of identical radius  $r$  and mass  $m$ . As in [1-6], we assume the liquid and impurity to be continuous media, interpenetrating and interacting with each other, and neglect interaction between the particles. The volume fraction of particles is assumed to be so low that the Einstein correction to liquid viscosity can be neglected. The density of the particle material  $\rho_p$  is much greater than the density of the carrier medium  $\rho$ . The left force acting on the particles is negligibly small, since it is proportional to the ratio  $\rho/\rho_p \ll 1$ . Interaction between the phases as they undergo relative motion follows the Stokes law. The equations describing the behaviour of an incompressible fluid with an impurity of heavy solid particles have the form [7, 8]. Based on those equations, equations were obtained [6] in the Boussinesq approximation for the free convection of an incompressible medium with a heavy additive:

$$\begin{aligned} \frac{\partial \vec{u}}{\partial t} + (\vec{u} \nabla) \vec{u} &= -\frac{\nabla p}{\rho} + \nu \Delta \vec{u} - \frac{a}{\tau_v} (\vec{u}_p - \vec{u}) + (1+a) \vec{g} \beta T, \\ \frac{\partial \vec{u}_p}{\partial t} + ((\vec{u}_p + \vec{u}_s) \nabla) \vec{u}_p &= \frac{1}{\tau_v} (\vec{u}_p - \vec{u}), \\ \frac{\partial T}{\partial t} + (\vec{u} \nabla) T &= \chi \Delta T + \frac{ab}{\tau_t} (T_p - T), \\ \frac{\partial T_p}{\partial t} + ((\vec{u}_p + \vec{u}_s) \nabla) T_p &= -\frac{1}{\tau_v} (T_p - T), \\ \text{div } \vec{u} &= 0, \quad \frac{\partial \rho_p}{\partial t} + \text{div}(\rho_p (\vec{u}_p + \vec{u}_s)) = 0, \end{aligned} \quad (1)$$

$$\rho_p = mN, \tau_v = \frac{m}{6\pi r \rho \nu}, \tau_t = \frac{mb}{4\pi r \rho \chi}, a = \frac{\rho_p}{\rho},$$

where  $\vec{u}$  is the liquid velocity;  $T$  is temperature;  $p$  is pressure of the fluid measured with respect to the hydrostatic pressure renormalized because of the settling particles;  $c$  is the heat capacity of the fluid at constant pressure;  $\beta$ ,  $\nu$  and  $\chi$  are the coefficient of volume expansion of the fluid, its kinematic viscosity, and thermal diffusivity; quantities with the subscript “ $p$ ” refer to the particle cloud, where  $\vec{u}_p$  is the velocity acquired by the particles as a result of their interaction with the moving fluid measured with respect to the rate of particle settling  $\vec{u}_s$ ;  $c_l$  is the heat capacity of the particle material;  $N$ , number of particles per unit volume; and  $\vec{g}$ , acceleration of gravity. The quantities  $\tau_t$  and  $\tau_v$  have the dimensionality of time and are, respectively, the time required for the temperature difference between fluid and particles to decrease by factor  $e$  and the time required for the velocity of the particles relative to the fluid to decrease by factor of  $e$  in comparison with its original value.

We consider isothermal motion of incompressible fluid containing an additive in a plane layer between infinite parallel vertical surfaces at  $x = \pm h$ , which are maintained at the constant temperature  $\Theta$ , respectively. The particles, the concentration of which is not uniform, move through the fluid.

We obtain a steady-state solution of the equation system (1) describing plane-parallel convective motion in such a structure,

$$\begin{aligned} u_x = u_y = 0, \quad u_z &= u_0(x), \quad T_0 = \text{const}, \quad p_0 = p_0(z), \\ u_{px} = u_{py} = 0, \quad u_{pz} &= u_{p0}(x), \quad T_{p0} = \text{const}, \end{aligned} \quad (2)$$

$$N(\alpha, x) = \frac{4ch\alpha \frac{\alpha x}{h} - ch \frac{2\alpha x}{h} - ch 2\alpha - 2}{4ch\alpha - ch 2\alpha - 3},$$

where  $\alpha$  is a coefficient defining the impurity concentration near the boundary of the layer. Equation (2) describes well the distribution of settling particles in a vertical channel observed experimentally in [8].

The settling particles, nonuniformly distributed across the channel, interact with the liquid and set it in motion. We find the steady-state distribution of liquid and particle velocities from Eq. (1) with the assumption that trajectories of both liquid and solid particles are straight lines parallel to the  $z$  axis, closing at infinity above and below:

$$\begin{aligned} \frac{1}{\rho} \frac{dp_0}{dz} &= \nu \frac{d^2 u_0}{dx^2} - \frac{a}{\tau_v} (u_{p0} - u_0) - g, \\ \frac{1}{\tau_v} (u_{p0} - u_0) &= g. \end{aligned} \quad (3)$$

Here is  $u_0$  and  $u_{p0}$  are the vertical velocity components and the subscript 0 indicates the steady-state solution of Eq. (1).

The boundary conditions and closed flow condition are expressed by

$$u(\pm 1) = 0, \quad \int_{-h}^h u_0 dx = 0. \quad (4)$$

Solving the problem of Eqs. (3), (4), we obtain the steady-state distributions of liquid and particle cloud velocities over the layer section

$$\begin{aligned} u_0 &= \frac{gh^2}{\nu} B_1 \left[ \frac{1}{\alpha^2} \left( 4ch \alpha \frac{ch \alpha x}{h} - \frac{1}{4} ch \frac{2\alpha x}{h} \right) + B_2 \frac{x^2}{h^2} - B_3 \right], \\ u_{p0} &= u_0 - g\tau_v, \quad \nabla p_0 = \text{const}, \\ B_1 &= \frac{m}{\rho(4ch \alpha - ch 2\alpha - 3)}, \\ B_2 &= \frac{3}{4\alpha^2} \left( \frac{15}{4\alpha} sh 2\alpha - \frac{7}{2} ch 2\alpha - 4 \right), \\ B_3 &= \frac{45}{16\alpha^3} sh 2\alpha - \frac{7}{8\alpha^2} ch 2\alpha - \frac{1}{\alpha^2}. \end{aligned} \quad (5)$$

As is evident from Eq. (5), under the action of the settling particles within the layer a liquid motion is established with two ascending and one descending flow, symmetric about the  $z$  axis. The intensity of the motion decreases with increase in  $\alpha$  (as  $\alpha \rightarrow \infty$ ,  $u_0 \rightarrow 0$ ).

We will study the stability of the steady-state liquid flow of Eq. (5), produced by settling of the nonuniformly distributed impurity particles. To do this we impose upon the steady-state velocity fields  $u_0$ ,  $u_{p0}$ , pressure  $p_0$ , and number of particles per unit volume  $N_0$ , the small perturbations  $u$ ,  $u_p$ ,  $p$ ,  $N$ .

We write the equations for the perturbations in dimensionless form, using the following units to dedimensionalize: for distance,  $h$ ; time,  $h^2/\nu$ ; velocity,  $\nu/h$ ; pressure  $\rho\nu^2/h^2$ . Linearizing with respect to the perturbations, we obtain from Eq. (1).

$$\begin{aligned} \frac{\partial \bar{u}}{\partial t} (\bar{u}_0 \nabla) \bar{u} + (\bar{u} \nabla) \bar{u}_0 &= \nabla p + \Delta \bar{u} - \frac{\bar{u}_0}{\tau_v} (\bar{u}_p - \bar{u}) + G a \bar{\gamma}, \\ \frac{\partial \bar{u}_p}{\partial t} + (\bar{u}_{p0} \nabla) \bar{u}_p + (\bar{u}_p \nabla) \bar{u}_{p0} &= \frac{1}{\tau_v} (\bar{u}_p - \bar{u}), \\ \frac{\partial N}{\partial t} + \text{div}(N_0 \bar{u}_0 + N \bar{u}_{p0}) &= 0; \\ \text{div } \bar{u} &= 0; \\ u_0 &= G B_1 \left[ \frac{1}{\alpha^2} \left( 4ch \alpha \frac{ch \alpha x}{h} - \frac{1}{4} ch \frac{2\alpha x}{h} \right) + B_2 x^2 - B_3 \right], \\ u_{p0} &= u_0 - u_s, \quad \bar{u}_s = -G \tau_v \bar{\gamma}, \\ \tau_v &= \frac{2}{9} r^2 \frac{\rho_1}{\rho}, \quad a = \frac{mN}{\rho}, \quad a_0 = \frac{mN_0}{\rho}, \quad G = \frac{gh^3}{\nu^2}, \\ N_0 &= \frac{4ch \alpha \frac{ch \alpha x}{h} - ch 2\alpha x - ch 2\alpha - 2}{4ch \alpha - ch 2\alpha - 3}, \end{aligned} \quad (6)$$

where  $u_s$  is the particle settling velocity;  $G$  is the Galileo number;  $\tau_v$  is the dimensionless relaxation time;  $\bar{\gamma}$  is a unit vector directed vertically upward.

For a liquid with impurity [6, 10], as for a pure liquid [9], it has been demonstrated at the problem of stability with respect to spatial perturbations reduces to the problem of stability with respect to planar perturbations. In the case under consideration planar perturbations are more dangerous, i.e., they correspond to lower Galileo numbers, so that in studying stability it is sufficient to limit ourselves to the study of planar normal perturbation:

$$\begin{aligned} \bar{u}_p(x, z, t) &= \bar{v}_p(x) \exp[ik(z - ct)], \\ N(x, z, t) &= n(x) \exp[ik(z - ct)], \\ \Psi(x, z, t) &= \varphi(x) \exp[ik(z - ct)], \\ u_x &= -\frac{\partial \Psi}{\partial z}, \quad u_z = \frac{\partial \Psi}{\partial x}. \end{aligned} \quad (8)$$

Here  $\Psi$  is the flow function;  $\varphi$ ,  $v_p$ ,  $n$  are the perturbation amplitudes;  $k$  is the real wave number;  $c = c_r + ic_i$  is the complex phase velocity of the perturbations ( $c_r$  is the phase velocity,  $c_i$  is the decrement).

$$\begin{aligned} &(\varphi^{IV} - 2k^2 \varphi'' + k^4 \varphi) + ik(\varphi'' - k^2 \varphi) \left( c - u_0 + \frac{a_0}{ik\tau_v} \right) + \\ &+ iku_0' \varphi = \frac{a_0}{\tau_v} (v_{pz}' - \varphi') + Gn', \\ v_{px} &= \frac{ik\varphi}{ik\tau_v(u_{p0} - c) - 1}, \\ v_{pz} &= \frac{-\varphi' + u_{p0}' \tau_v v_{px}}{ik\tau_v(u_{p0} - c) - 1}, \\ n &= \frac{ikv_{pz} N_0 + N_0' v_{px} + N_0 v_{px}}{ik(u_{p0} - c)} \end{aligned} \quad (9)$$

with boundary conditions

$$\varphi(\pm 1) = \varphi'(\pm 1) = 0. \quad (10)$$

The stability boundary for flow of the liquid with impurity Eq. (7) is determined by the condition  $c_i = 0$ . The complex phase velocity  $c$  depends on the problem parameters  $G$ ,  $k$ ,  $a$ ,  $\tau_v$ . To solve the boundary problem Eqs. (9) and (10), i.e., to determine the stability limits of the flow under consideration and calculate the decrement spectrum, we use the Runge - Kutta method of step-by-step integration.

Calculations performed for a wide range of values of the parameter  $\alpha$  ( $0.5 \leq \alpha \leq 70$ ) show that instability of steady-state motion of the liquid with heavy particles is caused by the interaction of oppositely directed flows: the descending central flow and two ascending flows near the walls. Instability in the motion is produced by lower modes of hydrodynamic perturbations, while the decrements of normal perturbations prove to be complex (traveling perturbations).

The settling particles generate oscillatory (traveling) perturbations and encourage their transport. With decrease in the parameter  $\alpha$  the stability of the flow induced by particle settling decreases. In fact, at low  $\alpha$  the particle distribution in the layer has a sharply expressed "tonguelike" character and the flow intensity is high; decrease in  $\alpha$  leads to an increase in flow velocity and disruption of stability. This conclusion is confirmed by calculations of neutral stability curves ( $c_i = 0$ ,  $\tau_v = 0.009$ ,  $\alpha_1 = 20$ ,  $\alpha_2 = 30$ ,  $\alpha_3 = 40$ ,  $\alpha_4 = 45$ ,  $\alpha_5 = 50$ ,  $\alpha_6 = 65$ ). The character of the heavy particle distribution across the layer affects the stability of the flow induced by the impurity intensely.

3. We consider convective motion of a fluid containing an additive in a plane layer between infinite parallel vertical surfaces, which are constant temperatures  $-\Theta$  and  $\Theta$ , respectively. The particles, the concentration of which is nonuniform, move through the fluid. We obtain a steady-state solution of the equation, describing plane-parallel convective motion and we used boundary conditions  $u_0(\pm h) = 0$ ,  $T_0(-h) = \Theta$ ,  $T_0(h) = -\Theta$  and the closure condition for convective flow. We obtain the distribution of velocities and temperatures of the fluid and particle cloud over a section layer:



$$\begin{aligned}
 U_0 = Gr \left\{ \frac{x^3}{6} + \frac{m}{\rho_0(4ch\alpha - ch2\alpha - 3)} \left( \frac{4ch\alpha}{\alpha^2} (xch(\alpha x) - \frac{2sh(\alpha x)}{\alpha}) - \frac{1}{4\alpha^2} (xch(2\alpha x) - \frac{2sh(2\alpha x)}{\alpha}) - \frac{ch2\alpha + 2}{6} x^3 \right) + C_1 x \right\} + u_0, \\
 U_{p0} = U_0 + u_s, T_0 = T_{p0} = -x,
 \end{aligned} \quad (11)$$

$$\begin{aligned}
 C_1 = -\frac{1}{6} - \frac{m}{\rho_0(4ch\alpha - ch2\alpha - 3)} \left( \frac{8ch\alpha}{\alpha^2} (ch\alpha - \frac{2sh2\alpha}{\alpha}) - \frac{1}{2\alpha^2} (ch2\alpha - \frac{sh2\alpha}{\alpha}) - \frac{ch2\alpha + 2}{3} \right); \\
 \tau_t = \frac{3Pr\tau_v b}{2}, b = \frac{C_1}{C}, Pr = \frac{\nu}{\chi}, Gr = g \frac{g\beta\Theta h^3}{\nu^2}.
 \end{aligned}$$

We write the equations in dimensionless form, using the following units of measurement: distance  $h$ , time  $h^2/\nu$ , velocity  $\nu/h$ , pressure  $\rho\nu^2/h^2$ , and temperature  $\Theta$ .

4. The stability of convective motion. We investigate the stability of the steady-state motion of a medium containing a heavy additive as defined by Eqs. (11). To do this, we consider the perturbed fields for velocity, temperature, pressure and number of particles per unit volume.

As in the case of a pure fluid [9], one can show for a medium containing an additive that the problem of stability with respect to spatial perturbations reduces to the corresponding problem for plane perturbations. Plane perturbations are more dangerous in the case of vertical orientation of the layer, i.e., lower Grashof numbers  $Gr$  are associated with them. Consequently, it is sufficient to continue the investigation to plane perturbations in a study of stability.

We consider plane normal perturbations

$$\begin{aligned}
 N(x, z, t) &= n(x) \exp[ik(z - ct)], \\
 \Psi(x, z, t) &= \varphi(x) \exp[ik(z - ct)], \\
 u_{px}(x, z, t) &= v_{px}(x) \exp[ik(z - ct)], \\
 u_{pz}(x, z, t) &= v_{pz}(x) \exp[ik(z - ct)], \\
 T(x, z, t) &= \theta(x) \exp[ik(z - ct)], \\
 u_x &= -\frac{\partial \Psi}{\partial z}, u_z = \frac{\partial \Psi}{\partial x}.
 \end{aligned} \quad (13)$$

Where  $\psi$  is a stream function;  $\varphi$ ,  $\theta$ ,  $n$  are the amplitudes of the perturbations. We obtain a system of amplitude equations (primes denote differentiation with respect to  $x$ )

$$\begin{aligned}
 (\varphi^{IV} - 2k^2\varphi'' + k^4\varphi) + ik(\varphi'' - k^2\varphi) \cdot \\
 \left( c - u_0 + \frac{a_0}{ik\tau_v} \left( \frac{1}{A} - 1 \right) \right) + \frac{a_0'\varphi'}{\tau_v} \left( \frac{1}{A} - 1 \right) + \\
 + \varphi(iku_0'' + \frac{ik}{A^2} (a_0u_{p0}'' + a_0'u_{p0}') + \\
 \frac{2a_0k^2\tau_v u_{p0}'}{A^3}) + (1 + a_0)Gr \cdot \vartheta' + a' = \\
 = GrT + aGrT' + a_0'Gr\vartheta = 0,
 \end{aligned} \quad (14)$$

$$\begin{aligned}
 \frac{1}{Pr} (\vartheta'' - k^2\vartheta) + \vartheta \left( \frac{a_0b}{\tau_t} \left( \frac{1}{B} - 1 \right) + ik(c - u_0) \right) + \\
 ik\varphi T' \left( \frac{a_0b}{AB} + 1 \right) = 0,
 \end{aligned}$$

$$A = ik\tau_v(u_{p0} - c); B = ik\tau_t(u_{p0} - c) + 1;$$

$$n = \frac{\tau_v}{A - 1} \left( \frac{2N_0k^2\tau_v u_{p0}'\varphi}{A^2} + \frac{N_0'ik\varphi}{A} \right).$$

Boundary conditions are

$$\varphi(\pm 1) = \varphi'(\pm 1) = 0 \quad (15)$$

The boundary-value problem (14) - (15) determines the spectrum of characteristic perturbations and their decrements. The complex phase velocity  $c$  depends on seven independent parameters of the problem:  $Ga, Pr, Ga, k, a, \tau_v, \tau_t, \alpha$ . The limit of stability for steady-state flow is determined from the condition  $c_i = 0$ . To solve the resultant boundary-value problem, i.e. to determine the decrement spectrum and the flow stability limits, the Runge - Kutta - Merson method of stepwise integration was used with orthogonalization of solutions at each step in the integration. The method used made it possible to carry out calculations to sufficiently large values of the problem parameters:  $Gr \sim 10^6, Pr \sim 10^3, Ga \sim 10^6$ .

The presence of added particles shows up primarily in the spectrum of perturbation decrements. In contrast to the spectrum for a layer of pure fluid and the spectrum for a layer with transverse seepage fluid, the perturbation spectrum is now considerably richer because of the appearance of perturbations associated with the particle cloud. As shown by calculations, however, perturbations associated with the transport medium remain responsible for the instability of the equilibrium state.

Transverse motion of the particles leads to a considerable change in the perturbation spectrum for a stationary layer of pure fluid. Oscillational perturbations now appear in the spectrum; they arise as the result of coalescence of real levels. With an increase in Rayleigh number, these complex-conjugate pairs break down into two real levels. Instability, as in the case of a stationary layer of pure fluid, is caused by the real branches of the spectrum and has monotone nature.

The effect of particle setting rate on the stability of a layer shows the dependence of the minimum critical number  $Ra_m$  on the particle setting rate  $u_s$ . Layer stability rises rapidly with increase in  $u_s$ . The wavelength of the most dangerous perturbations decreases. In a layer of air 2 cm thick, motion of wood particles at a velocity  $\approx 25\text{cm/sec}$  ( $a = 0.15, r = 0.008\text{ cm}$ ) increase the stability by factor of almost 18. With an increase in the particle setting rate, however, the rate of rise in the minimum critical Rayleigh number slows down (for  $|u_s| \geq 180$ ).

With an increase in particle setting rate, a thermal boundary layer begins to form at the lower boundary of the layer. As a result, the effective thickness of the stratified layer of gas is decreased ( $h_{eff} < h$ ). The characteristic temperature difference of  $2\Theta$  remains fixed in this case. The critical temperature difference is found from the condition  $(1+a)g\beta\Theta h_{eff}^3/\nu\chi = const$  and therefore the critical Rayleigh number, which is determined in the usual manner from the halfwidth  $h$  of the layer, is increased in proportion to the decrease in  $h_{eff}$ , i.e., to the rise in  $|u_s|$ . This occurs as long as the particles "blowup" the distribution of gas temperature increase the thickness of the thermal boundary layer at the lower surface. It turns out that at high values of the setting rate, further increase leads to insignificant distortion of the established distribution of gas temperature and so to a small rise in stabilizing effect.

Intensification of the distorting effect of particles on the distribution of gas temperature is also observed when there is an increase in the mass concentration  $a$  of the additive. The stabilizing effect of the particles on equilibrium stability increases in this case. With an increase in the mass concentration  $a$  by a factor of two from 0.15 to 0.37, the minimum critical Rayleigh number increases from 780 to 2035 and the critical wavenumber  $k_m$  increases from 2.2 to 2.9. Convective equilibrium stability in our case is much higher than the stability of a pure fluid. Stability rises with an increase in the relative heat capacity  $b$  of the particles. Particles having a higher heat capacity better absorb the perturbations that are the most dangerous.

The behavior of the minimum critical Rayleigh number  $Ra_m$  as a function of particle radius (or of relaxation time  $\tau_v$ ) is similar to the behavior of the minimum critical Grashof number in the problem of the stability of convective flow in a minimum containing an additive in a vertical layer. An increase in  $r$  leads to an increase in equilibrium stability up to some limiting value  $r_* = 0.0045$  at which  $Ra_m = 3139$ . The stabilizing effect decreases when  $r > r_*$ . The critical wave number  $k_m$  increase in  $r$  and reaches a value of 3.19, and then decreases with further increase in  $r$ . In contrast to the problem of the stability of steady-state convective motion of containing additive, the increase in convective equilibrium stability with increase in particle size is associated with a decrease in the length of dangerous standing perturbations.

5. A comparison of these results with the results of [10] shows that settling particles produce a considerably greater stabilizing effect on steady-state flow of a fluid than suspended particles. In fact, neglect of particle settling rate in comparison with the velocity of steady-state flow of a fluid valid for sufficiently fine particles of not too great a density (with respect to the density of the transporting medium). Coarse dense particles are more inert than fine particles, and it is impossible to neglect their settling rate. The particle slip rate with respect to the fluid is of the order of the quantity  $u_s$ . The resultant relative motion of fluid and particles leads to additional dissipation of perturbation energy in comparison with the case of suspended particles.

## REFERENCES

1. Gupalo Yu. P. "Stability of laminar flow of a liquid with heavy impurity," *Izv. Akad. Nauk SSSR, Otd. Tekh. Nauk, Mekh. Mashinostr.*, 1960; No. 6, 38-46.
2. Saffman P. G. "On the stability of laminar flow of a dusty gas," *J. Fluid Mech.*, 1962; 18, No. 1, 120-128.
3. Michael D. H. "The stability of plane Poiseuille flow of a dusty gas," *J. Fluid Mech.*, 1964; 18, No.1, 19-32.
4. Zheltukhin I. D. "Stability of a laminar boundary layer in an incompressible gas carrying a heavy impurity," *Izv. Akad. Nauk SSSR, Mekh. Zhidk. Gaza*, 1971; No.2, 103-110.
5. Gupalo Yu. P., Ryazantsev Yu. S., Sergeev Yu. A. "Convective instability of a homogeneous suspended layer," *Izv. Akad. Nauk SSSR, Mekh. Zhidk. Gaza*. 1982; No. 3, 112-114
6. Dement'ev, O. "Convective stability of a medium containing a heavy solid additive". *Zhurnal Prikladnoi Mekhaniki i Tekhnicheskoi Fiziki*, No. 3. 1976, P. 105-115.
7. Marble F. E. "Dynamics of dusty gases," *Mekhanik.*, 1970; No. 6, 397-404.
8. Sow S. "Hydrodynamics of Multiphase Systems" [Russian translation], Mir, Moscow, 1971. P. 576.
9. Gershuni, G.Z., Zhukhovitskii E.M., Nepomnjashchy A.A. "Stability of convective flows". Moscow, Nauka. 1989, P. 320.
10. Dementiev O. "Stability of steady-state flows of a liquid with a heavy impurity", *Z. angew. Math. und Mech.*, 1996; v. 5, 112-114.

# Motorcycle accidents reconstruction and simulation - application of hybrid human body model

Tomasz Bonkowski<sup>1,\*</sup>, Ludek Hyncik<sup>1</sup>, Jan Spicka<sup>1</sup>, Jan Vychytil<sup>1</sup>

Department of Biomechanical Human Body Models, New Technologies – Research Centre, University of West Bohemia,  
Univerzitní 8, 301 00 Pilsen, Czech Republic <sup>1</sup>  
tomasz@ntc.zcu.cz

**Abstract:** Motorcycle accidents with opposite vehicles are among the most difficult to reconstruct due to complicated kinematics and interactions between multiple participants. The Multi-Body System approach commonly applied in software packages as PC-Crash and Virtual-Crash, allows for proper reconstruction of the crash kinematics but did not take into account the full deformation of the vehicles and occupants. On the other hand, the Finite Element Method approach, especially the explicit formulation, used in the field of crashworthiness gives a way to describe the proper material behavior of the participant components during dynamic events. For the analysis of the accident, the full FEM approach becomes too complicated and time-consuming (both for preparation of the simulation and for the simulation run). The authors would like to propose a hybrid approach which couples and FEM and MBS models in VPS numerical environment (Pam-crash solver). This paper presents an analysis of the accident between the maxi-scooter and the opposite vehicle. As the representation of the PTW driver, a Virthuman hybrid human body model was used. This model in opposition to full FEM models allows the fast calculation of the simulation. Besides the kinematics of the accident, prescribed injury criteria were assessed on the human body model.

**Keywords:** VULNERABLE ROAD USERS, HUMAN BODY MODEL, VIRTUMAN, MOTORCYCLE ACCIDENTS

## 1. Introduction

An accident reconstruction is a procedure of creating the linkage between the causes and the effects of an accident. This procedure could be carried out in two ways. The first way is a backward-looking, in which the reconstruction starts from the known post-crash position of crash participants. The information about the deformation and the post-crash movement guide to the impact speed, and then to the driving speed. The second way of the accident reconstruction is a forward reconstruction.[1,2]

In the forward reconstruction, the accident is replicated by the numerical model. This method aims to replicate the final position by the solution of the model. Proper numerical models of participants and interaction between them are crucial to conducting the backward reconstruction procedure. For a regular PTW to a car accident, at least four numerical models are required (car, PTW, rider, helmet). Due to its multi-directional validation and scaling possibility, the Virthuman model can be used as a representation of the PTW rider. Moreover, the classical injury criteria like the HIC and the Nij could be assessed on the Virthuman model.

## 2. Materials

The cases were simulated in the numerical environment: Virtual Performance Solution (former PamCrash). The simulation was performed for the FEM models (the OV, the helmet) using an explicit approach. The main aim of the simulation was the reconstruction of the PTW occupant injury pattern. Due to the nature of the Virthuman [3] (MBS), the injuries could be only found by monitoring the nodal accelerations and forces which appear in the joints [4,5]. Based on these parameters, the injury criteria can be calculated (e.g. HIC - head injury criteria).

During the simulation, four macroscopic objects were used (the PTW, the OV, the occupant, and the helmet) [6]. Before starting the numerical calculation, these objects must be positioned and coupled. The procedure for coupling was as follows:

- Virthuman scaling according to the PTW occupant description
- Coupling Virthuman to the helmet
- Positioning Virthuman to a sitting position,
- Coupling Virthuman to the PTW (at the contact points),
- Positioning the PTW with the occupant (according to the backward reconstruction),
- Setting the initial velocities of the PTW and the OV.
- Injury criteria evaluation

After the simulation, two injury criteria were evaluated:

- Nij - normalized neck injury criterion,

- HIC - head injury criterion.

The Nij injury criterion could be calculated as follows [7]:

$$N_{ij} = \frac{F_Z}{F_{int}} + \frac{M_Y}{M_{int}},$$

where:

$F_Z$  - the axial load,

$F_{int}$  - the critical intercept value of load used for normalization,

$M_Y$  - the flexion/extension bending moment,

$M_{int}$  - the critical intercept value for moment used for normalization.

The HIC can be defined as follows [7]:

$$HIC = \left\{ \left[ \frac{1}{t_2 - t_1} \int_{t_1}^{t_2} a(t) dt \right]^{2.5} (t_2 - t_1) \right\}_{max}$$

where:

$t_1$  - the initial time of the interval in which the HIC has a maximum value,

$t_2$  - the final time of the interval in which the HIC has a maximum value,

$a(t)$  - the magnitude of the acceleration of the head center of gravity.

### 2.1 Case 1

The first step for an accident simulation is the positioning of the vehicles and the occupant. In Case 1, the OV and the PTW were positioned according to the figures from the case description. The angle between the vehicles was equal to 114 deg.

- OV: Ford Fiesta (2004) with a mass of 1300 kg,
- The PTW mass: 260 kg (vehicle with driver)
- The PTW speed: 55 km/h,
- The OV speed: 10 km/h.



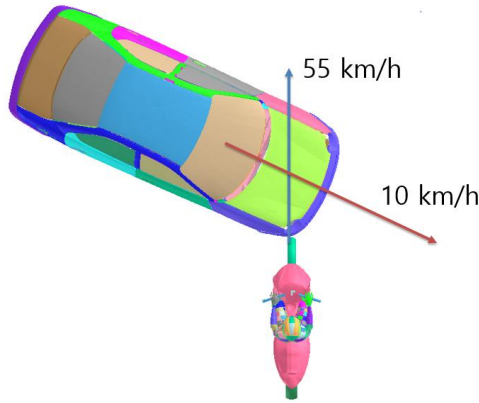


Figure 1. Case 1 setup.

## 2.2 Case 2

According to the procedure, the first step was Virthuman scaling. The basic model was scaled to the anthropometric parameters of the real PTW occupant. Next, the model was positioned, coupled with the helmet and coupled with the motorcycle. Then the OV model was trimmed to the mass reported in police records (1130 kg). After these steps, the PTW model was positioned against the OV model (Figure 2.). The angle between the vehicles was approximately 111 deg.

- ▶ OV: Fiat Grande Punto (2009) with a mass of 1130 kg,
- ▶ The PTW mass: 260 kg (vehicle with driver)
- ▶ The PTW: 56 km/h,
- ▶ The OV: 9.5 km/h.

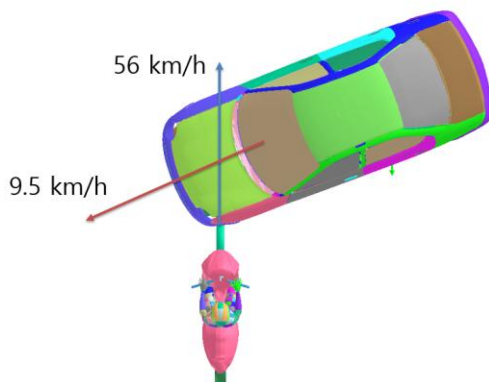


Figure 2. Case 2 setup

## 3. Results

### 3.1 Case 1

The kinematics of the accident is shown in the foregoing figures. All sub-phases of the PTW crash can be easily seen. Firstly, the front fork of the PB is compressed (0 – 30 ms). Next, the fork starts to deform (30 – 60 ms). The third step of the kinematics is the rotation of the PTW around the contact point.

During these sub-phases, the movement of the occupant can be described as follows. Firstly, the body of the driver starts to slide out from the seat, due to the PTW's loss of speed. The occupant's hands start to be compressed against the handlebar. After reaching the 450 N of the contact force between the hands and the handlebar, the contact ends. The upper part of the driver's body starts to overtake the PTW. The lower part of the body is continuously

compressed by the inertia forces on the PTW front frame. Due to this, the lower extremities are blocked by the PTW frame. This situation results in the appearance of the torque which acts on the rider's body. This torque results in rotation of the occupant around the point of the abdomen – motorcycle contact (90 - 120 ms). Because of the body rotation, the occupant finally hits the OV hood with the head.

- ▶ 0 – 30 ms sliding on the seat
- ▶ 30 ms reaching maximum handlebar grip force (450 N)
- ▶ 30 – 60 ms continuous sliding from the seat
- ▶ 60 ms first contact between the occupant's abdomen and the PTW frame
- ▶ 60 - 180 ms rotation of the body until the head-to- hood impact (175 - 185 ms).

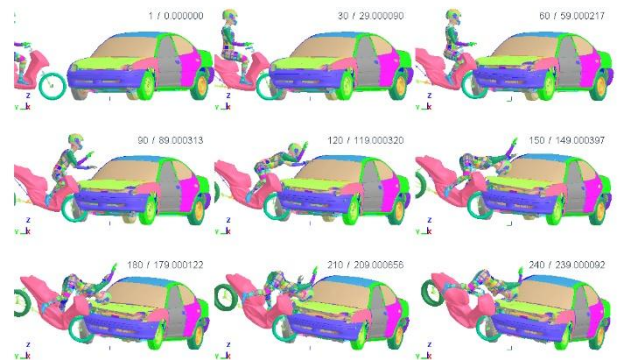


Figure 3. Case 1 kinematics.

The initial momentum and angle of the OV result in the change of the PTW path (the path starts to rotate clockwise). This situation results in contact between the left side of the PTW and the left leg of the occupant (150 - 240 ms). The contact force between the leg and the PTW side can result in an extensive leg injury. By analyzing the acceleration, which was acting on the head center of gravity (COG), the head injury criteria (HIC) can be calculated. In the reconstructed case the HIC is equal to 489 (Figure 4.). This value is in line with the medical examination of the PTW driver – the examination did not find injuries higher than AIS1.

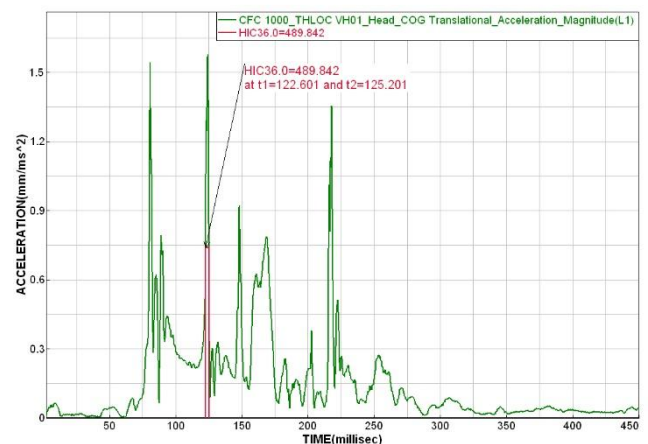


Figure 4. Case 1 HIC assessment.

After the filtration, the Nij was calculated. The calculation has been placed in the 50<sup>th</sup> percentile male corridor (Figure 5.). This

figure shows that the corridor has been exceeded. This situation occurs because of the high peak of the neck extension force at 75 ms and 120 ms. However, the medical examination of the area did not report any neck injuries.

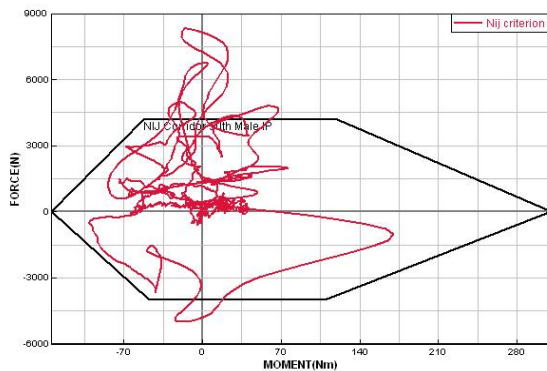


Figure 5. Case 1 Nij corridor.

### 3.2 Case 2

The kinematics of the crash are presented in the foregoing figures. The crash starts with the first contact between the PTW front wheel and the left fender of the OV. In the first 20 ms, the fork of the PTW is exposed to compression. After this period, the fork starts to bend (20 - 45 ms) until the first contact between the PTW front wheel and the PTW frame. At 45 ms, the PTW starts to rotate around the vehicles' contact point (Y-axis of the PTW). This results in the rear part of the PTW lifting.

During the crash, the PTW driver's movement passes through the following steps:

- ▶ 0 – 30 ms sliding on the seat
- ▶ 30 ms reaching maximum handlebar grip force (450 N) – releasing the hands
- ▶ 30 – 60 ms continuous sliding from the seat
- ▶ 60 ms first contact between the occupant's abdomen and the PTW frame
- ▶ 60 - 180 ms rotation of the body until the head-to- hood impact (175 - 185 ms)

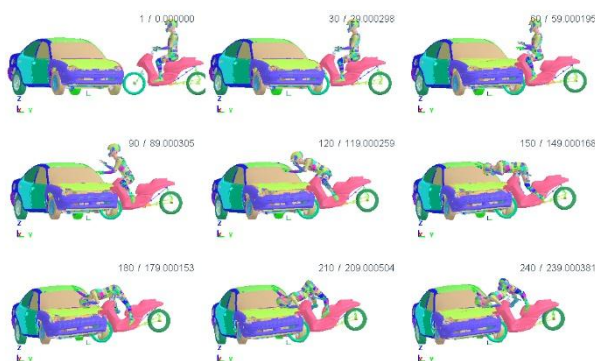


Figure 6. Case 2 kinematics.

The analysis of the signal from the head COG virtual accelerometer (Грешка! Источникът на препратката не е намерен.) shows that the biggest peak of the acceleration was around 180 ms. This data corresponds to the contour plot of the

simulation (180 ms, Грешка! Источникът на препратката не е намерен. 6.). The calculated HIC criterion (399) is in line with the medical reports (no head injuries were reported).

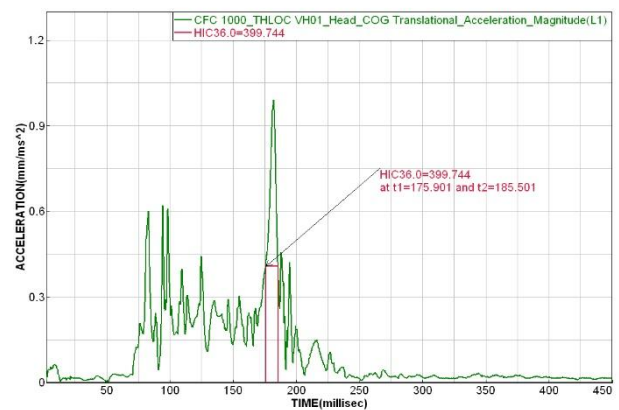


Figure 7. Case 2 HIC assessment.

The analysis of the Nij criterion (Figure 8.) shows that during the accident the PTW occupant was constantly inside the safe corridor for the neck. This is in line with the medical examination – neck injury was not reported.

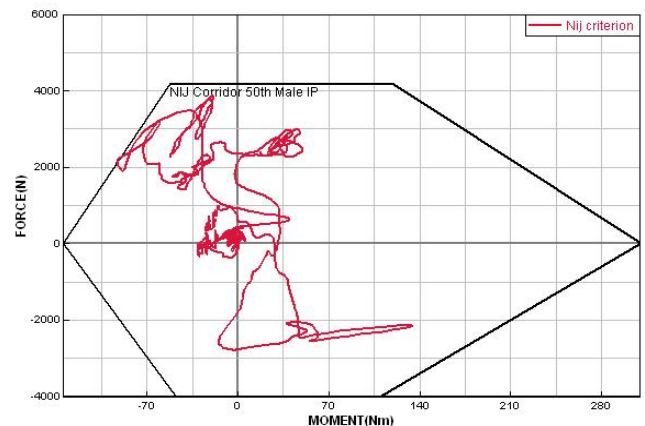


Figure 8. Case 2 Nij corridor.

### 3. Conclusions

The VPS Virthuman shows in simulated cases a good recreation of the PTW occupant kinematics. Its main advantage is the scaling possibility and acceptable calculation time. In comparison with more complicated FEM human body models (THUMS, GHBM), the Virthuman is easier to position. However, it should be mentioned that even improved MBS models of the human body can only be used to evaluate predefined and existing injury criteria. They do not have any built-in mechanisms for real injury simulation (e.g. lung puncture). From the engineering point of view, numerical accident simulation can be a booster for PPE development teams, but, as with every tool, they are only as good as the people who use them.

### 4. Acknowledge

The work has been supported by the research project CZ.02.1.01/0.0/0.0/17\_048/0007280 Application of Modern Technologies in Medicine and Industry and the internal grant project SGS-2019-002 Biomechanical models of human body, biological tissues and biomechanical processes with application in industry and medicine

#### 4. References

- [1] R. Noon, Introduction to forensic engineering, Boca Raton: CRC Press, 1992.
- [2] R. Noon, Forensic engineering investigation, Boca Raton: CRC Press, 2001.
- [3] J. Vychytil, J. Manas, H. Cechova, S. Spirk, L. Hyncik and L. Kovar, "Scalable Multi-Purpose Virtual Human Model for Future Safety Assessment," *SAE Technical Paper*, Vols. 2014-01-0534, 2014.
- [4] G. Kasanický and P. Kohút, Analýza nehôd jednotopových vozidiel, Žilina: Žilinská univerzita v Žiline, 2000.
- [5] D. Kirk, Vehicular accident investigation and reconstruction, Boca Raton: CRC Press, 2000.
- [6] A. Chwla and S. Mukherjee, "A Road Crash Reconstruction Technique," *Institute of Engineers Journal*, vol. 91, pp. 3-8, 2010.
- [7] R. Eppinger, E. Sun, F. Bandak, M. Haffner, N. Khaewpong, M. Maltese, S. Kuppa, T. Nguyen, E. Takhoumts, R. Tannous, A. Zhang, and R. Saul, "Development of Improved Injury Criteria for the Assessment of Advanced Automotive Restraint Systems - II," NHTSA, 1999.



# Injury prevention during childbirth: A model of pelvic floor

Hana Čechová<sup>1\*</sup>, Linda Havelková<sup>1</sup>, Tomáš Zítka<sup>1</sup>, Zdeněk Rušavý<sup>2</sup>, Vladimír Kališ<sup>2</sup>, Khaled Ismail<sup>2</sup>

University of West Bohemia in Pilsen, Pilsen, Czech Republic<sup>1</sup>

Charles University in Pilsen, Pilsen, Czech Republic<sup>2</sup>

hcechov@ntc.zcu.cz

**Abstract:** During vaginal delivery women suffer with several kinds of injuries which may negatively influence their quality of life. Different techniques are used for perineal protection during the second stage of the delivery. A method called manual perineal protection (MPP) is used to decrease the risk of severe perineal trauma. In order to quantify this method a special measuring glove was designed and forces generated by the obstetricians during real deliveries were measured. Measured forces were then used in computer simulation of the MPP method. The forces were applied on a previously developed FEM model of the pelvic floor during simulation of the vaginal delivery. The stress distribution in the perineal area was monitored. Reactions of perineal tissues were evaluated. The simulations of childbirth with and without MPP were compared

**Keywords:** VAGINAL DELIVERY, FINITE ELEMENT MODEL, PELVIC FLOOR, MANUAL PERINEAL PROTECTION

## 1. Introduction

Female pelvic floor dysfunctions are very often associated with injuries of pelvic floor structures during vaginal delivery. It is reported that only 9.6% and 31.2% of women deliver with an intact perineum at their first and second births respectively [Smith]. Therefore, it is imperative that strategies that decrease the extent of perineal trauma are developed, assessed and promoted.

In the certain cases the method called manual perineal protection (MPP) can be used to successfully protect the integrity of the perineum during vaginal delivery [7]. Proper execution of the MPP is a complex problem with a high variation of obstetrical variables described by the accoucheurs [5]. Due to the nature of vaginal delivery, it is not possible to precisely repeat a modification of MPP in order to study its efficacy. Virtual modeling linked with measuring techniques seems to be a promising way how to improve the maneuvers and helps in better understanding of this topic.

The correct virtual modeling should always stay on relevant experimental data. (Several studies were published.) As the pilot research the stereophotogrammetry was presented [11]. Large deformations of the perineal skin were quantified, however, no information concerning acting forces was known. For this reason, a special measuring glove was designed and used by obstetricians during real deliveries. This unique measurement was published [10].

So far, the MPP has been simulated based on stereophotogrammetry data only [3,4]. The simplified model covering the rigid fetal skull and superficial perineal structures represented by a homogenous material were modelled. The forces applied by obstetricians were supplied by boundary conditions.

The main objective of this study is to improve the existing female pelvic floor FE model [6] and to simulate a delivery of a fetal head. The second aim is to simulate the MPP at the time of the head expulsion using hand forces measured during the real delivery.

## 2. FE Pelvic Model

Previously published finite element female model was used as a basis [6, 2]. Originally, the model consisted of the female pelvis, the levator ani muscle (LAM) with the fetal head modelled as a rigid body. Other surrounding structures were substituted by boundary conditions. For the refined FE model muscles forming the pelvic floor such as ischiocavernosus, bulbospongiosus and transversus perinei including anal sphincters and the anococcygeal ligament and the perineal membrane were added. The geometry of all structures was based on a live-subject's MRI data and anatomical cadaveric measurements. Complete model geometry is shown in the Fig. 1.

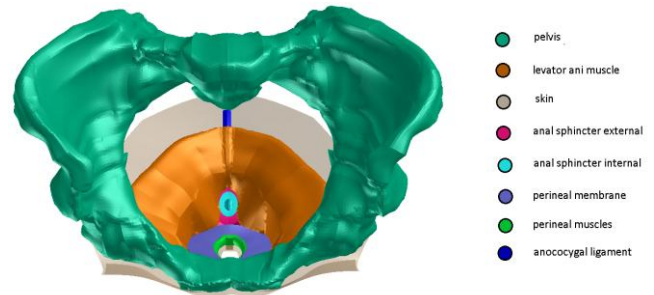


Fig. 1 Setup of the pelvic model.

The fetal head model and its trajectory through the pelvic floor structures was reconstructed based on the dynamic magnetic resonance of a vaginal delivery [1]. However, the fetal head was scaled up to ensure that its main dimensions corresponded to those of an average size term fetus.

Bones were modelled as rigid bodies, soft tissues as hyperelastic Ogden material to allow for large deformation. The muscle material constants were fitted using the stress-strain characteristic measured during a uniaxial tensile test and utilizing information from porcine samples or characteristics published previously in [2]. The perineal membrane was modeled as a layered membrane with perpendicular layers of fibers and a surrounding matrix. The skin was modelled by elastic shells. Material characteristics such as skin and ligaments were based on literature search.

## 3. Delivery Simulation

Using the new FE model, the vaginal delivery was simulated for the optimal fetal head size, position and orientation – i.e. left occipito-anterior position.

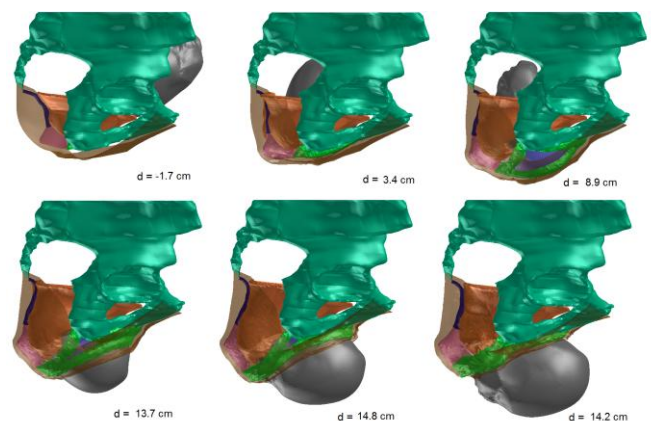


Fig. 2 Phases of the delivery in side view displayed in chosen stations marked as d.

The simulation was prepared and results were analysed by VPS. The stress and strain distribution of the pelvic floor structures during birth was analysed by the Virtual Performance Solution (VPS 9.0; ESI Group, Paris, France) commercial software. The head station was defined as the distance between the interspinous diameter and the head vertex. The interspinous diameter is the distance between the tips of the ischial spines. The vertex denotes the top of the head in the upright position. The delivery simulation starts with the head placed in the upper part of the pelvis then rotates and descends according to prescribed trajectories. The head in chosen positions – stations - is shown in Fig. 2.

#### 4. Measuring of forces during MPP

Several variations of the MPP maneuver exists. The used Finnish technique of MPP (FMPP) involves application of the thumb, the index finger and the middle finger of the dominant hand on the perineal skin. The thumb and the middle finger press anterolaterally to the fourchette to reduce midline perineal strain. The flexed middle finger is used to apply pressure against the perineal body to facilitate the process of the fetal head extension. The non-dominant hand controls the speed of the fetal head expulsion and facilitates the fetal head extension [10].

Since it is difficult to evaluate the actual contribution of the individual components of FMPP in a clinical setting a special measuring glove was designed, see Fig. 3. Using this glove forces applied by the obstetrician during FMPP were measured. This right-handed glove was designed in order to gather forces generated by the obstetrician during the head expulsion. The wireless sensors are placed on the thumb, the index finger and the middle finger. The glove is a part of system, which collects, transfers and stores data onto a PC. All detailed information including pilot measurements are published in [10].

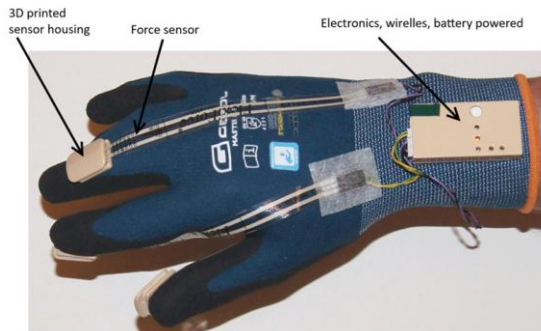


Fig. 3 Measuring glove with force sensor.

During the delivery the glove was put on the accoucheur's right hand and covered by the sterile medical glove. At the moment of the head expulsion the forces were measured

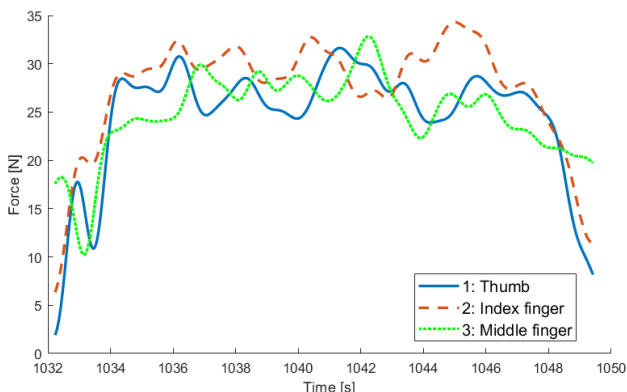


Fig. 4 Measured time-force dependencies of fingers during MPP. The curve no. 1 denotes thumb, no. 2 denotes index finger and no. 3 the middle finger.

. In [10] twenty first term spontaneous deliveries were undertaken by two expert obstetricians using the measuring glove. Measured samples were processed. The courses of finger forces of one chosen case are displayed in Fig. 4.

#### 5. Simulation of MPP

The proper time-force dependencies of fingers of the one chosen delivery are implemented to the pilot simulation of the FMPP. As the first step the preliminary simulation of the “hands on” technique was prepared and only the pressure loading of fingers without head delivery were implemented to control perineal structures reaction. Further the complete delivery with “hands on” was simulated. The obstetrician fingers acting during the maneuver are supplied by prescribed pressure loading as is shown in Fig. 5. Measured forces are converted to pressures since the sensor surfaces are known.

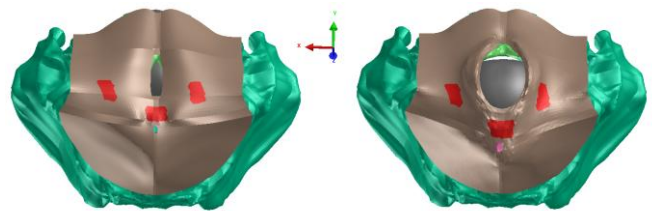


Fig. 5 Pelvis in inferior view at the beginning of the simulation (left) and with the head station at 11.4 cm (right). The positions of the finger sensors are red colored.

According to [3] the fingers during delivery are applied when the vaginal introitus is dilated to 8 cm anteroposteriorly and 4 cm transversely which corresponds to the head station equal to 11.4 cm in the presented model. At this moment, which corresponds to the beginning of the head expulsion, pressure loadings increase and continues till the end of the simulation.

#### 6. Results and discussion

Our study confirmed the hypothesis that pelvic floor structures undergo large stress and deformation during the second stage of the labor, see Fig. 2. The caudal displacement of the LAM was 2.4 cm and 4.1 cm for the head station equal to 8.9 cm and 14.2 cm respectively. It corresponds to a 166% elongation of the LAM in the caudal direction. The perineal caudal displacement was 4.9 cm for the head station equal to 14.7 cm.

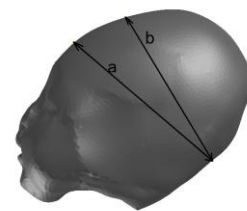


Fig. 6 Fetal head diameters; a) suboccipito-frontal, b) suboccipito-bregmatic diameter.

The stress values at the LAM were the highest at the anterior attachments to the tendinous arches when the head station was equal to 8.9 cm and reached 30.8 MPa. This was followed by a decrease in the LAM stress level as the stress in the perineal structures starts to increase with further head descent. The stress in the perineal body reached its maximum when the suboccipito-frontal diameter of the head was passing through the introitus. It was later than the priori expectation that this would happen when this area is stretched by the suboccipito-bregmatic diameter of the head. The suboccipito-bregmatic diameter passed through the introitus at the head station

equal to 14.7cm. Described head diameters are demonstrated in the Fig. 6. All monitored first principal stress values are summarized in the **Грешка! Источникът на препратката не е намерен.** and displayed in the Fig. 7.

**Table 1** Summary of maximal values of the first principal stress on the LAM and the perineum muscles.

Muscle / region	Head station [cm]	Max first principal stress [MPa]
LAM / insertion to tendinous arches	8.9	30.8
Transversus perinei / perineal body	13.7	33.6
Transversus perinei / perineal body	14.7	91.47

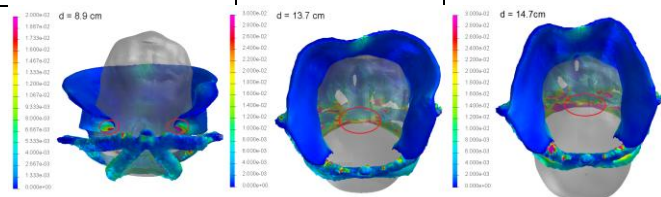


**Fig. 7** The first principal stress distribution in the LAM and perineal muscles,  $d$  denotes the head station. Red circles mark the LAM attachments to the tendinous arches (left) and the area of perineal body (middle and right).

Concerning the simulation of the FMPP the stress and strain distribution is influenced by the missing subcutaneous structures. These structures are not crucial for the own delivery simulation. Currently they are substituted by appropriate linking elements. Skin deformations shows Fig. 8. Although the acting finger forces are similar, deformations caused by thumb and index finger are much higher than by the middle finger.

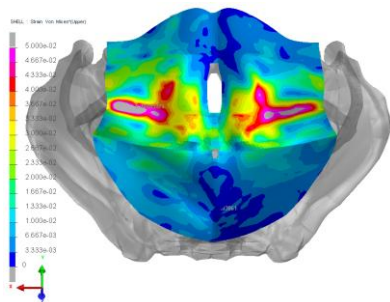


**Fig. 8** Strains of the loaded skin. Simulation without delivery.

Differences in the stress distribution of the perineal skin during delivery are shown in Fig. 9. In case of “hands on” the stress moves from the posterior fourchette to the perineal body. The posterior fourchette is a critical place for tearing. The FMPP influences the stress distribution in this critical region.

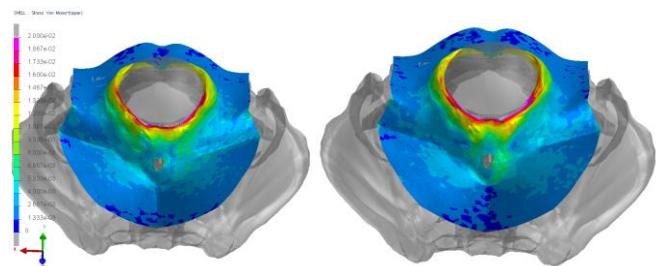


**Fig. 9** Comparison of stress distribution in the model with “hands off” (left) and “hand on” (right) technique during delivery.

## 7. Conclusion

We were able to develop a complex model of the pelvic floor, to simulate the delivery of the fetal head and to simulate the MPP method. The main advantage of this model is that it allows detailed evaluation of individual pelvic floor structures hence increasing the internal validity of our findings and enables extending future applications of the model. Current state of the model enables further applications as the simulation of the manual perineal protection (MPP).

The pilot simulation of MPP shows a weakness of the model, which is the missing connective tissue between the skin and the perineal structure. Although the connective tissue is substituted by linking elements, it should be improved since it would influence the force transmission between perineal structures. Despite that the study confirmed the influence of the fingers pressure on the perineal skin during the vaginal delivery.

## 8. References

1. C. Bamberg, G. Rademacher, F. Guttler, U. Teichgraber, M. Cremer, C. Buhner, C. Spies, L. Hinkson, W. Henrich, K.D. Kalache, J.W. Dudenhausen, *Am J Obstet Gynecol*, 206, 6 (2012).
2. L. Havelkova, L. Krofta, P. Kochova, V. Liska, V. Kalis, J. Feyereisl, *Int Urogynecol J*, 31, 7 (2019).
3. M. Jansova, V. Kalis, Z. Rusavy, R. Zemcik, L. Lobovsky, K. Laine, *Int Urogynecol J*, 25 (2014).
4. M. Jansova, V. Kalis, L. Lobovsky, L. Hyncik, J. Karbanova, Z. Rusavy, *Int Urogynecol J*, 25 (2014).
5. H. Kleprlikova, V. Kalis, M. Lucovnik, Z. Rusavy, M. Blagajne, R. Thakar, et al, *Acta Obstet Gynecol Scand*, 99, 4 (2020).
6. L. Krofta, L. Havelkova, I. Urbánková, M. Krcmar, L. Hyncik, J. Feyereisl, *Int Urogynecol J*, 28, 2 (2017).
7. K. Laine, F.E. Skjeldestad, L. Sandvik, Staff AC, *ISRN Obstet Gynecol* (2013).
8. N. Sindwani, C. Bamberg, N. Famaey, G. Callewaert, J.W. Dudenhausen, J. Deprest, *Am J Obstet Gynecol*, 217, 2 (2017).
9. L.A. Smith, N. Price, V. Simonite, E.E. Burns, *BMC Pregnancy Childbirth*, 7 (2013).
10. V. Kalis, Z. Rusavy, L. Havelkova, T. Zitka, D. Tolar, K.M. Ismail, *BMC Pregnancy Childbirth*, 20 (2020).
11. R. Zemcik, J. Karbanova, V. Kalis, L. Lobovsky, M. Jansova, Z. Rusavy, *Int Urogynecol J*, 119 (2012).

## Acknowledgements

This work was supported by the project n. 182 “Obstetrics 2.0 – Virtual models for the prevention of injuries during childbirth” realised within the frame of the Program INTERREG V-A: Cross-border cooperation between the Czech Republic and the Federal State of Germany Bavaria, Aim European Cross-border cooperation 2014-2020. The realisation is supported by financial means of the European Regional Development Fund (85% of the costs) and the state budget of the Czech Republic (5%).

# A study of convergence of $\xi$ approximations transform by region depended given as determined by $\sigma_n(t)$ Functions on entire complex plane

Işım Genç Demiriz

Department of Mathematics, Davutpaşa Campus-Yıldız Technical University of İstanbul, Turkey  
idemiriz@yildiz.edu.tr

**Abstract:** In this study, the convergence behavior of the  $\xi$  approximants transform given as determined by  $\sigma_n(t)$  functions for the exponential operators is investigated on the entire complex plain. An algorithm is developed to observe how to transform a initial region on the complex plane defined by  $\xi$  approximants.

**Keywords:** LIE OPERATORS, COMPLEX RECURSIVE FUNCTIONS, EVALUATION OPERATORS

## 1. Introduction

In this study, the convergence behavior of the  $\xi$  approximants transform given as determined by  $\sigma_n(t)$  functions for the exponential operators is investigated on the entire complex plain and an algorithm is developed to observe how to transform a initial region on the complex plane defined by  $\xi$  approximants.

System with n degrees of freedom will be characterized by  $x_1, x_2, \dots, x_n$  complex variables, which are considered as the coordinates of a point or components of a vector in an n-dimensional complex vector space.

$\{x_1(t), x_2(t), \dots, x_n(t)\}$  : System

$x_1, x_2, \dots, x_n$  : Phase space vector components in this system.

Hence  $Q(t_f, t_i)$  global evolution operator is defined as

$$x(t_f) = Q(t_f, t_i).x(t_i)$$

where  $t_i$  and  $t_f$  denote the initial and final states respectively. If factorization of evolution operators is considered as a sequence of rather simple global evolution operators then the evolution operator can be written as follows

$$Q(t_f, t_i) = e^{(t_f - t_i)S}$$

where S is defined through

$$S = \sum_{j=1}^N f_j(x_1, x_2, \dots, x_N) \frac{\partial}{\partial x_j}$$

so Q evolution operator can be assumed to be written as

$$Q = e^{t f(x) \frac{\partial}{\partial x}} = \prod_{j=1}^{\infty} e^{\sigma_j(t) x^j \frac{\partial}{\partial x}} \quad \sigma_j(t) = t f_j$$

where  $L = f(x) \frac{\partial}{\partial x}$  and

$$f(x) = \sum_{j=1}^{\infty} f_j x^j \quad |x| < \rho$$

This equation is factorization formula for the one-dimensional case.

The essential approximation is to truncate

$$Q = \prod_{j=1}^{\infty} e^{\sigma_j(t) x^j \frac{\partial}{\partial x}} \quad \sigma_j(t) = t. f_j$$

to a finite order. By this way it produces the following approximation.

$$\bar{\xi}_n(x, t) = \left\{ \prod_{j=1}^n Q^{(j)} \right\} x$$

If the infinite product representation of Q converges then the following result can be obtained:

$$\bar{\xi}(x, t) = Qx = e^{t f(x) \frac{\partial}{\partial x}} x = \lim_{n \rightarrow \infty} \bar{\xi}_n$$

A recursion relation for these approximants can be shown as follows:

$$\bar{\xi}_{n+1} = \frac{\bar{\xi}_n(x, t)}{[1 - n \sigma_{n+1}(t) \bar{\xi}_n^n(x, t)]^{\frac{1}{n}}}$$

And this is a recursion relation with an initial member evaluated as follows:

$$\bar{\xi}_1(x, t) = e^{\sigma_1(t) x \frac{\partial}{\partial x}} x = x e^{\sigma_1(t)} = x e^{f_1 t}$$

Although this is a simple recursion relation, the existence of  $f_1$  may not be suitable for numerical purpose depending on the value of  $f_1$ . So we can normalize  $\xi$ - approximants as follows:

$$\bar{\sigma}_{n+1} = n \sigma_{n+1} e^{n f_1 t}$$

Then the final recursion relation becomes as follows:

$$\xi_{n+1}(x, t) = \frac{\xi_n(x, t)}{(1 - \bar{\sigma}_{n+1}(t) \xi_n^n(x, t))^{\frac{1}{n}}}$$

The relation between the final and the previous approximants can be given as

$$\bar{\xi}_n(x, t) = \xi_n(x, t) x e^{f_1 t}$$

In this study the convergence of the  $\xi$ -approximant sequences in the complex plane is main issue. The above transformation of  $\xi_n$  to  $\xi_{n+1}$  can be interpreted as applying some basic elementary transformations consecutively

$$\xi_{n+1} = \frac{\xi_n}{(1 - \sigma_{n+1} \xi_n^n)^{\frac{1}{n}}}$$

Here  $\sigma_n(t)$  functions are assumed to be given and the  $\xi$ -approximants' nature are determined by these  $\sigma_n(t)$  functions. The main purpose of the examination of this convergence is to give important information about the convergence of finite product sequences that appears during the factorization of these sequences.

In this study an algorithm is developed to find out or observe how the above recursion relation defined via  $\xi$ -approximants transform a given initial region on the complex plane defined by  $\xi$ -approximants and a develop a computer program based on this algorithm.

A singular point taken in the domain can carry us to infinity on the  $\xi_{n+1}$ -plane as can be noticed through

$$\xi_{n+1} = \frac{\xi_n}{(1 - \sigma_{n+1} \xi_n^n)^{\frac{1}{n}}}$$

Therefore one can obtain a singularity free initial region on  $\xi_n$  - plane by determining the locations of these singularities and discarding them from the domain.

In this study, the original contribution is the separation of the recursion relation between two consecutive  $\xi$ -approximants into basic simple consecutive transformations.

The other contributions are the construction of an algorithm that evaluates the region variations through the consecutive transformations and to develop a computer program to execute this



algorithm. The computer program is written in C++ language and Mathematica is used for graphics.

## 2. Examining of The Convergence

If we assume that the functions represented by  $\sigma_n(t)$  are given quantities, we need to trace how the  $\xi$ -approximants behave on the complex number plane.

$$\xi_{n+1} = \frac{\xi_n}{(1 - \sigma_{n+1} \xi_n^{\frac{1}{n}})}$$

Although it is important that the functions  $\sigma_n(t)$  depend on  $t$ , it will be assumed that the  $\sigma_n(t)$  take into for a certain value of  $t$ , that is, we will deal with pointwise convergence.

Let us consider  $\sigma_{n+1}(t)$  function sequences as constant, but convergent or non-convergent sequences.

For  $|\xi_1| = R$  circle, we obtain iterative functions as below.

$$\begin{aligned}\xi_1 &= \xi_1 \\ \xi_2 &= \frac{\xi_1}{1 - \sigma_2 \xi_1} \\ \xi_3 &= \frac{\xi_2}{(1 - \sigma_3 \xi_2^2)^{\frac{1}{2}}} \\ \xi_4 &= \frac{\xi_3}{(1 - \sigma_4 \xi_3^2)^{\frac{1}{3}}} \\ &\vdots\end{aligned}$$

If the sequences  $\sigma_1, \sigma_2, \sigma_3, \dots, \sigma_n$  are taken as constant arrays such as  $1, n, \frac{1}{n}, \frac{1}{n^2} \dots$   $\xi$ -approximants will show different behavior.

It is impossible to solve the  $\xi_{n+1}$  sequences by analytically except by taking  $n = 1$ , for  $|z| = R$  and  $\sigma = \text{const}$ .

However, it may be possible to examine the graphs found by some operations on functions.

The graphs in Figure 1 show four consecutive transformations, taking the  $\sigma_n(t) = n$  sequence of the  $|\xi_1| = 1$  unit circle in the complex number plane.

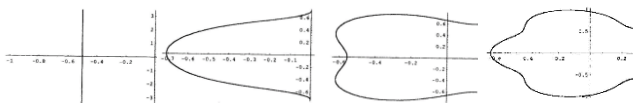


Figure 1

Here it can be easily seen that the transformation obtained with  $\xi_2$  transforms into the line  $u = -\frac{1}{2}$ , and the inside of the unit circle transforms into the region to the right of the line  $u = -\frac{1}{2}$ .

In the next step, the line  $u = -\frac{1}{2}$  turn into a parabola with its peak around  $x = -0.7$  and its arms extending to  $x = +\infty$ .

The region to the right of  $u = -\frac{1}{2}$  has turned inside of the parabola. The arms of the parabola cut the y-axis around  $\pm 0.7$ .

In the next transformations, generally appear look likes these parabolas.

However, they are not smooth due to error congestion.

The graphs in Figure 2 show four consecutive transformations, taking the  $\sigma_n(t) = 1$  sequence of the  $|\xi_1| = 1$  unit circle in the complex number plane.

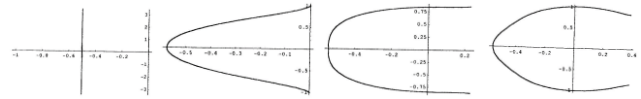


Figure 2

The graphs in Figure 3 show four consecutive transformations, taking the  $\sigma_n(t) = \frac{1}{n}$  sequence of the  $|\xi_1| = 1$  unit circle in the complex number plane.

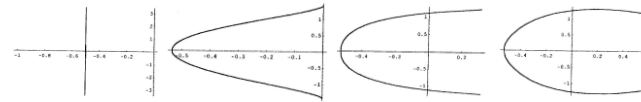


Figure 3

## 3. Conclusion

In this study has shown for the  $\sigma_n(t)$  sequences that the equivalent in the  $\xi_n$ -plane of a circular region without a singularity for the  $\xi_1$ -plane will remain without singularity in the  $\xi_n$  series, regardless of  $n$  and time.

Here all the transformations remain open at infinity because they are the branch points of systems.

## 4. References

1. Feynman R.P., Phys. Rev., (1951)
2. Aizu K., Math. Phys., (1963)
3. Demiralp M., Rabitz H., Factorization of Certain Evaluation Operators Using Lie algebra: Formulation Method, J. Math. Chem., Vol.6, pp:165-192, (1991)
4. Demiralp M., Rabitz H., Factorization of Certain Evaluation Operators: Convergence Theorems, J. Math. Chem., Vol.6, pp:193-208, (1991)

# Mathematical modeling of automated production systems

Associate Professor Ph.D. Sergii P. Vysloukh, Professor dr. eng. Viktor S. Antonyuk,  
associate Professor Ph.D. Kateryna S. Barandych, assistant Professor Oksana V. Voloshko

Faculty of instrument-making, National Technical University of Ukraine "Igor Sikorsky Kyiv Polytechnic Institute", Ukraine

**Abstract:** The paper theoretically substantiates and practically implements mathematical methods of modeling production systems, proves the adequacy of mathematical models and optimization methods, as well as selected rational optimization methods and created software that implements the selected methods in practice. The analysis of methods of modeling and optimization of production technological systems is performed, the most effective methods of solving these problems for discrete production are selected. The main provisions of infinite-valued logic and ordinal determinants, on which the structural-logical approach to the study of complex systems, which include production systems in instrument making, are considered.

**KEY WORDS:** production system, mathematical modeling, optimization, structural-logical method, the method of branches and boundaries.

## 1. Introduction

Development of methods for modeling and optimization of production systems is a promising scientific and technical task, which is of great importance for creating the optimal structure of the production system, which will reduce production costs without investing significantly in re-equipment, development of technological equipment [1–3].

Solving this problem involves various aspects of production, one of the main ones being the manufacturing time of the product. Along with the improvement of technological processes and material and technical base, the optimal loading of the production system equipment allows to significantly reduce the manufacturing time of products by minimizing equipment downtime. Thus, the optimization of the loading of technological equipment is an urgent problem in modern instrumentation. This problem is solved by modeling the operation of production systems [3–5].

To date, there is no single method of modeling production systems in general, i.e. those that would adequately and accurately describe the parameters of production systems of different structures, so to model a particular type of system, or at least several similar types of structures use different mathematical models [6–9].

To model the loading of technological equipment of production systems, it is proposed to apply the structural-logical method, as it can be used in production systems of various structures, namely: serial, parallel, parallel-serial, serial-parallel. In addition, this method is easily formalized and programmatically implemented [10, 11].

## 2. Fundamentals of structural and parametric optimization of production systems

When designing technological processes and operation of production equipment, the main set of tasks is related to the choice of the best version of the production system on a set of technical and economic indicators. These problems have several varieties, which correspond to three levels of optimization [11]:

- the first level of optimization is to choose the best technical idea or principle of operation of the projected object;
- the second - in search of the best structure or scheme within the chosen principle of action;
- the third - in determining the best values of parameters for the selected structure (scheme).

The division into three levels is conditional, and it is impossible to draw a strict line between them. The expediency of such a division is due to the need to distinguish between simpler and more complex and time-consuming tasks, which belong to different stages of technology design and at the same time differ significantly in the methods of solution.

First-level tasks are specific to the external design stages and are solved using heuristic programming approaches and methods. Modern systems of automated design of technological processes are focused on the stages of internal design. In this case, the problems of the second and third level are typical, which are called structural and parametric optimization problems, respectively.

When solving these problems, the term production technological system means a system whose purpose is to manufacture a certain number of products in a certain time, using a clearly defined amount of equipment. Strictly speaking, in this case we will describe the production system in terms of queuing theory.

Here, the system, which in connection with possible technical, economic and other applications, is considered structural, in contrast to the abstract system, which is the subject of study of general systems theory. An element of the system is an arbitrary indivisible object in this problem.

The indivisibility of an element is conditional and is caused by the desire to simplify the problem. It is possible that the transition from one task to another will require the decomposition of one element or, conversely, the combination of several elements into one. An object that does not decompose in this but may decompose in another problem is a block.

The system is a defined set of blocks (elements), combined by some set of connections to achieve a common goal. In service systems, this goal is to perform a given set of jobs. Each job consists of a number of different operations performed by the respective blocks.

The system as a whole provides a consistent passage of each job through certain blocks, a set of operations in which ensures the performance of this job. We believe that the operation is the smallest, indivisible part of the job.

In this regard, in the study of queuing systems, quantitative characteristics (parameters) of operations must be specified.

These parameters can be set by a matrix:

$$A = \|a_{ij}\|,$$


where  $a_{ij}$  is the quantitative effect of the  $i$ -th operation in the  $j$ -th job.

Values  $a_{ij}$  – can mean either the cost of time resources, or income and so on. The specific content of these values affects the formulation of problems of studying systems. The parameters  $a_{ij}$  express the quantitative characteristics of the queuing system as a whole.

The functioning of an arbitrary system is a set of rules that determines what the system must do to achieve its goal; these rules do not necessarily use the knowledge of building a system. In general, according to the level of abstraction adopted in the study of the system, its operation can be described by more or less detailed rules.

Thus, the operation of queuing systems is usually described at the level of system structure. Under the structure of an arbitrary system we understand the set of a set of blocks (elements) and a set of connections between them. The structure of the service system is usually represented by a digraph, in which the vertices denote the blocks (elements) of the system, and the arcs - the directions of movement of works from block to block in the process of their execution.

To quantify the degree of achievement by an arbitrary system of the goal set before it, various characteristics of its functioning are introduced. Each individual characteristic evaluates one side of the system, and only together they allow to assess how the system has achieved its goals.

Production systems form structures that can be serial, parallel, parallel-serial, serial-parallel, where  is the block of the production system, i.e. the machine [10].

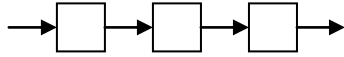


Fig. 1. An example of a serial structure of the system.

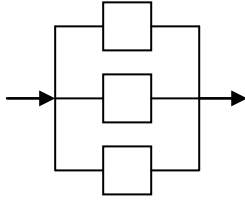


Fig. 2. An example of a parallel system structure.

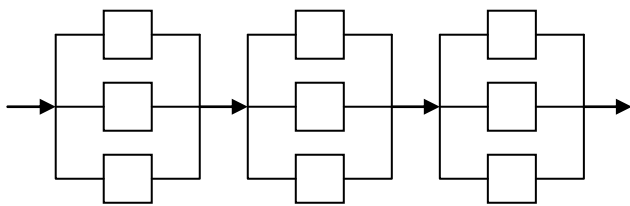


Fig. 3. An example of a parallel-serial structure of the system.

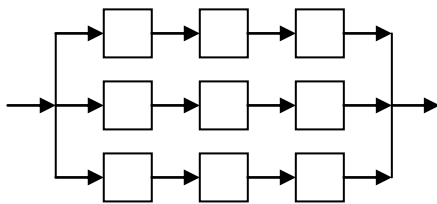


Fig. 4- Example of a serial-parallel structure of the system.

The quality of operation of any system can be assessed using certain characteristics. In this case, each performance characteristic, as a rule, evaluates a separate component of the quality of system operation, although generalizing characteristics are possible. Each class of systems has its own types of performance characteristics, although there are universal characteristics that apply to all classes of systems. Below is a short list of types of characteristics with an indication of the components of the quality of systems functioning evaluated by them. Some of these characteristics are universal, others belong to separate classes of systems.

The performance characteristics of the systems are universal. They evaluate the speed of operation of the systems. As such characteristics in service systems usually use the total execution time of the system of a fixed set of works or the number of works performed per unit time (speed of operation of the system). In other systems, performance is assessed similarly.

The boot characteristics of the systems are also universal. They assess the degree of employment of individual units and the set of units in achieving the goal of the system. As such characteristics in service systems apply a fraction of time during which the block is occupied with performance of works (average loading of the block); average for all blocks the share of employment time (average system load), etc. In other systems, the load is estimated similarly. The load is related to the performance of the systems as follows: the higher the load, the (other things being equal) the higher the performance.

The stability characteristics of the systems quantify the ability of any system to continue to function properly (albeit with poorer performance, load, etc.) in the event of block failures. To assess the

stability usually use the maximum number of blocks, with the simultaneous failure of which still retains the correct operation of the system. Stability, as well as speed and load, is a universal characteristic of the system.

The cost characteristics in the systems show the generalized costs (financial, material, energy, etc.) that are necessary for the normal functioning of the system. For service systems, such characteristics may be the total cost of the system to perform a fixed set of works; specific costs per work performed or per unit of system operation time, etc. Costs are not a universal characteristic of system operation. They relate mainly to technical, organizational, economic and production systems.

Characteristics of profit in systems estimate the generalized profit (financial, material, etc.) which appears as a result of system functioning. In service systems, these characteristics may be the total income that arises as a result of performing a fixed set of works; specific income per work performed or per unit of system operation time, etc. Profit is not a universal characteristic of systems. It applies only to organizational and economic systems.

The characteristics of the efficiency of systems are generalizing characteristics that bring together the assessments of all the above individual components of the quality of systems. The efficiency of the system shows the degree of achievement of the goal of the system. The characteristic of efficiency is often taken as the probability of achieving the goal of the system. Efficiency is a universal characteristic of the functioning of systems.

There are a number of limitations to the structure of the input data, namely:

- completely fixed structures of systems of the four above-mentioned types are taken into consideration: serial, parallel, parallel-serial and serial-parallel;
- the system has a completely fixed number of blocks, in addition, usually the number of blocks is determined by an integer;
- the system receives a clearly defined number of works, the number of which is also an integer;
- each block of the system performs a certain job for a certain time, then the matrix of time of work is the input data for calculating the parameters of the system.

The following assumptions should also be taken into account, namely:

- absolute reliability of all blocks of the service system;
- for each work is set many components of its operations, the order of execution of which is proposed by some given order ratio, and each operation is not more than one previous and one subsequent operation;
- no more than one operation can be performed simultaneously in any work;
- at any time, each block can perform no more than one operation;
- the operation started by any block is performed to the end.

To model the load of production systems it is necessary to solve a number of problems, namely: system representation, system calculation, system analysis and synthesis.

Representation of the system is the presentation of all given information about the system in a compact form, which facilitates the description of the system, as well as the formulation and solution of problems of its calculation, analysis and synthesis.

The calculation of the system is to determine the expressions or numerical values of various characteristics of the system according to the given structure of the system, the mode of its operation, the order of work entering it, and the numerical value of the parameters of its blocks.

The analysis of the system is to determine the type of dependence of various characteristics of the system on its structure, the mode of its operation, the order of execution of works in it, the values of the parameters of its blocks. The analysis allows to establish the degree of influence of these factors on the characteristics of the system. Due to this, it is possible to calculate the accuracy (stability) of the system when changing its parameters and structure.

The synthesis of the system is to find its structure and / or the order of execution of works in it on a given set of works to be performed, the values of the parameters of the blocks forming the structure, and the required values of the various characteristics of the system.

As an adequate mathematical apparatus for describing systems, infinite-valued logic is chosen - the theory of functions, the domain of which is a set of real numbers, and the main operations - disjunction, ie maximum, and conjunction, ie minimum, which are similar in properties to binary disjunctions and conjunctions. Using the structural representation of the studied system, it is possible to express any of its characteristics through similar characteristics of the blocks, using these logical operations.

This opens the way for the uniform solution of problems of calculation, analysis and synthesis. As an adequate mathematical apparatus for a compact representation of a given information about a complex system selected logical determinants - a kind of extreme numerical characteristics of rectangular matrices, expressed through the elements of the matrix by operations of infinite logic and their properties resemble ordinary determinants of square matrices.

To optimize the loading of technological equipment of the production system (ie to find the optimal order of launching parts into the system) it is advisable to use the method of branches and networks, because it is the most flexible. This method includes standard elements, namely: branching, estimation and clipping, combined into a typical optimization algorithm, consisting of a single first step and repeated the second step. The specificity for each type of system is manifested only in the form of an evaluation function.

The study of any real system is carried out on a model that is a simpler system than the original, while maintaining its essential features. Models are divided into physical and abstract, which in turn are divided into conceptual and mathematical.

Conceptual models characterize only causal relationships that are essential to describe the functioning of the system; while leaving aside the quantitative and qualitative aspects of this description.

The mathematical model is based on the conceptual and characterizes the functioning of the system in quantitative and qualitative terms.

The mathematical model of the production or technological system itself is described as follows.

There are some set of products  $B$  that need to be manufactured, and some set of units of technological equipment (machines)  $M$ , as well as workers for the manufacture of these products. Each product is characterized by its technological route, ie the sequence of passage of a certain subset  $M$ , which leads to the finished product.

The system in this case is a set of sets  $B$  and  $M$ , and its purpose – the manufacture of all products from the set  $B$ . The machines are blocks of the system, and various products - robots to be performed in this system. The technological route of the product is an ordered set of operations, which consists of the manufacturing process of this product. Each operation is performed by a separate machine (block). The effect of the operation is measured by the time required, costs, and so on.

All machines with connections between them form the structure of the system. The directional connection between the two machines shows that after performing the operation in one of them, the operation can be performed in the other.

The functioning of the system is to lay routes in its structure, in accordance with the specified technological routes of individual products, and the agreed passage of certain routes of all products until their full manufacture.

The task of structural modeling and optimization is to investigate the mathematical apparatus, which would adequately describe the structure of the production system and would allow to algorithmize the procedures for calculating the most important parameters of this system.

Usually in detailed consideration, this problem is divided into several subtasks:

a) analyze the work of production equipment for different structures and explore the features of modeling each of them;

b) choose a method of modeling the equipment of the production system, which would describe as fully as possible the parameters of the system and would allow to obtain its adequate model;

c) choose a method of optimizing the operation of equipment that would meet the given constraints and would have the best possible convergence;

The classification of systems aims, if possible, to unify the quantitative characteristics of systems, the tasks of their study and methods of solving these problems.

The classification of systems can be based on various features, so the paper considers only some of them, namely - on the structures of deterministic queuing systems.

Production systems, depending on the conditions of a particular production can have a series, parallel, parallel-series or series-parallel structure, and in the case of the intended return of the finished product to correct the defect - the structure of the feedback system. Thus, production systems can have a diverse structure.

According to the mode of operation of the units, all systems are divided into: systems with single-program and multi-program mode; static and dynamic; without downtime and with downtime of blocks. Systems with single-program (multi-program) mode of operation include those in which only one action (several actions) is performed simultaneously (for service systems - one job (several works)).

Static are systems in which during the execution of the purpose of the system (in service systems - during the execution of a given set of works) each block performs its operation not more than once, dynamic - those in which there are blocks that perform their operations for a specified time at least twice.

According to the mode of submission of works, service systems are divided into: systems with waiting and without waiting; systems with free and forced on time of receipt of works; conveyor and non-conveyor; systems with stationary and non-stationary workflow; systems with one and with several works.

Waiting systems (without waiting) include those in which the work after the previous operation is waiting for the release of the unit performing the next operation (immediately transferred to the free unit performing the next operation).

In the system with free time of work receipt all works are available already at the initial moment  $t = 0$  of start of system therefore the moments of actual occurrence of works are not specified. The works are entered into the system for their execution in accordance with the presence of free blocks in it.

In systems with forced time of work, the latter appear at specified points in time, in the general case later than the moment  $t = 0$  of the system startup. Here works are submitted to the system only after its appearance and in the presence of free blocks in it. Conveyor type includes systems in which the order of work is the same for all operations, and non-conveyor - other systems.

In systems with a stationary flow of work, the flow parameters do not change over time, and in systems with a non-stationary flow - change.

According to the discipline of service of works waiting in blocks, it is possible to allocate systems of service of types: 1) "came first - served first", 2) "came first - served last", 3) "came first - served average in order". 4) in ascending order of some indicator (usually the time required to complete this work in the system), 5) random service.

The scheme of the system in general is very important for its correct modeling, because often the methods of mathematical modeling are able to adequately describe only a certain, one structure and are not acceptable for modeling others.

Structural optimization of the technological systems created on the basis of the production equipment is connected with variation of their components: types and options of manufacturing of products, types, sequence and options of concentration of technological operations.



Each variant of the system is formed of elements  $w_g, g = \overline{1, G}$ , indicators of which  $f_{\omega g}$  have different meanings for implementation:  $w_g = \overline{1, W_g}$ .

The set of elements  $w_g$  and the relationship between them characterize the structure of the technological system, and the task of optimization is to choose a set of combinations of elements  $w_g$  of variant  $s^*$ , which is optimal in terms of the specified technical and economic requirements:  $F_i^*, i = \overline{1, I}$ .

Possibilities of change of the listed components are defined by a variety of two sets and communications between them:

- production objects

$$R \subset \times \{r_j : j \in J\},$$

where  $\subset$  – sign of relations;

$\times$  – sign of a Cartesian multiplication;

$r_j = \overline{1, R_j}$  – sets of numbers of production objects  $j$ -th name;

$J$  – set of indexes for names of production objects;

– technological operations

$$V \subset \times \{v_t : t \in T\},$$

where  $v_t = \overline{1, V_t}$  – set of numbers of technological operations  $t$ -th name;

$T$  – set of name indexes for technological operations.

Thus, the structure of the technological system is a set of elements  $r_i \in R, v_t \in V$  and the relationships between them.

In this case, it is convenient to consider the technological system in the form of a relation on a nonempty set of production objects and technological operations:

$$S \subset R \times V. \quad (1)$$

The elements of the set (1) are pairs of vectors  $r, v$

$$s_l = (r, v), s_l \in S, l = \overline{1, L}.$$

Here

$$r = (r_1, \dots, r_j, \dots, r_I), j = \overline{1, J}, r_j = \overline{1, R_j};$$

$$v = (v_1, \dots, v_t, \dots, v_T), t = \overline{1, T}, v(t) = \overline{1, V_t}.$$

Denote the common pair of elements  $(r_j, v_t) = w_g, g = \overline{1, G}$ .

Then

$$s_l = (w_1, \dots, w_g, \dots, w_G), l = \overline{1, L}, \quad (2)$$

Where  $w_g = \overline{1, W_g}, g = \overline{1, G}$  – elements of the technological system;

$L$  – the total number of variants of the technological system.

Universal methods of structural optimization take into account only the combinatorial nature of the formation of options. Therefore, only partial problems of choosing the optimal structure of technological systems can be solved on their basis.

One way to solve them is to go over and over. It involves a preliminary synthesis of options that can be obtained by forming all possible combinations of elements:  $w_g = \overline{1, W_g}, g = \overline{1, G}$ .

Then, for each implementation of the system, the values of the indicators are calculated  $F_i, i = \overline{1, I}$ , and the choice of the optimal option is carried out.

The positive side of a full search is the review of all permitted combinations, which ensures high reliability of the optimal decision.

This approach has shortcomings that impose limitations on its application.

First, the lack of mathematical models that take into account the system connections of production facilities and technological operations requires the formalization of the allowed combinations for each partial problem, which significantly increases the cost of preliminary preparation of the automated solution.

Secondly, the total number of variants of the technological system is quite significant, and the machine time required to generate them becomes unacceptable.

Third, in the case of multiple technical and economic requirements, the search for the optimal system leads to additional costs for re-research and analysis in the field of trade-offs.

An approach aimed at limiting the number of pre-synthesized variants is abbreviated random search.

However, due to the lack of mathematical models of structural optimization of the technological system, it is impossible to build targeted search procedures that predict the position of the system in the space of indicators, which reduces the reliability of incomplete search. In addition, it is not always possible to justify the condition of stopping an uncontrolled random search process.

A formalized approach to taking into account the combinatorial nature of structural optimization is achieved on the basis of discrete programming methods, because the components  $w_g$  variations are given on a discrete set  $\overline{1, W_g}$ .

Technological systems used in the manufacture of parts of devices and their assembly are discrete systems, so to model and optimize their work should use appropriate methods [11].

### 3. Method choice for modeling of production systems

The production system in General is a system with a fixed number of equipment (system units) that process a fixed number of parts (perform certain work).

Unfortunately, today there is no single method of modeling production systems in general, ie those that would adequately and with sufficient accuracy would describe the parameters of production systems of different structures, so to model a particular type of system, or at least several closely related types of various mathematical models. They are somehow able to model the production system, but usually each of them has its limits of application.

Models obtained by linear integer programming can only be used if a large number of constraints are imposed on the problem. In addition, to apply these methods, it is necessary to obtain the appropriate dependencies, which could be used to calculate the parameters of the system. Therefore, mathematical programming methods can be used as optimization methods in the presence of well-formalized system models [11].

Models of queuing systems are acceptable only for workflows with a random number and time of passage, because they use the apparatus of probability theory. You can usually consider degenerate cases where a random stream is replaced by a stream with predefined parameters. Therefore, we will consider deterministic queuing models that describe very well processes similar to those that need to be modeled. But such models are very different from each other depending on the type of system structure.

Models based on the provisions of graph theory differ from others by the simplicity and clarity of representation of both input and output data, and the image of the structure of the system itself.

Methods of classical modeling and optimization are well studied, widely used in theoretical problems, but have several significant shortcomings, in particular in terms of modeling systems in their application it is difficult to develop an adequate objective function that would satisfy the limitations of this method. would be able to interpret the results of further calculations, in particular the results of model optimization.

Statistical methods have been used for a long time and allow to determine the factors that most affect the characteristics of the system. However, they require a large amount of experimental data and therefore are more likely to be useful for solving problems of optimization of empirical processes, ie where it is impossible to establish unambiguous relationships between system parameters.

Structural-logical method of modeling is acceptable from the point of view of clarity of representation of system and calculations of its parameters, quite well algorithmized, has good convergence at

application of the corresponding optimization methods, and also is suitable for modeling of systems with various types of structures. clarity of presentation of the system.

Based on the analysis of methods of modeling production systems in order to optimize their work, it is established that the most interesting are the structural-logical method of research of technological systems and methods based on graphical representation of production structures using Petri nets. These methods are discussed in this article.

#### 4. Structural and logical method of modeling and optimization of production systems

There are two main directions in the methods of research of production systems: general (abstract) systems theory, which studies the behavior of the system out of connection with its structure, as the ratio of inputs and outputs, and structural systems theory, which studies the functioning of the system depending on its structure.

The possibility of constructing a deterministic theory of service systems on the basis of the mathematical apparatus of infinite logic and logical determinants was first shown in, where the problem of synthesis of one class of static systems was solved. Subsequently, the possibility of applying this apparatus to the synthesis of other classes of systems, as well as to their analysis was shown.

The advantages of the apparatus of infinite logic and logical determinants are realized within the structural-logical approach to the study of service systems, which involves structural representation of the studied system and expression of its characteristics through the characteristics of subsystems using infinite logic and logical determinants.

Structural-logical method does not have most of the shortcomings of other methods of modeling and optimization of production systems, ie it is acceptable in terms of clarity of the system and calculations of its parameters, quite easy to formalize, has good convergence in the application of appropriate optimization methods, and that most importantly, suitable for modeling systems with different types of structures, namely: serial, parallel, parallel-serial and serial-parallel. This approach makes it possible on the basis of a small number of such algorithms to calculate, analyze and synthesize the optimal structure of the production system.

#### 5. Construction of mathematical models of production systems

The tasks of studying systems are very diverse and are largely determined by the class of the studied system. However, there are universal types of problems that are essential for many classes of systems: representation, calculation, analysis and synthesis.

Representation of the system is a representation of all given information about the system in a compact form, which facilitates the description of the system, as well as the formulation and solution of problems of its calculation, analysis and synthesis.

The calculation of the system is to determine the numerical values or expressions of various characteristics of the system according to the given structure of the system, the mode of its operation (for the service system - also the order of work coming to it) and the numerical value of its blocks.

The problem of system calculation is important for all classes of systems. It reveals the possibilities of existing natural (biological, social) and underlies the design of artificial (technical, organizational and economic) systems.

The analysis of the system consists in determining the type of dependence of various characteristics of the system functioning on its structure, the mode of its functioning (for the service system - also the order of execution of works in it), the values of its blocks.

The analysis allows to establish the degree of influence of these three factors on the characteristics of the system. Due to this, it is possible to perform calculations of accuracy (stability) of the

system at different values of its parameters and structure and calculations in the design of systems in order to achieve the desired values of system characteristics by some change in their parameters and structure.

The synthesis of an arbitrary system consists in determining its structure and mode of operation for a given purpose of the system, the values of the parameters of its blocks and the required values of the characteristics of the system.

The synthesis of the service system is to find its structure and the order of execution of works from a given set of works to be performed, the values of the parameters of the blocks that form the structure of this system, and the required values of various characteristics of the system.

The task of system representation is important only for complex systems, while the tasks of calculation, analysis and synthesis are essential for any system - both simple and complex. In our case, service systems are considered, for which the problems of representation, calculation, analysis, and synthesis problems are solved in the form of the problem of finding the optimal order of execution of a given set of works in the system, which provides optimal values of certain system characteristics. The structure of the system and the parameters of its blocks are considered specified.

The paper considers deterministic problems of representation, calculation, analysis and synthesis of service systems with a typical structure (serial, parallel, parallel-serial, serial-parallel), with different modes of operation of units and submission of works, with the possibility of imposing restrictions on the operation of units.

Here are the mathematical models for each type of system, according to the problems to be solved. The tasks of calculation and analysis of the service system are respectively:

- a) calculation of its various characteristics (performance, load, etc.) in accordance with the specified similar characteristics of its units, the scheme of their connection, the number of works entering the system, and the mode of operation of the system;
- b) determining the nature and degree of influence of all given factors on the characteristics of the system.

The solution of the first problem must precede the solution of the second.

The complexity of solving both problems significantly depends on the scheme of connection of blocks to the system (serial, parallel, etc.), the mode of operation of the system (single-program or multi-program, waiting for work or without waiting, etc.), the number of jobs entering the system. A single-work system can only be without waiting and with a single-program execution mode.

Analysis of such systems is not a problem and is not considered here. Of the other systems, serial systems are the most convenient for calculation and analysis. Consider a system in the form of  $m$  series-connected blocks, designed to sequentially perform  $m$  different operations.

The system receives  $n$  different works, each of which breaks down into  $m$  of the above operations. Opening times  $a_{ij}$  ( $i = \overline{1, m}$ ) for jobs  $j$  ( $j = \overline{1, n}$ ) given by the matrix:  $A = \|a_{i,j}\|$ .

Execution of works in the system can be carried out in two modes: single-program and multi-program.

In the first mode, first all the operations of the first work are performed sequentially, then in the same order all the operations of the second work, and so on.

In the second mode of operation are started in the system and pass its successive blocks  $1, 2, \dots, m$  in the same order  $P_n = (j_1, j_2, \dots, j_n)$ ; here  $j_k$  is the number of the work that follows the  $k$ -th in order.

Thus moments of receipt of works in system are not specified (free on time of receipt of works), the block 1 is loaded and starts to carry out the operation in the next work  $j_k$  immediately after release from the previous work  $j_{k-1}$  (ie in the block there are no downtimes); loading of the first work  $j_1$  occurs at the initial moment  $t = 0$ .

However, block 2 begins to perform its second operation in the next job  $j_k$  not immediately after the release of the previous job, but only after the end in block 1 of the first operation of work  $j_k$ .

Similar time relations between the operation of units 2 and 3, 3 and 4, ...,  $m-1$ ,  $m$ . Thus, in blocks 2, 3, ...,  $m$  downtime is possible. But it is possible that the work that comes to the unit, finds him busy with previous work.

In this case, the unit works without downtime, but the work coming to it is waiting, forming a queue served by the unit as a rule: first come - first served. So, a multi-program system is a standby system.

For a *serial system*, the total time  $To(m, n)$  of the passage of all  $n$  works through all  $m$  blocks of the system with a single-program mode of execution of works is equal to the summing logic determinant from the matrix  $A = \|a_{ij}\|$  times of operations, and for the case of multiprogram mode  $Tm(m, n)$  – disjunctive logic determinant from the matrix  $A = \|a_{ij}\|$ .

In the case of a **parallel system**, it is represented in the form of  $m$  parallel connected blocks 1, 2, ...,  $m$ , which are designed for parallel performance of the same type of work. The blocks are functionally equivalent, ie they can perform each of the works.

However, the speed of the blocks in the general case is different - the execution time in the work block is  $a_{ij}$ . Times  $a_{ij}$  form a matrix of working times  $A = \|a_{ij}\|$  sized  $m \times n$ .

The system works in multi-program dynamic mode as follows. Works 1, 2, ...,  $n$  are fed into the system in a given order  $Pn = (j_1, j_2, \dots, j_n)$ , where  $j_k \in \{1, \dots, n\}$ , but without specifying the moments of receipt, ie free time.

In this case, at the initial moment  $t = 0$  at the same time work  $j_1$  is loaded into block 1 (which immediately begins to perform its operation), similarly work  $j_2$  – in block 2 and so on – work  $j_m$  – in block  $m$ .

After that, all blocks of the system are loaded by performing the first  $m$  works  $j_1, \dots, j_m$ . Therefore, the next job  $j_{m+1}$  will have to wait until the first  $j^{(1)}$  of the loaded jobs  $j_1, \dots, j_m$  is performed, and then take its place in the vacated block.

The next job  $j_{m+2}$  will have to wait for its loading into the system until the moment when the first of the new set of jobs  $\{j_1, \dots, j_m, j_{m+1}\}$  that are currently in the system and so on will be performed. It follows that the considered system works without downtime (ie with a load equal to 1) in the standby mode of the start of its execution.

Simultaneously with the tasks of calculation and analysis, the problem of system representation is solved, using the apparatus of ordinal logical determinants.

Matrix  $T(m, n) = \bigvee_{k=1}^n t_k$  is the basic ratio for calculating the system speed. It reduces the definition of the performance characteristic of the system  $T(m, n)$  to the calculation of the vector of moments of completion of work in the system.

In the case of using **parallel-serial and serial-parallel systems**, they are represented in the form of  $M$  series-connected stages (groups, blocks), designed to perform work consisting of  $M$  different operations.

Let the  $i$  degree ( $i = \overline{1, M}$ ) serves to perform the  $i$ -th operation and is a subsystem in the form of  $m_i$  parallel connected blocks 1, 2, ...,  $m_i$ . All blocks of one stage are functionally equivalent, ie configured to perform one operation, and the  $i$ -th stage can perform simultaneously  $m_i$  such operations of the same type (according to the number of blocks in it).

We believe that all blocks of one degree have the same speed (ie degrees are homogeneous in blocks). The system receives a set of  $n$  different works, each of which consists of  $M$  of the above operations. Time  $a_{ij}$  execution of the  $i$ -th operation ( $i = \overline{1, M}$ ) for job  $j$  ( $j = \overline{1, n}$ ) are given and form a matrix  $A = \|a_{ij}\|$ .

Execution of jobs in the system is possible in two modes: single-program and multi-program.

In the first mode, first all operations of work 1 are performed sequentially, then in the same order all operations of work 2 and so on.

In the second mode, the system operates as follows. The order  $P_{1n} = (j_{11}, j_{12}, \dots, j_{1n})$  of start of works on the first operation (the first stage of system) where  $j_{1k}$  – number of the work started  $k$ -th on an

order is specified. At the same time the moments of receipt of separate works are set, that is we have system with free on time receipt of works.

Execution of the first operation in the next work  $j_{1k}$  begins as soon as among the blocks of the first stage engaged in execution of this operation in the previous works  $j_{11}, \dots, j_{1, k-1}$  any block is released.

Execution of any  $i$ -th ( $i = \overline{1, M}$ ) the operation in the next work  $j_{ik}$  begins as soon as the execution of the previous ( $i-1$ )-th operation in this work ends and among the blocks of the  $i$ -th degree, occupied with the execution of the  $i$ -th operation in the incoming  $j_k$  works, any block will be released.

The mathematical apparatus of infinite logic can serve as an adequate means of describing deterministic service systems. This adequacy is manifested in the fact that for an arbitrary system, any characteristic of functioning can usually be expressed through the parameters of the system using logical operations of infinite-valued logic (sometimes supplemented by ordinary algebraic addition).

In this case, formally, the difference between the characteristics comes down to the fact that some of them receive simple expressions (containing few of these operations), and others - complex (because they contain many operations). Using the rules of equivalent logical transformations developed in infinite logic, the received expression of the characteristic of functioning can always be led to this or that convenient kind. This type depends on the system problem to be solved.

Thus, to solve the calculation problem, the most convenient is the minimum expression of the characteristic that contains the smallest possible number of logical and other operations; to solve the problem of analysis - the expression of a characteristic with a selected parameter, the impact of which on the system is analyzed; to solve the problem of synthesis - the expression of characteristics in a form that is sensitive to changes in the order of work in the system.

This possibility of flexible representation of different characteristics of systems functioning in terms of operations of infinite logic opens the fundamental possibility of the same, based on the rules of equivalent logical transformations of infinite logic, solving the whole set of problems of systems research - calculation, analysis, synthesis.

This possibility of the same solution of problems of calculation, analysis and synthesis of service systems using the apparatus of infinite logic is directly realized only for fairly simple systems, where the number of blocks is small, and the links between them are not developed. In complex systems due to the presence of a large number of blocks with developed links between them on the way to the implementation of this possibility there are additional difficulties associated with the need to solve the problem of system representation.

In overcoming these difficulties the main role is played by the mathematical apparatus of logical determinants. Since the logical determinant is a parameter of the enlarged description of the studied system, they allow to present all given information about the system in a compact, accessible form, which makes the system "simple" and opens the way to its study by the above methods of studying simple systems based on the apparatus of infinite logic. In addition, the apparatus of logical determinants allows to make in the process of studying complex service systems and a number of other significant simplifications.

The method of modeling and optimization of loading of production technological systems on the basis of structural-logical approach to the study of complex systems is tested on real examples.

The use of structural-logical approach to modeling and optimization of production systems has the following advantages:

a) unification with the help of logical determinants of computational procedures in the study of systems leads to the fact that all tasks of calculation and analysis, as well as the synthesis of complex systems are reduced to the calculation of certain logical determinants, ie are the same from a computational and mathematical point of view;

b) obtaining analytical conditions for the optimality of the order of work in the system and on their basis - the procedures for the synthesis of some classes of complex systems have a reduced complexity of calculations;

c) modification of the procedure of branches and boundaries, which is used in the synthesis of complex systems to improve its accuracy and speed, allows to intensify the clipping of unpromising options by additional use of information contained in optimal conditions, and obtaining a more accurate estimates that in addition, it has reduced computational complexity.

The above advantages of using infinite logic and logical determinant are realized within the structural-logical approach to the study of production systems, which involves structural representation of the studied system and expression of its characteristics through the characteristics of subsystems using infinite logical logic and logical determinant.

## 6. Conclusions

The article theoretically substantiates and implements mathematical methods of modeling production systems, which allow to choose rational conditions for their work.

It is shown that increasing the efficiency of instrument-making production can be achieved by modeling and optimizing the equipment load of production systems.

The analysis of modeling methods for production systems has shown that at the decision of this problem it is expedient to apply modern methods of mathematical and simulation modeling based on use of the structural-logical approach to mathematical modeling of systems.

Methods of infinite logic and logical determinants allow to describe the mathematical model of the production system and its characteristics, and the method of branches and boundaries - to optimize its work. The basic provisions of infinite logic and ordinal determinants, on which the structural-logical approach to the study of complex systems is based, which include production systems in instrument making, allow to create a mathematical model of the system of arbitrary structure.

The actual application of this method of modeling production systems can reduce non-production losses of time, thereby saving production resources without the use of any other measures of administrative or technical nature.

## 7. Literature

1. Tamm B.G. i dr. Analiz i modelirovanie proizvodstvennykh sistem / B.G. Tamm, M.E. Puusepp, R.R. Tavast; Pod obsch. red. B.G.

Tamma. – M.: Finansyi i statistika, 1987.- 191 s.: il. <https://www.twirpx.com/file/2128170/>  
 2. Buslenko N.P. Modelirovanie slozhnykh sistem. – M.: Nauka, 1978. –400 s. <https://www.twirpx.com/file/1655389/>  
 3. Sovetov V.Ya., Yakovlev S. A. Modelirovanie sistem. – M.: Vysshaya shkola, 1985.- 271s. <https://lib-bkm.ru/14025>  
 4. Moiseev N.N. Matematicheskie zadachi sistemnogo analiza - M.: Nauka, 1981.- 487s. <http://www.library.fa.ru/files/Moiseev.pdf>  
 5. Skurihin V.I. i dr. Matematicheskoe modelirovanie / V.I. Skurihin, V.B. Shifrin, V.V. Dubrovskiy. – K.: Tehnika, 1983. 270 s. <https://www.twirpx.com/file/505366/>  
 6. Mitrofanov V.G. Matematicheskoe obespechenie SAPR tehnologicheskoy podgotovki proizvodstva. – M.: Mashinostroenie, 1991. –52 s. [http://library.lp.edu.ua/opac/page\\_lib.php?docid=11538&mode=DoCBibRecord](http://library.lp.edu.ua/opac/page_lib.php?docid=11538&mode=DoCBibRecord)  
 7. Solomentsev Yu.M., Ostafev V.A., Antonyuk V.S., Vyisloukh S.P. i dr. SAPR. Tipovyye matematicheskie modeli i algoritmyi rascheta optimalnykh rezhimov odnoinstrumentalnoy obrabotki materialov rezaniem. Metodicheskie rekomendatsii MR 119-85. – M.: VNIINMASH, 1985. – 120 s.  
 8. Antonyuk V.S., Vyisloukh S.P., Filippova M.V. Avtomatizirovannoe proektirovanie tehnologicheskikh protsessov sborki izdeliy priborostroeniya. Sborka v mashinostroenie i priborostroeni. M. Mashinostroenie. 2007. - #6 – S.3-6. [http://library.ztu.edu.ua/e-copies/Zbirnyk/Process\\_obrobky\\_6/3.pdf](http://library.ztu.edu.ua/e-copies/Zbirnyk/Process_obrobky_6/3.pdf)  
 9. S.P. Visloukh Determination of process parameters of new tool, J. Superhard Mater., 2001, vol. 23, no. 5, pp. 65–69. <https://www.scopus.com/record/display.uri?eid=2-s2.0-0035550254&origin=resultslist&sort=plf-f&src=s&sid=7af691b6a48f6aedbb73486821d6d62d&sot=autdocs&sdt=autdocs&sl=17&s=AU-ID%287801645204%29&relpos=0&citeCnt=0&searchTerm=>  
 10. Levin V.I. Strukturno-logicheskie metodyi issledovaniya slozhnykh sistem s primeneniem EVM. – M.: Nauka, 1987. – 304 s. [https://litmy.ru/knigi/tehnicheskie\\_nauki/130378-strukturno-logicheskie-metody-issledovaniya-slozhnykh-sistem-s-primeneniem-evm.html](https://litmy.ru/knigi/tehnicheskie_nauki/130378-strukturno-logicheskie-metody-issledovaniya-slozhnykh-sistem-s-primeneniem-evm.html)  
 11. Vysloukh, S.P., *Informatsiyni tekhnologiyi v zadachakh tekhnologichnoyi pidgotovky prylado- ta mashynobudivnogo vyrobnutstva. Monografiya* (Information Technologies in the Tasks of Preproduction Engineering for Instrument- and Machine-Building Industries. Monograph), Kiev: NTUU “KPI”, 2011. [in Ukrainian] [http://old.kafvp.kpi.ua/media/books/Vysloukh.Inf\\_tech\\_v\\_zad\\_tpv.pdf](http://old.kafvp.kpi.ua/media/books/Vysloukh.Inf_tech_v_zad_tpv.pdf).